MARCO FEDELE DI LIBERTO

QUANTUM PHASE TRANSITIONS IN LOW-DIMENSIONAL OPTICAL LATTICES

Quantum phase transitions in low-dimensional optical lattices

Kwantumfaseovergangen in laagdimensionale optische roosters

(met een samenvatting in het Nederlands)

Proefschrift

ter verkrijging van de graad van doctor aan de Universiteit Utrecht op gezag van de rector magnificus, prof. dr. G.J. van der Zwaan, ingevolge het besluit van het college voor promoties in het openbaar te verdedigen op maandag 22 juni 2015 des middags te 2.30 uur

door

Marco Fedele Di Liberto

geboren op 11 april 1986 te Carini, Italië

CONTENTS

PUBLICATIONS

The main chapters of this thesis are based on the following publications:

- Chapter 2 is based on M. Di Liberto, C. E. Creffield, G. I. Japaridze, and C. Morais Smith, *Quantum simulation of correlated hopping models with fermions in optical lattices*, Phys. Rev. A **89**, 013624 (2014), arXiv:1310.7959.

- Chapter 3 is based on M. Di Liberto, D. Malpetti, G. I. Japaridze, and C. Morais Smith, *Ultracold fermions in a one-dimensional bipartite optical lattice: Metal-insulator transitions driven by shaking*, Phys. Rev. A **90**, 023634 (2014), arXiv:1405.4756.

- Chapter 4 is based on M. Di Liberto, T. Comparin, T. Kock, M. Ölschläger, A. Hemmerich and C. Morais Smith, *Controlling coherence via tuning of the population imbalance in a bipartite optical lattice*, Nature Communications **5**, 5735 (2014), arXiv:1412.4040.

Other publications to which the author has contributed:

- M. Di Liberto, O. Tieleman, V. Branchina, C. Morais Smith, *Finite - momentum Bose-Einstein condensates in shaken 2D square optical lattices*, Phys. Rev. A **84**, 013607 (2011), arXiv:1310.7959.

- V. Branchina, M. Di Liberto, I. Lodato, *Mapping fermion and boson systems onto the Fock space of harmonic oscillators*, Phys. Rev. E **81**, 011120 (2010), arXiv:1001.3041.

- V. Branchina, M. Di Liberto, I. Lodato, *Dark energy and Josephson junctions*, Journal of Cosmology and Astroparticle Physics (JCAP) **08** (2009) 011.

1

INTRODUCTION

The physics of ultra-cold gases has proved to be an almost unlimited source of beautiful phenomena. When the temperature is low enough, such that the thermal wavelength is comparable to the inter-particle spacing, atoms become governed by the laws of quantum mechanics. This regime is quite different, for instance, from room temperature physics, where atoms can be considered for most purposes as point-like classical objects. At low temperatures (of the order of 100 nK), the atoms behaves as extended waves that overlap and interfere [1]. These interference effects are the ones leading to the spectacular phenomenon known as Bose-Einstein condensation (BEC), where (bosonic) atoms massively occupy one quantum state and behave as a macroscopic matter wave.

With the realization of the first BEC in 1995 [2, 3], a completely new world has come within reach. Although the proposal of this new state of matter dates back to the 20's, when Einstein first put forward this idea after receiving a letter from Bose on the quantum statistics of photons [4, 5], more than 70 years of research have been necessary to overcome the technical limitations. Helium, the primary candidate for BEC, cannot undergo condensation because, at low temperatures, it becomes a strongly interacting liquid and the atoms cannot occupy a macroscopic quantum state. Nevertheless, another quantum mechanical phenomenon sets in, namely the liquid can flow without dissipating energy and forms a superfluid.

On the contrary, alkali atoms preserve their gaseous state and can therefore be employed to reach Bose-Einstein condensation. The drawback is the requirement of very low density, which lowers unfortunately by orders of magnitude the critical temperature to observe BEC. The quest for the experimental realization of extremely low temperatures stimulated a lot of work in developing cooling techniques, such as laser cooling and evaporative cooling, that ultimately led to the achievement of BEC [1]. Since then, many different types of atoms have been cooled and the techniques have been refined to deal with the challenges that the different atomic species exhibit.

Over the years, the field of cold atoms has considerably grown, going far beyond the achievement of Bose-Einstein condensation. The high degree of control allowed in experiments is the crucial reason behind its success. One can tune interactions, effective mass of the particles, lattice geometry, density and much more [6]. As a first example, we briefly describe the BEC-BCS crossover, one of the phenomena that cold atoms have made possible to observe and realize.
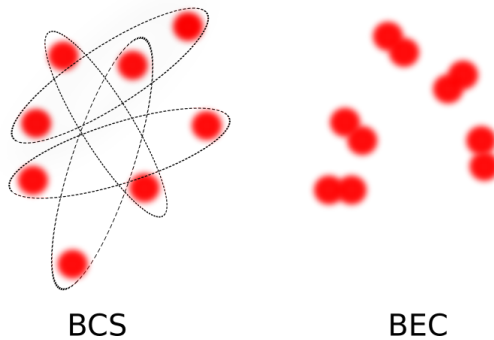
FIGURE 1.1: BEC-BCS crossover. In the BCS limit the electrons form weakly-bound pairs, whereas in the BEC limit the electrons are tightly bound into molecules that form a Bose-Einstein condensate.

In the presence of a weakly-attractive interaction, Fermi gases exhibit superconductivity at sufficiently low temperatures, as described by the theory of Bardeen, Cooper and Schrieffer (BCS) [7]. Fermions form weakly-bound pairs (Cooper pairs), the size of which is, in general, much larger than the average interparticle spacing. When the attraction becomes stronger, the size of the pairs starts decreasing and, ultimately the two atoms will form a bound state. These tightly-bound pairs can be considered to all intents as bosons that can condense and form a BEC. Although the two regimes are very different with respect to each other because the former is a state of matter that arises because of a many-body instability while the latter is a consequence of the two-body attraction[1], there is no symmetry change between these two scenarios. Therefore, no phase transition occurs, but a rather smooth crossover, known as the BEC-BCS crossover [8].

At first, it was difficult to imagine an experiment that could verify this theoretical proposal. However, the high tunability available in cold atoms allows one to control the effective two-body interaction described at low temperature by a single quantity, the s-wave scattering length a_s, by using an external magnetic field (Feshbach resonances) that plays the role of a knob [9, 10]. In this way, it has been possible to tune interactions from the weakly to the strongly-interacting regime and explore the behaviour of the degenerate Fermi gas through the crossover [11–13].

---

1 The wave function in the BCS state manifests oscillations with the periodicity set by the Fermi momentum, while for the BEC bound state there are no oscillations but an exponential decay.

1.1 QUANTUM SIMULATION AND PHASE TRANSITIONS

Condensed matter physics typically deals with the understanding of the behavior of electrons in solids, where they usually move on the periodic crystalline potential created by the atoms. Very often, this is an extremely complicated problem to address theoretically. What if we can design a system where the role of the electrons is played by a certain type of quantum objects (for instance fermionic atoms at very low temperature) and make them experience a periodic potential? In this way one could simulate the behavior of the electrons in a crystalline material. Certainly, atoms are objects quite different from electrons: besides having a much larger mass and a complicated internal structure, they are also electrically neutral. However, many features and physical phenomena are quite general and occur as a consequence of the generic model describing the system. Hence, as long as we are able to implement a specific model of interest in a controlled experiment, we can explore the type of physics that it describes, provided that we can tune the parameters in the required region of phase space. This is quite similar to what a computer does when implementing a simulation, except for the fact that the cold-atom system can span the exponentially large Hilbert space of the model that we want to understand because it is an intrinsically quantum system itself [14].

Systems of cold atoms provide, for this reason, a rich playground for physicists [6, 15]. The possibility to tune interactions discussed previously is not, however, the only freedom that is available to experiments. In 1998, just a few years after the realization of the first BEC, Jaksch *et al.* [16] proposed a scheme to realize the Bose-Hubbard model in optical lattices. As for the BEC-BCS crossover, also in this case cold atoms provided a platform to make possible the observation of physical phenomena theoretically proposed beforehand [17].

In the proposal by Jaksch *et al.* [16] and in its subsequent experimental implementation [18], a cloud of bosonic atoms (in the experiment Rubidium 87) is trapped by a magnetic field. Counter-propagating laser beams are used to create an optical "lattice" on top of the magnetic trap. The intensity of the lasers allows one to control the lattice depth V_0, i.e. the height of the potential barrier between neighboring wells, and therefore the tunneling amplitude. In typical experimental condition, atoms occupy the lowest exponentially-localized quantum state in each well of the periodic potential and tunnel to the nearest-neighbor wells with hopping amplitude J. Because the lattice depth controls the height of the potential barriers between two neighboring wells, it allows to control J, which decreases when V_0 increases. Repulsive contact interactions lead to an energy cost U when two atoms occupy the same localized state. Contrary to the hopping, U becomes larger upon increasing V_0 because more localized states have a larger overlap of the wave functions describing each of the two interacting atoms. The ratio J/U therefore depends monotonically on the lattice depth V_0.

The phase diagram of the Bose-Hubbard model displays a second-order phase transition as a function of J/U [17, 19, 20]. Let us focus for simplicity on integer filling, say n particles per site, with $n = 1, 2, \ldots$. When the hopping J is dominant, particles are free to delocalize and form a condensate, occupying the zero-momentum state. This is the superfluid phase. When instead the interactions, governed by the single parameter U, are dominant, the energy is minimized by having an insulating and incompressible state, the Mott insulator phase, with vanishing particle-number fluctuations on each site and a gap in the excitation spectrum. The phase transition has been observed by varying the lattice depth V_0, and therefore J/U, in a three-dimensional optical lattice and recording the momentum distribution [18].

After the realization of the superfluid - Mott insulator phase transition, many possibilities to engineer models of physical interest were devised [15, 21]. Ultra-cold atoms in optical lattices became the paradigm to concretize the idea of quantum simulator envisaged by Feynman years before [22]. The simulation of a many-body quantum system on a classical computer would require an exponentially large amount of time because the Hilbert space of a many-body system grows exponentially with its size. However, a quantum simulator is instead a system that can directly encode the quantum degrees of freedom and process their dynamics. The key element is to engineer a mapping between the model to simulate and the degrees of freedom to be used in the quantum simulator.

There are two ways to look at this problem. On one side, one can use a cold-atom system to simulate a certain model known in condensed matter, with the aim of understanding whether such a model can describe the behaviour observed in a specific class of materials. This would be the case of the simulation of the Fermi-Hubbard model [23, 24] to understand whether it describes the phase diagram of high-temperature superconductors [25, 26], for example. On the other side, a quantum simulator can be seen as a platform to observe novel physical phenomena that have been only theoretically predicted. In typical condensed-matter systems, the parameters cannot usually be tuned: not only the crystalline potential is fixed, but also the type of particles, their mass and their interaction strength. In a cold-atom system, instead, many parameters can be controlled, thus allowing one to explore quantum phase transitions for many classes of models [27]. This is the case for some old problems in condensed matter, such as the Bose-Hubbard model [17], the Hofstadter butterfly [28], the Haldane model [29] and many others [14].

Other theoretical speculations which have no analog in solid-state systems have also been implemented in experiments. A remarkable example is Bose-Einstein condensation in higher orbitals [30, 31]. When bosons condense in a higher orbital, the many-body wave function is not constrained to be real and unique, as Feynman's no-node theorem requires [32, 33]. Time-reversal symmetry, which corresponds to complex conjugation of the bosonic wave
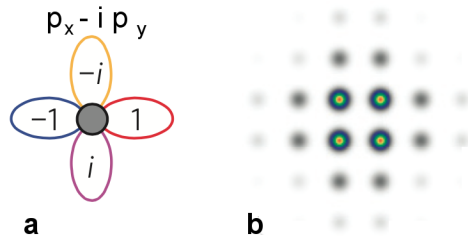
FIGURE 1.2: P-band condensates. (a) The lobes represent the p_x and p_y orbitals. The phases of the wave function are indicated, corresponding to a $p_x - ip_y$ state with non vanishing angular momentum tha breaks time-reversal symmetry. (b) Time-of-flight pattern showing the orbital condensation signature at finite momenta $(\pi/a, 0)$ and $(0, \pi/a)$, where a is the lattice spacing. The figures are adapted from Ref. [34].

function, can therefore be spontaneously broken and the emergent superfluid phases may have intriguing properties. A recent realization of a condensate in p-bands [34] and f-bands [35] has made use of a chequerboard optical lattice to stabilize a long lived condensate in an excited state. The experiment has shown that a new class of phenomena is within reach: bosons condense in states with finite crystalline momentum, non-zero angular momentum and staggered orbital currents [36].

States that break time-reversal symmetry have been introduced to explain controversial phases of matter, such as the π-flux phase or the Varma phase, both proposed to describe the pseudo-gap regime of high-T_c superconductors [26]. We will show in Chapter 5 how condensates in p-bands can be used to simulate bosonic analogs of the Varma phases in an optical Lieb lattice, which is the lattice of the Cu-O plane of cuprate superconductors. In particular, we will show how to generate a Varma phase that, in the fermionic version, displays anomalous Hall effect as for the Haldane model [37].

1.1.1 *Hubbard models in cold-atom systems*

The Bose-Hubbard model, being the prototype of a typical cold-atomic realization in optical lattices, has been the object of a thorough investigation over the years. The superfluid - Mott insulator phase transition has been addressed in one [38], two [39] and three [18] dimensions. New imaging techniques have been invented, allowing to probe single lattice-site occupation and therefore the many-body wave function [40, 41]. Thermalization properties and the effect of correlations, e.g., have been investigated using this technique. These studies revealed the full power of the quantum simulator because numerical approaches on classical computers are unable to capture the highly-entangled relaxation process observed at long times in the experiments [42]. In this experiment, a bichromatic one-dimensional lattice is used to generate an initial

density wave with occupations $|\ldots, 1, 0, 1, 0 \ldots\rangle$ which forms a Mott insulator with inhomogenous density, when the tunneling is inhibited by a large potential barrier. The dynamics is studied by quenching the lattice depth to lower values such that the atoms can start tunneling again.

However, an open question to address is how the transition from a superfluid to an inhomogeneous Mott insulator occurs. In Chapter 4, we focus on a static bipartite lattice in which Mott insulators with imbalanced population are generated by detuning the potential depth of neighboring wells. This procedure is different from the one used in Ref. [42] to prepare the initial state of the experiment, where the Mott phase is realized by imposing a large potential barrier to prevent the atoms to tunnel to the neighboring empty sites. Using a mean-field theory supplemented by perturbative calculations, we show that detuning nearest-neighbor wells can destroy coherence and drive the system into Mott insulators with inhomegeneous density. Our findings suggest that the physics of static Bose-Hubbard models has still many aspects that remain to be explored.

A significant effort has been devoted also to the simulation of the Fermi-Hubbard model [24], which is exactly solvable in one dimension [43], but represents a challenge in dimensions higher than one. In two dimensions, in particular, it has been proposed to describe the elusive high-temperature superconducting cuprates [44]. The simulation of the Fermi-Hubbard model with cold atoms could shed some light into its phase diagram, for which theoretical and numerical efforts have not provided conclusive answers [26, 45]. The scheme for the simulation of the Fermi-Hubbard model with cold atoms was discussed shortly after the proposal for the Bose-Hubbard model [24]. Its experimental implementation has been successfully achieved by using a two-component Fermi gas in a three dimensional optical lattice [46, 47]. Two hyperfine states of the atoms are the degrees of freedom used in this setup to mimic spin.

In the Hubbard model at half-filling (one particle per site on average) with strongly repulsive interactions $U \gg J$, the Mott phase appears when lowering the temperature below $T \sim U$. In this phase, double occupation and number fluctuations are suppressed and the system is an insulator, with a gap in the excitation spectrum of the order of U [48]. Clearly, this phenomenon is quite similar to the bosonic counterpart described earlier. An experiment performed in this regime by the group of Esslinger [47] showed the formation of a Mott insulator for a Fermi gas described by the repulsive Hubbard model. In this experiment, Feshbach resonances were used to tune the interactions.

Cooling further the system, the next temperature scale to achieve is the one leading to Néel antiferromagnetism, which is set by the exchange energy $T \sim J^2/U$. The strongly-repulsive Hubbard model can indeed be mapped into a Heisenberg model [48, 49], for which spin-spin correlations become important when the temperature is sufficiently low. Exploring quantum magnetism is the next frontier in the experimental study of strongly-correlated

Fermi systems with cold atoms. However, limitations of cooling techniques still do not permit to go below the Néel scale. Recent experimental efforts showed quite some progress by getting close to the transition temperature by less than a factor of two [50] or by engineering special geometries that can enhance magnetic correlations [51]. On the theoretical front, some procedures have also been proposed to limit the entropy gain (and therefore the temperature) during the loading of the Fermi gas into the optical lattice [52], which is the major source of non-adiabaticity [53].

From a theoretical perspective, cold-atomic gases offer not only the opportunity to investigate fermionic models that are relevant to understand solid state materials, but also to discover novel phenomena and unconventional phase transitions. In the next paragraph, we will describe how time-dependent driving forces can be used for quantum simulation of bosonic and fermionic systems. In particular, in Chapter 2 and 3, we will use specific driving protocols to engineer lattice models for fermions described by generalized Hubbard models that can support exotic superconducting states and transitions to metallic states with a non-trivial Fermi surface.

1.2 SHAKING AND DRIVING FORCES FOR QUANTUM SIMULATION

Among the many methods that have been used to realize systems and Hamiltonians of interest in cold atoms during the last years, time-dependent forces have played a prominent role. The seminal papers by Eckardt *et al.* [54] and Creffield *et al.* [55] suggested that the Mott insulator - superfluid phase transition could be achieved using a dynamic protocol to control the ratio J/U, instead of tuning the lattice depth. The procedure involves the shaking of the lattice with a large frequency ω, much larger than the characteristic energy scales in the problem. This periodic time-dependent model can be effectively studied using the so-called Floquet formalism, based on a time-independent effective Hamiltonian operator. The effective description works at stroboscopic times, namely when the time t is a multiple of the period $T = 2\pi/\omega$, leading to a renormalization of the hopping parameter J by a Bessel function of zeroth order, the argument of which depends on the ratio between the driving force and the frequency. As a result, one can reduce the magnitude and change the sign of the hopping. When tuning the driving parameters close to a zero of the Bessel function, the hopping is dynamically suppressed and a Mott insulator is formed.

This proposal is not only very appealing, but it has proved to be experimentally realizable [56, 57]. The phase transition from a superfluid to a Mott insulator was observed with time-of-flight imaging [57], and the renormalization of the hopping by a Bessel function was detected by measuring the expansion rate of the cloud when the magnetic trapping is turned off [56]. It was noticed that higher-order hopping terms become important to understand the experimental data near the vanishing of the Bessel functions [58].
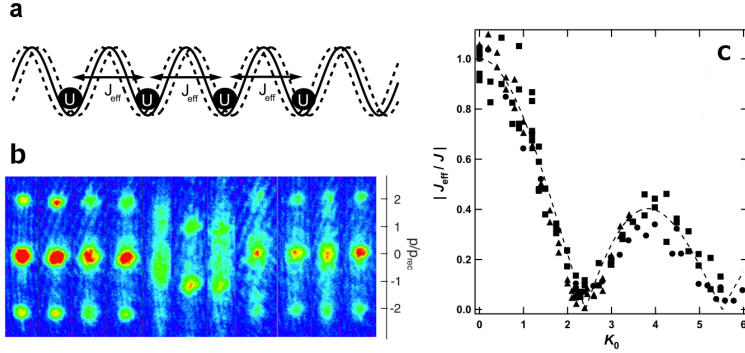
FIGURE 1.3: Dynamic superfluid - Mott insulator transition. (a) Lattice shaking in one dimension. The on-site interaction U is not affected by the shaking procedure, whereas the hopping J is renormalized to the effective value $J_{eff} \equiv J\mathcal{J}_0(K_0)$, where K_0 is the driving parameter (see text). (b) Time-of-flight pattern as a function of the driving parameter K_0 showing the dynamic loss of coherence. The figure also shows a condensation at π/a, corresponding to the sign inversion of the hopping. (c) Measured effective hopping as a function of the driving displaying the characteristic Bessel function behavior. The nodes are the points where the tunneling is coherently suppressed corresponding to the Mott insulating phase. Figures are adapted from Ref. [56, 57].

Considering the growing interest in the study of fermionic systems in optical lattices, a natural question is whether one can observe metal-insulator transitions dynamically generated. We show in Chapter 3 how that is possible, by considering a one-dimensional dimerized lattice at half-filling that is a band insulator (Peierls insulator) in the static case. A shaking protocol allows to close such a gap and obtain several metal-insulator transitions. One of these transitions leads to a non-standard metal with four Fermi points.

Driving forces have been investigated not only in the limit when the frequency is much larger than the other energy scales, but also at lower frequencies, in resonant regimes. For instance, the coupling of the lowest two bands by a resonant shaking has been used to generate a single-particle spectrum with two minima, which leads to very interesting physics [59, 60]. It is observed that atoms form spatially distinct ferromagnetic domains, in which each domain corresponds to condensation in one of the two minima [59], and the excitation spectrum displays a roton minimum [61], typical of superfluid helium [62].

In two dimensions the problem is even richer because one has the freedom to shake the lattice along different trajectories. In particular, an elliptical trajectory allows one to control the hopping parameters of a triangular lattice [63] and generate a model that leads to the simulation of frustrated classical magnetism [64]. In this system, the phase of the condensate in each site of the triangular lattice plays the role of classical spin degrees of freedom.

These last experiments are examples of the interest in using cold atoms to understand magnetic properties of matter. Coupling the electronic charge with an external electromagnetic field can lead to striking phenomena. The most prominent example is the quantization of the transverse conductivity described by the quantum Hall effect, which is the prototype of a class of phases of matter known as topological insulators [65–67]. In the presence of the lattice, beautiful effects can arise, such as the fractalization of the energy spectrum known as the Hofstadter butterfly [28], provided that the flux per plaquette is large enough. Such phenomena are, in principle, out of reach in optical lattices because atoms are neutral objects. However, it has also been possible to engineer artificial gauge potentials via shaking [68], among other possible methods[2] [71]. A synthetic engineering of the gauge potential can therefore overcome these technical limitations imposed by Nature. The first experiment to simulate a synthetic gauge potential using shaking was a one dimensional realization with bosons [68], but later two-dimensional experiments have been performed for Abelian [72] and also proposed for non-abelian fields [73].

Recently, the topological Haldane model has been realized by using resonant shaking [74] in an optical lattice with honeycomb geometry [75, 76]. This achievement made possible the observation of a topological transition in absence of a net magnetic field, as theoretically proposed long ago by Haldane [29]. At the same time, it is the first realization of a fermionic topological insulator in cold atoms and it leaves no doubts that a lot of room is available to explore topological states of matter in optical lattices. For instance, the quantum spin Hall effect predicted for graphene by Kane and Mele [77, 78] has never been observed because of the small spin-orbit coupling present in this material[3]. However, methods exist in cold atoms to engineer synthetic spin-orbit interactions and synthetic magnetic fields [71, 80], and probably not in the far future we will see a realization of this state of matter and many others [66].

All the accomplishments obtained through the use of shaking techniques described above are based on a manipulation of the single-particle physics. On the other hand, by modulating the interactions in time, one can reach a completely different regime in which particle correlations become highly non-trivial. In the bosonic case, it has been shown that one can generate non-standard Bose-Hubbard models [81], in which the hopping depends on the particle density [82]. The model is intrinsically strongly correlated and supports exotic states of matter such as pair superfluidity, namely a phase in which the condensate is made of pairs of particles (or holes).

This scheme has not been realized in experiments yet, but it turns out to be a very promising method to engineer classes of models otherwise out of

---

2 The simulation of the Hofstadter model with cold gases has been achieved very recently using Raman assisted tunneling [69, 70].

3 It has instead been observed in CdTe/HgTe quantum wells [79].

reach. We explore in Chapter 2 the consequences of modulating interactions in time for a fermionic gas in an optical lattice. The effective theory in this case is an extended Hubbard model with additional nearest-neighbor interactions that affect the hopping processes. The new interactions make possible the realization of an unconventional type of superconductivity, known as η-pairing superconductivity, introduced by Yang in 1989 for the Hubbard model [83]. Superconductivity originates from pairs of fermions with zero size and lattice momentum π/a, with a the lattice spacing. This state can be thought of as a condensate of molecules (as in the BEC side of the BEC-BCS crossover discussed before) but with molecules having a finite crystal momentum, as for the elusive FFLO superconductivity [84–86].

Contrary to the BEC limit of interacting fermions, in this case there is no need for strong attractive interactions because the existence of these eigenstates relies simply on the symmetries of the model. Unfortunately, in the Hubbard model they are never the ground state but rather metastable higher-energy states that can, in principle, be accessed after a quench scheme [87]. In the model that we propose to simulate, this is not the case because the ground state phase diagram in one dimension has η pairs in a certain regime of parameters where the model is exactly solvable [88]. However, the macroscopic degeneracy of the ground state prevents the observation of this exotic superconducting state. It is well possible that this degeneracy may be removed in favor of the η-superconductivity by moving away from the integrable point. Moreover, the richness of the model appears also in other peculiar features, such as the appearance of spin and charge density correlations that are incommensurate with the lattice spacing.

Recently, a new proposal, in which the lattice shaking is combined together with the modulation of interactions, has shown that one can extend the parameter phase space of the model to regimes where, for instance, triplet superconductivity appears [89]. Quantum simulation of these models can therefore reveal novel phases of matter. The effect of dimensionality and special geometries is yet to be explored, both theoretically and experimentally. On the experimental part, the quantum simulation of this strongly-correlated model could be also useful in the search for quantum magnetism. Indeed, we have noticed from quantum Monte Carlo simulations in one-dimensions (see Chapter 2) that the new interaction terms enhance antiferromagnetism in the regime of repulsive contact interactions. In three dimensions, where true long-range order can be realized, one might speculate that this effect can be used to push the Néel transition temperature to larger values and allow experiments in cold-atoms to finally glance at antiferromagnetism.

1.3   OUTLINE

In this thesis, we discuss quantum phase transitions in low-dimensional optical lattices, namely one- and two-dimensional lattices. The dimensional con-

finement is realized in experiments by suppressing the hopping in the extra dimensions through a deep potential barrier that prevents the atoms to tunnel across dimensions [6]. The dimensionality considerably affects the physical behavior of the system. For instance, in one dimension, the celebrated Fermiliquid theory does not describe the many-body behavior of a fermionic system. Using bosonization to single out the correct degrees of freedom, a new type of liquid, known as Luttinger liquid, emerges. In this type of liquid there are no single particle excitations, but instead collective behavior, and spin and charge degrees of freedom are decoupled [90].

In the first part of this thesis, we consider one-dimensional fermionic gases under the effect of time-dependent driving forces. In Chapter 2, we describe a proposal to realize non-standard Hubbard models that display correlated-hopping terms. The extra terms describe hopping processes that depend on the particle-density difference in neighboring sites. These processes emerge when the interactions are modulated through a time-dependent magnetic field that controls the interaction strength. The effective model is obtained in arbitrary spatial dimensions, but only in one-dimension it is known to be exactly solvable for specific values of the parameters [88]. Moreover, an SU(2) symmetry in the charge sector allows to construct non-trivial superconducting eigenstates (η states), discovered by Yang as excited states of the Hubbard model [83].

In the one-dimensional case at the integrable limit, the additional hopping terms lead to these eigenstates in the ground-state phase diagram [88]. The only drawback is the fact that the ground state is macroscopically degenerate. It is possible that by moving away in the parameter space from the integrable limit one may remove the degeneracy and single out η-pairs. This question is at the moment still open. However, we have investigated the charge and spin sectors in the case of half-filling (one fermion per site on average), and found that the density-dependent hopping terms generate spin and charge correlations that are incommensurate with the lattice spacing.

In Chapter 3, we study a one-dimensional bipartite optical lattice with fermionic atoms at half-filling. The lattice potential barriers have heights alternating in magnitude. As a consequence, the hopping amplitudes also alternate in magnitude and the elementary unit cell has two sites. This system is known to display Peierls dimerization at half-filling [91]: the fermions form dimers in neighboring sites that inhibit transport and open a gap in the spectrum, thus forming an insulator. A famous example is given by the Peierls distortion in polyacetylene [92].

We derive the single-particle spectrum describing the low-energy physics of the model, which reveals that the insulating behavior at half-filling is given by a gap at momemtum π/a between the two lowest bands. We then consider the effect of shaking on this system, and find that the renormalization of the hopping coefficients in the effective model can lead to several scenarios when tuning the driving parameter κ. The second band inverts and the

energy spectrum displays an indirect gap that closes at a critical value of κ. We demonstrate in this way that we can induce a phase transition from an insulating to a metallic state through shaking. Moreover, the fact that the band closing is realized through an indirect gap leads to an unconventional metallic phase with four Fermi points. After bosonization of the model, we obtain a qualitative picture of the effect of interactions on the gap opening.

The second part of this thesis describes bosonic systems in two-dimensional optical lattices. In Chapter 4, we consider a square optical lattice with alternating deep-shallow wells arranged in a checkerboard pattern. This lattice is realized in the experimental laboratory of Prof. Hemmerich in Hamburg. The relative depth of neighboring wells can be tuned with a high degree of control and it has been used to achieve Bose-Einstein condensation in excited bands [34, 93]. In the experiment, the *visibility* is extracted from the time-of-flight imaging to quantify the phase coherence of the bosonic gas [94]. The observation that a modest detuning can destroy the phase coherence in the trapped gas is object of a detailed theoretical investigation.

We develop a mean-field theory and determine the phase diagram of this model. The detuning between neighboring wells is accounted for by introducing a staggered chemical potential. Mott insulating phases with integer (but non uniform) density arise. We interpret the experimental data by assuming that at large detuning, only the deeper wells are populated and form an imbalanced Mott insulator with empty shallow wells and integer density on the deeper wells. We support this hypothesis by large-scale calculations using a variational mean-field approach for the wave function, the Gutzwiller ansatz. Taking into account the parameters of the experiment (e.g. the trapping potential), we compute the condensed fraction and the density profiles. We find an excellent agreement between the loss of coherence in the experiment and the vanishing of the population of the shallower wells, which corresponds to the localization of the atoms in the deeper wells and the formation of the Mott insulator. We also develop a perturbative theory to compare directly with the measured visibility data at large detuning.

In Chapter 5, we investigate a system of bosons in the Lieb lattice, which is the lattice geometry of the Cu-O plane in cuprates [26]. We consider configurations of the optical potential where s and p orbitals sitting on neighboring wells become resonant and hybridize, which can be achieved by tuning the relative depth of the neighboring wells. The interest in this problem comes from the possibility to realize time-reversal broken phases, usually known as Varma phases [95], which have been proposed to explain the pseudogap regime of cuprate superconductors. Time-reversal symmetry breaking involves the appearance of loop currents in the ground state of the system, driven by interactions.

One of the time-reversal symmetry-broken states discovered by Varma is topologically non-trivial [37, 96], and displays Quantum Anomalous Hall Effect. It can be considered to be the equivalent of the Haldane model on the

Lieb lattice. After the recent realization of the Haldane model for fermions in a honeycomb optical lattice [74], a bosonic analog exhibiting a chiral-superfluid phase and a Mott insulator phase with topological excitations has also been theoretically investigated [97]. Similarly to this case, we discuss how to realize bosonic analogs of the Varma phases. The recent achievement of Bose-Einstein condensation in higher bands of optical lattices [34, 93] makes possible to break time-reversal symmetry by two-body on-site interactions [31]. In the Lieb geometry, we show the conditions under which the symmetry breaking can lead to states with loop currents as in Varma's case. We study a four-band model with bosons realizing a condensate phase that does not break translational and inversion symmetry, but breaks mirror symmetry. In the fermionic case, this condition is sufficient to realize the anomalous Hall effect. Here, we will show that the lowest branch of the excitation spectrum has a non-vanishing Chern number and therefore supports topological excitations.

2

QUANTUM SIMULATION OF CORRELATED-HOPPING MODELS WITH FERMIONS

By using a modulated magnetic field in a Feshbach resonance for ultracold fermionic atoms in optical lattices, we show that it is possible to engineer a class of models usually referred to as correlated-hopping models. These models differ from the Hubbard model in exhibiting additional density-dependent interaction terms that affect the hopping processes. In addition to the spin-SU(2) symmetry, they also possess a charge-SU(2) symmetry, which opens the possibility of investigating the η-pairing mechanism for superconductivity introduced by Yang for the Hubbard model. We discuss the known solution of the model in 1D (where η states have been found in the degenerate manifold of the ground state) and show that, away from the integrable point, quantum Monte Carlo simulations at half filling (performed with the code of Charles Creffield) predict the emergence of a phase with coexisting incommensurate spin and charge order.

2.1 INTRODUCTION.

The use of ultracold atoms in optical lattices as condensed matter simulators has brought a major advance in physics in the last decade. Both bosonic [16, 18] and fermionic [24, 47] Hubbard models have been theoretically and experimentally investigated, and the simulation of artificial gauge fields [71, 98] and Quantum Hall physics [69, 70, 99] are some of the many phenomena that this active field is unveiling [6, 15, 100].

The realization of the fermionic Hubbard model opens the possibility of using quantum simulators to treat strongly-correlated fermionic systems, with the ultimate goal of understanding high-T_c superconductivity. While it is more challenging to cool fermionic systems than bosonic ones, state-of-the-art techniques have recently allowed fermionic atoms to be cooled sufficiently to reach the regime where quantum magnetism manifests [101].

A particular interest with ultracold gases is the use of time-dependent driving potentials. Using this technique, it has been possible to observe the transition from a Mott-insulator to a superfluid phase in the Bose-Hubbard model by a dynamical suppression of tunneling [54–56], as well as the simulation of frustrated classical magnetism [63, 64], and schemes for the realization of abelian [68] and non-abelian gauge fields [73]. More recently, a time-dependent modulation of Feshbach resonances has been proposed for a system of ultracold bosons, leading to a model with density-dependent hop-

ping coefficients, and exotic phenomena like pair superfluidity, and holon and doublon condensation [82].

In this chapter we extend this idea to fermionic atom systems. We show how a time-dependent manipulation of the interaction strength allows us to simulate an unusual class of "correlated-hopping models" [102], opening a window for the experimental observation of a novel and elusive form of superconductivity called η-superconductivity proposed by Yang in 1989. After discussing the model derivation and its symmetries, we focus on the 1D case at half-filling and perform quantum Monte Carlo (QMC) simulations for arbitrary values of the Hubbard interaction U and of the correlated-hopping parameter γ. Our results show that the model can exhibit an interesting phase, with coexisting incommensurate spin- and charge-density-wave order.

2.2 MODEL

We consider a system of (pseudo) spin-1/2 fermions in the lowest band of an optical lattice, and use a Feshbach resonance to modulate the interactions in time [82]. The Hamiltonian of the model reads

$$H = -J \sum_{\langle i,j \rangle, \sigma} (c_{i\sigma}^{\dagger} c_{j\sigma} + \text{h.c.}) + \bar{U}(t) \sum_{i} n_{i\uparrow} n_{i\downarrow} \tag{2.1}$$

where J is the fermion hopping amplitude between nearest-neighbor sites $\langle i,j \rangle$, and $\bar{U}(t) \equiv U + U_1 \cos(\omega t)$ is the time (t) dependent amplitude of the two fermion coupling at the same site.

According to Floquet theory [103], a time-periodic Hamiltonian $H(t) = H(t + T)$ is described by a set of Floquet modes $|u_n(t)\rangle$ which are time-periodic with the same period T, and a set of quasienergies E_n which are solutions of the eigenvalue equation

$$\mathfrak{H}(t)|u_n(t)\rangle = E_n|u_n(t)\rangle, \tag{2.2}$$

where $\mathfrak{H}(t) \equiv H(t) - i\hbar\partial_t$ is called the Floquet Hamiltonian. Solutions $|\psi_n(t)\rangle$ of the Schrödinger equation thus have the form $|\psi_n(t)\rangle = \exp(-iE_n t/\hbar)|u_n(t)\rangle$, and are unique up to a shift $E_n' = E_n + m\hbar\omega$ of the quasienergies by an integer multiple m of $\hbar\omega$, which thus gives a Brillouin-zone structure in quasienergy. The eigenvalue problem is defined in the composite Hilbert space [104] $\mathcal{H}' = \mathcal{H} \otimes \mathcal{H}_T$, where $\mathcal{H}$ is the standard Fock space and $\mathcal{H}_T$ is the Hilbert space of time-periodic functions. Let us define the following Floquet basis

$$|\{n_{j\sigma}\}, m\rangle = |\{n_{j\sigma}\}\rangle e^{-i\frac{U_1}{\hbar\omega}\sin(\omega t)\sum_j n_{j\uparrow}n_{j\downarrow}+im\omega t}, \tag{2.3}$$

where m labels the basis of the periodic functions, and $|\{n_{j\sigma}\}\rangle$ indexes the Fock states. The unitary transformation performed by the operator

$$\exp[-i(U_1/\hbar\omega)\sin(\omega t)\sum_j \hat{n}_{j\uparrow}\hat{n}_{j\downarrow}], \tag{2.4}$$

leads to the time-independent Floquet Hamiltonian. The main goal is now the calculation of the Floquet quasienergy spectrum, for which one needs the matrix elements $\langle\langle\{n_{j\sigma}\}, m|\mathfrak{H}(t)|\{n'_{j\sigma}\}, m'\rangle\rangle_T$. The symbol $\langle\langle\dots\rangle\rangle_T$ means that the ordinary scalar product defined in $\mathcal{H}$ has been time-averaged, defining the natural scalar product in $\mathcal{H}'$. In the high-frequency regime, $\hbar\omega \gg J, U$, states with different label m decouple, and the Floquet Hamiltonian matrix elements can be approximated by

$$\langle\langle\{n_{j\sigma}\}, m|\mathfrak{H}(t)|\{n'_{j\sigma}\}, m'\rangle\rangle_T \approx \delta_{m,m'} \left(\langle\{n_{j\sigma}\}|H_{\text{eff}}|\{n'_{j\sigma}\}\rangle + m\hbar\omega\delta_{n,n'}\right), \quad (2.5)$$

defining an effective static Hamiltonian

$$H_{\text{eff}} = -J \sum_{\langle i,j\rangle,\sigma} (c_{i\sigma}^\dagger c_{j\sigma} + \text{h.c.})\mathcal{J}_0\left[K(n_{i\bar\sigma} - n_{j\bar\sigma})\right] + U\sum_i n_{i\uparrow}n_{i\downarrow}. \quad (2.6)$$

The function $\mathcal{J}_0\left[K(n_{i\bar\sigma} - n_{j\bar\sigma})\right]$ is a Bessel function of the first kind. Its argument is the density operator difference between sites i and j relative to the spin $\bar\sigma$, where $\bar\sigma \equiv \downarrow (\uparrow)$ if $\sigma = \uparrow (\downarrow)$, and the parameter $K = U_1/\hbar\omega$.

We now perform a Taylor expansion of the Bessel function to rewrite the hopping term. Using the fact that the Bessel function is an even function, we can write its Taylor series (without necessarily specifying the coefficients of the expansion) as

$$\begin{aligned}
\mathcal{J}_0\left[K(n_{i\sigma} - n_{j\sigma})\right] &= \sum_{m=0}^\infty c_{2m}K^{2m}(n_{i\sigma} - n_{j\sigma})^{2m} \\
&= 1 + \left[\mathcal{J}_0(K) - 1\right](n_{i\sigma} + n_{j\sigma} - 2n_{i\sigma}n_{j\sigma}). \quad (2.7)
\end{aligned}$$

In deriving (2.7) we noted that the first term in the expansion with $m = 0$ is just 1, and have used the fermion identity $(n_{i\sigma} - n_{j\sigma})^{2m} = n_{i\sigma} + n_{j\sigma} - 2n_{i\sigma}n_{j\sigma}$ for arbitrary $m > 0$. This allows the Hamiltonian to be rewritten as

$$\begin{aligned}
H_{\text{eff}} &= -J \sum_{\langle i,j\rangle,\sigma} (c_{i\sigma}^\dagger c_{j\sigma} + \text{h.c.})\left\{1 - X(n_{i\bar\sigma} + n_{j\bar\sigma} - 2n_{i\bar\sigma}n_{j\bar\sigma})\right\} + U\sum_i n_{i\uparrow}n_{i\downarrow} \\
&\equiv H_J + H_U, \quad (2.8)
\end{aligned}$$

where we define $X = 1 - \mathcal{J}_0(K)$.

Eq. (2.8) can be easily recognized as the Hamiltonian of the Hubbard model with a correlated-hopping interaction [23, 102]. Similar interaction terms have appeared in a different context in cold atoms. If one considers a fermionic lattice system very close to the Feshbach resonance (which is not the regime studied here) in a static magnetic field, the behavior of the system cannot be described using the one-band Hubbard model because the on-site interaction energy exceeds the energy gap and higher bands play an important role. The physics in this regime can be described by an effective one-band model with density-dependent tunneling rates [105, 106].

Let us now discuss some limits of the Hamiltonian (2.8). In the absence of the driving ($U_1 = K = 0$), the Bessel function $\mathcal{J}_0(K) = 1$, and so the effective Hamiltonian (2.8) coincides with the Hamiltonian of the standard Hubbard model. Tuning the driving to $K = 2.4048..$, where $\mathcal{J}_0(K) = 0$ and $X = 1$, produces a Hamiltonian that coincides, in $d = 1$, with an exactly solvable limit of the correlated-hopping model (2.8), in which the strongly correlated dynamics of the electrons ensures separate conservation of the doubly occupied sites, empty sites, and singly occupied sites [88]. Interest in models with this particular type of fermionic dynamics was triggered by the concept of η-superconductivity proposed by C. N. Yang [83]. Motivated by the discovery of high-T_c superconductivity, Yang proposed a class of eigenstates of the Hubbard Hamiltonian which have the property of off-diagonal long-range order, which in turn implies the Meissner effect and flux quantization [107–109], i.e. superconductivity. These eigenstates are constructed in terms of operators $\eta_\pi^\dagger \equiv \sum_{\mathbf{r}} e^{-i\pi\cdot\mathbf{r}} c_{\mathbf{r}\uparrow}^\dagger c_{\mathbf{r}\downarrow}^\dagger$ that create pairs of electrons of zero size with momentum π. Yang also proved, however, that these states cannot be ground states of the Hubbard model with finite interaction; η-superconductivity is only realized in the Hubbard model at infinite on-site attraction in $d \geq 2$ [110]. Later, several generalizations of the Hubbard model showing η-superconductivity in the ground state (for a finite on-site interaction) were proposed [111–115].

The exactly solvable limit of the model (2.8) ($X = 1$ in $d = 1$) has been analyzed in detail by Arrachea and Aligia [88, 116]. Away from the exactly solvable limit, the model has been mainly studied in the weak-coupling limit ($X \ll J$) using the continuum limit bosonization treatment and finite-chain exact diagonalization studies [117, 118].

The infrared behaviour of the system (2.8), determined by the unusual correlated dynamics of fermions, is also strongly influenced by its high symmetry. The three generators of the spin-$\mathfrak{su}(2)$ algebra

$$S^+ = \sum_i c_{i\uparrow}^\dagger c_{i\downarrow}, \qquad S^- = \sum_i c_{i\downarrow}^\dagger c_{i\uparrow}, \qquad S^z = \frac{1}{2}\sum_i (n_{i\uparrow} - n_{i\downarrow}), \qquad (2.9)$$

commute with the Hamiltonian (2.8), which shows its spin-$SU(2)$ invariance.

To keep the discussion as general as possible, let us consider the case of bipartite lattices that we label A, B and introduce the index α_i that assumes values $\alpha_i = 1$ if $i \in A$ and $\alpha_i = -1$ if $i \in B$. In $d = 1$, in particular, one can choose A to be the even sites and B to be the odd sites and one simply has $\alpha_i = (-1)^i$. The electron-hole transformation $c_{i,\sigma} \to (-1)^{\alpha_i} c_{i,\sigma}^\dagger$ leaves the Hamiltonian unchanged and therefore the model is characterized by the electron-hole symmetry. Moreover, for the case of half-filling that we consider in this work, the model (2.8) possesses an additional $SU(2)$ symmetry. The transformation

$$c_{i\uparrow} \to c_{i\uparrow}, \qquad c_{i,\downarrow} \to (-1)^{\alpha_i} c_{i\downarrow}^\dagger, \qquad (2.10)$$

interchanges the charge and spin degrees of freedom and converts

$$H_{\text{eff}}(J, U, X) \rightarrow H_{\text{eff}}(J, -U, X). \tag{2.11}$$

In this case therefore, the charge sector is governed by the same $SU(2)$ symmetry as the spin sector, and the model has the $SU(2) \otimes SU(2)$ symmetry [88] with generators

$$\eta^+ = \sum_i (-1)^i c_{i\uparrow}^\dagger c_{i\downarrow}^\dagger, \quad \eta^- = \sum_i (-1)^i c_{i\downarrow} c_{i\uparrow}, \quad \eta^z = \frac{1}{2} \sum_i (1 - n_{i,\uparrow} - n_{i,\downarrow}). \tag{2.12}$$

Henceforth we will focus on the case $d = 1$ where an exact solution of the model exists both for $X = 0$ (Hubbard model) and $X = 1$, as previously mentioned. For the half-filled Hubbard model the $SU(2) \otimes SU(2)$ symmetry implies that the gapped charge and the gapless spin sectors for $U > 0$ are mapped by the transformation Eq. (2.10) into a gapped spin and a gapless charge sector for $U < 0$. Moreover, at $U < 0$ the model is characterized by the coexistence of CDW and singlet superconducting (SS) instabilities in the ground state [119].

Contrary to the on-site Hubbard interaction U, the X term remains invariant with respect to the transformation Eq. (2.10). For a given X, this immediately implies that,

- for $U = 0$ the properties of the charge and the spin sectors are identical;

- in the limit in which $U \gg X$ one expects that the large onsite repulsion would open a gap in the charge sector. Since for $U = 0$ the spin and charge degrees of freedom have the same properties because of the X symmetry, there must exist a critical value of the Hubbard coupling $U_c \geq 0$ corresponding to a crossover from the X dominated regime into a U dominated regime.

- The Luttinger-liquid parameters of the model characterizing the gapless charge (K_ρ) and spin (K_σ) degrees of freedom are $K_\rho = K_\sigma = 1$.

In the following sections, we will separately consider the exactly solvable cases ($X = 0$ and $X = 1$), and the physically relevant case of ($0 < X < 1$).

2.3   EXACTLY SOLVABLE CASE: $X = 1$, $d = 1$.

In this section, we mainly follow the route developed by Arrachea and Aligia [88]. At $X = 1$, the hopping of an electron with spin σ from a site i to a neighboring site j is only possible if there are no other particles on the sites ($n_{i\bar{\sigma}} = n_{j\bar{\sigma}} = 0$), or if both sites are occupied by electrons with opposite spin ($n_{i\bar{\sigma}} = n_{j\bar{\sigma}} = 1$). Thus, the only allowed hopping processes in this limit are

exchange processes of a singly occupied site with a holon (e.g. $|0,\uparrow\rangle \leftrightarrow |\uparrow,0\rangle$), and a doublon with a singly-occupied site (e.g. $|\uparrow\downarrow,\uparrow\rangle \leftrightarrow |\uparrow,\uparrow\downarrow\rangle$).

It is convenient to use the slave-particle formalism to rewrite the model in another basis, where all available processes are clearly displayed. One defines the mapping

$$|0\rangle_j \rightarrow h_j^\dagger|0\rangle \,, \quad |\sigma\rangle_j \rightarrow f_{j\sigma}^\dagger|0\rangle \,, \quad |\uparrow\downarrow\rangle_j \rightarrow d_j^\dagger|0\rangle \,, \tag{2.13}$$

where the slave particles must obey the constraint

$$h_i^\dagger h_i + d_i^\dagger d_i + \sum_\sigma f_{i\sigma}^\dagger f_{i\sigma} = 1 \tag{2.14}$$

at each lattice site. The constraint physically means that the slave particles act as hard-core particles, with an infinitely large on-site repulsion. The $h_i^\dagger$ and $d_i^\dagger$ bosonic operators describe, respectively, holons and doublons of the original system, while the fermionic operators $f_{i\sigma}^\dagger$ describe fermions with spin σ. Using this mapping, the Hamiltonian can be exactly rewritten in the form

$$H_{\text{eff}}^0 = -J \sum_{\langle i,j \rangle,\sigma} [f_{j\sigma}^\dagger f_{i,\sigma}(h_i^\dagger h_j - d_i^\dagger d_j) + \text{h.c.}] + U \sum_i d_i^\dagger d_i \,, \tag{2.15}$$

where one can immediately observe that the numbers N_h, N_d, $N_{f\uparrow}$ and $N_{f\downarrow}$ are *separately* conserved, because the Hamiltonian (2.15) can only interchange individual particles. This corresponds to a $U(1)$ symmetry for each slave particle sector. These particle numbers will therefore be used as quantum numbers to label the eigenstates. Notice that the U term plays the role of a chemical potential for doublons and that there is not, in general, a free part of the Hamiltonian for the slave particles. We stress the sign difference in the exchange process between doublons and holons in Eq. (2.15). The additional minus sign for the doublons is responsible for the η-symmetry with momentum π described by the operators in Eq. (2.12). While the restricted dynamics of hopping processes expressed in the Hamiltonian (2.15) is a very general property of the choice $X = 1$, it is only in $d = 1$ that there are additional symmetries (not discussed here) that allow the model to be solved exactly. The solution of this model in 1D for open boundary conditions was given in Ref. [88]. The physical properties of the 1D system described by Eq. (2.15) are very peculiar. When a doublon and a holon are neighbors, they act like hard-core bosons as previously mentioned, and cannot tunnel through each other because of the dimensionality of the system. Such a process would require the doublon and the holon to annihilate into two single fermions on the neighboring sites and then reform as a doublon and holon on exchanged sites. This process is forbidden at $X = 1$, but is possible for $X \neq 1$.

As a result, there are three regimes for the ground state phase diagram, as shown in Fig. 2.1: in region I there are only single fermions and holons (in region II, by particle-hole symmetry, only doublons and single fermions); the dashed line in Fig. 2.1 will be discussed later when we concentrate on
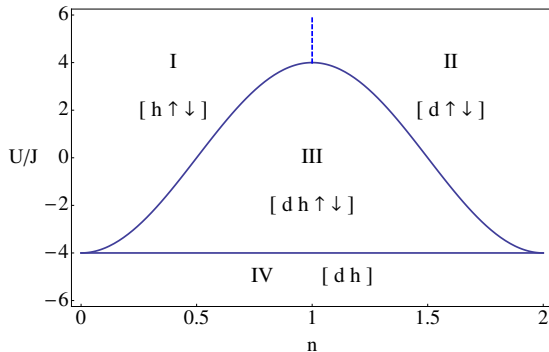
FIGURE 2.1: Phase diagram of model (2.8) obtained for $\mathcal{J}_0(K) = 0$ in $d = 1$ [88].

the regime $n = 1$; in region III all three types of particles are present, single fermions, holons and doublons; in region IV there are no single fermions but only doublons and holons. In all sectors the ground state is highly degenerate and, in region III and IV, one can show that also η-states belong to the ground state manifold. For further details, we refer the reader to Ref. [88].

In the following, we focus on the half-filled case $n = 1$, for which we perform QMC simulations in Par. 2.5. Since at $X = 1$ and half-filling the number of doublons N_d, holons $N_h = N_d$ and of the single occupied sites $N_f = N - 2N_d$ are integrals of motion, the delocalization energy of the system coincides with that of $2N_d$ hard-core bosons on a lattice of N sites. This equivalence allows one to write the density of energy at half-filling as

$$\epsilon(n_d) = -\frac{2J}{\pi} \sin\left(\pi - 2\pi n_d\right) + U\, n_d. \qquad (2.16)$$

For the half-filled case, the three regimes mentioned before become (see Fig. 2.1):

i. $U < -4J$. In this case, the ground state only contains doublons and holons ($n_d = n_h = 1/2$) that are frozen in the ground state since no dynamics is allowed in the absence of single fermions. The system is a doublon-holon insulator and its energy is $E_0 = NU/2$. The degeneracy of the ground state $\sim N$ diverges in the thermodynamic limit.

ii. $U > 4J$. In this case there are no doublons and holons in the ground state; all sites are singly occupied and particles cannot hop. The ground state has energy $E_0 = 0$ and is 2^N times degenerate, due to the freedom of distribution of spins of particles along the lattice. This state is thus a charge insulator.

iii. $-4J \leq U \leq 4J$. In this case, the ground state consists of a finite number of doublons and holons, separated by singly occupied sites to ensure their maximal delocalization along the lattice. It is clear that at $U = 0$ the minimum

of kinetic energy is reached at the densities $n_d = n_h = 0.25$. The doublon density now depends on the ratio U/J:

$$n_d = \frac{1}{2}\left[1 - \frac{1}{\pi}\arccos\left(-\frac{U}{4J}\right)\right].$$ (2.17)

2.4   AWAY FROM THE EXACT SOLUTION.

Deviation from the exactly solvable limit $X = 1$ produces the new term

$$2\gamma J \sum_{\langle i,j\rangle,\sigma}[f_{i\uparrow}^\dagger f_{j\downarrow}^\dagger(h_i d_j + h_j d_i) + \text{h.c.}],$$ (2.18)

where we have defined $\gamma \equiv \mathcal{J}_0(K) = 1 - X$. As these new terms allow doublons to convert into two single fermions on neighboring sites (and the reverse), the Hamiltonian no longer conserves the individual number of slave particles, and thus no exact solution is known. However, the η-symmetry *is* preserved and one expects that the enormous degeneracy of the ground state would again be removed. For $\gamma \simeq 1$, *i.e.* $|X| \ll 1$, the model can be treated using bosonization techniques and the phase diagram is known (also in the presence of nearest-neighbor interactions) [117] showing for $U < 0$ that superconducting correlations coexist with CDW. For the strongly-interacting case, exact diagonalization in 1D has been used [120, 121], for systems of up to 12-14 sites. Nakamura [121] presented a phase diagram at half and quarter filling (for $X = \pm 1/4$), and Arrachea *et al.* [120] have shown that superconducting correlations can appear for $n = 1$. Most recently, by using a double modulation, namely combining a modulation of interactions and also a shaking of the lattice, Greschner *et al.* have shown that the model discussed in this chapter can be generalized [89]. The density-dependent hopping terms (two-body and three-body interactions) display two independent coupling constants while here only the parameter X appears. The phase space is therefore enlarged. The results presented in their work have been obtained using density-matrix renormalization group (DMRG) techniques for the case $U = 0$. The half-filled case shows two possible phases: a bond-ordering wave and triplet superconductivity.

In the next section we will use the QMC technique to investigate the charge and spin ordering of the Hamiltonian given by Eq. (2.8) at general values of X and see how the results evolve between the two integrable cases ($X = 0$ and $X = 1$) for the specific case of half-filling.

2.5   QUANTUM MONTE CARLO METHOD

To treat the Hamiltonian (2.8), we employed a standard "world-line" algorithm [122] written for this work by Charles Creffield who produced the numerical data shown below. This is a finite-temperature method, operating

in the canonical ensemble, which is particularly well-adapted to treat lattice spin-charge Hamiltonians. In order to sample the zero temperature behavior of the system, it is important to set the inverse temperature of the system, $\beta = 1/kT$, to a sufficiently large value. By comparing the results for the ground state energy of the system with $\gamma = 1$ to the exact results for the Hubbard model available from the Bethe Ansatz, we established that a sufficiently low temperature was $\beta J = 48$, and accordingly we used this value in all the simulations. The Trotter decomposition of the imaginary time axis gives systematic errors which can be made arbitrarily small by increasing the number of timeslices, thereby reducing the imaginary-time discretization $\Delta\tau$. Our simulations demonstrated that the convergence of the results depended strongly on the value of γ. For the Hubbard model ($\gamma = 1$) a relatively coarse value of $\Delta\tau = 0.1$ was adequate. However, as γ was reduced, $\Delta\tau$ also had to be reduced further, the lowest values of $\gamma = 0.2$ requiring a discretization of $\Delta\tau \simeq 0.02$, with the simulation involving 2048 timeslices.

As well as the increased number of timeslices required, taking lower values of γ was also hindered by ergodic "sticking", in which local Monte Carlo (MC) updates are unable to evolve the system from local minima in energy. It was this factor that set the practical barrier on the lowest values of γ that we were able to simulate, and accordingly we only present results for $\gamma \geq 0.2$. In order to obtain results of high accuracy, typically 16,000 MC measurements would be made for each set of parameters, with each measurement being separated by the next by several MC sweeps in order to reduce autocorrelation between the data.

A particular advantage of the world-line method is that as it operates in the real-space occupation number basis, it is simple to evaluate operators diagonal in number operators, such as the onsite spin $\sigma_i = n_{i\uparrow} - n_{i\downarrow}$, the onsite charge $\rho_i = n_{i\uparrow} + n_{i\downarrow}$, the doublon number, and correlations between these operators. An especially useful quantity is the static structure function

$$S_\alpha(q) = \frac{1}{L} \sum_{m,n} e^{iq(m-n)} \langle \alpha_m \alpha_n - \alpha^2 \rangle \tag{2.19}$$

where m and n are integers labeling sites, $\alpha = \sigma$ (ρ) denotes spin (charge), and L is the number of lattice sites. As well as using the structure functions to investigate the type of spin and charge ordering present in the system, they can also be used to directly estimate the Luttinger-liquid parameters [123],

$$K_\alpha = \lim_{q\to 0} \frac{S_\alpha(q)}{\pi q} . \tag{2.20}$$

Thus, when the structure function is linear at low momentum, the Luttinger-liquid parameter is well-defined and is simply related to its slope. On the other hand, if the function is quadratic, this indicates that the Luttinger-liquid parameter is not well-defined and that this sector has a gap. In a uniform system, continuity requires that $S(q \to 0) = 0$. However, if phase separation

occurs $S(q)$ will have a peak at the smallest non-zero momentum, which will diverge as L increases. The regularity of $S(q)$ for small momentum thus also provides a first check that the system is not phase-separated.

2.5.1   *QMC results*

Doublon density –   In this section we will measure all energies in units of J. In Fig. 2.2 we show the doublon density as a function of γ for several different values of the Hubbard interaction U. In these simulations, γ was initially set to 1, and then reduced "quasi-statically" in steps of $\Delta\gamma = 0.01$. For each value of γ and U the ensemble was allowed to rethermalize and a number (typically 64) of MC measurements made. This technique permits a rapid scan to be made through the configuration space of the model, at the expense of only producing results of moderate accuracy.

From Fig. 2.2, we can first see that for $U = 0$, the doublon density does not depend on γ. This arises from the underlying symmetry of the Hamiltonian at half-filling. For negative U, we see that the doublon density increases as γ is reduced, interpolating smoothly between the results for the Hubbard model ($\gamma = 1$), and the exactly solvable case ($\gamma = 0$). The results for positive U mirror those for negative U, and can be related via

$$n_d(+|U|) = 0.5 - n_d(-|U|). \tag{2.21}$$

The validity of Eq. (2.21) is clear from the numerical results in Fig. 2.2. In addition, it can be easily proven, starting from Eq. (2.10) and recalling that $N_d = \sum_i n_{i\uparrow} n_{i\downarrow}$. Although $\gamma = 0$ is not directly accessible to our QMC simulation due to ergodic trapping, we can obtain estimates for the doublon density in this limit by extrapolating the data in Fig. 2.2. We present the results in Fig. 2.3. The agreement between the numerical results and the exact solution [88] is excellent, demonstrating the accuracy and reliability of the QMC simulation.

Correlation functions –   In Fig. 2.4(a) we show the static charge structure functions for strong repulsive interactions, $U = 4$. It can be clearly seen that for the Hubbard model ($\gamma = 1$) the charge sector is gapped, and that the structure function presents a weak peak at $k = 2k_F = \pi$. Reducing γ suppresses the structure function, and weakens this peak further. The spin structure function, shown in Fig. 2.4(b) shows a contrasting behavior. For the Hubbard model this function possesses a strong peak at $2k_F$, indicating the presence of strong antiferromagnetic ordering ($\uparrow, \downarrow, \uparrow, \downarrow$), and this peak is enhanced as γ is reduced. An infinitesimally small deviation of the coupling γ from zero opens channels for the exchange of spins on neighboring sites. This gives a preference for an alternating distribution of particles with opposite spins along the lattice, *i.e.* a spin-density-wave (SDW) structure. The spin excitations are gapless, and the spin-$SU(2)$ symmetry sets the Luttinger-liquid parameter $K_\sigma = 1$.
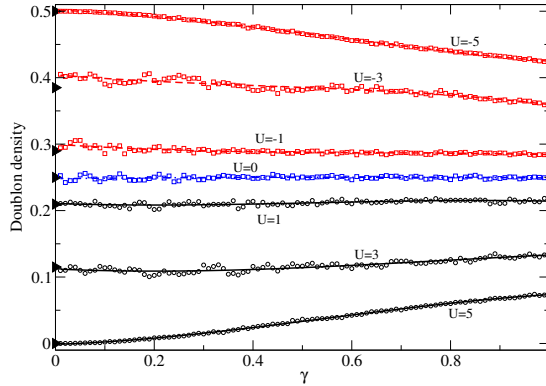
FIGURE 2.2: Doublon density measured as γ is quasi-statically reduced toward zero. For $U = 0$ (blue squares) the doublon density does not change, reflecting the symmetry of the model. For positive U (black circles) the density drops as γ is reduced; the reverse is the case for negative U (red squares). The data are symmetric about $n_d = 0.25$ (see Eq. (2.21)). The solid lines are cubic fits to the data to guide the eye. The arrows on the left indicate the analytic values obtained in Ref. [88] for the limit $\gamma = 0$. Parameters of the model: 32 sites, $\beta = 48$, $n_\uparrow = n_\downarrow$.
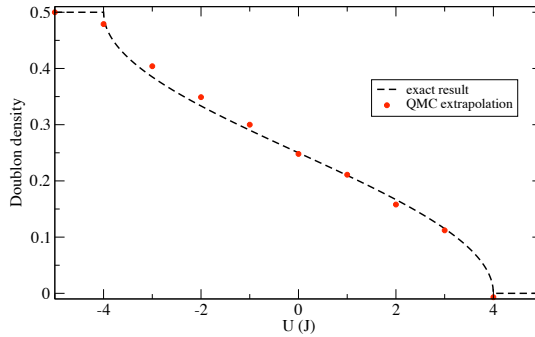

FIGURE 2.3: Comparison of the analytic results for the doublon density for $\gamma = 0$ with the results obtained by extrapolating the data shown in Fig. 2.2. The agreement is seen to be excellent.
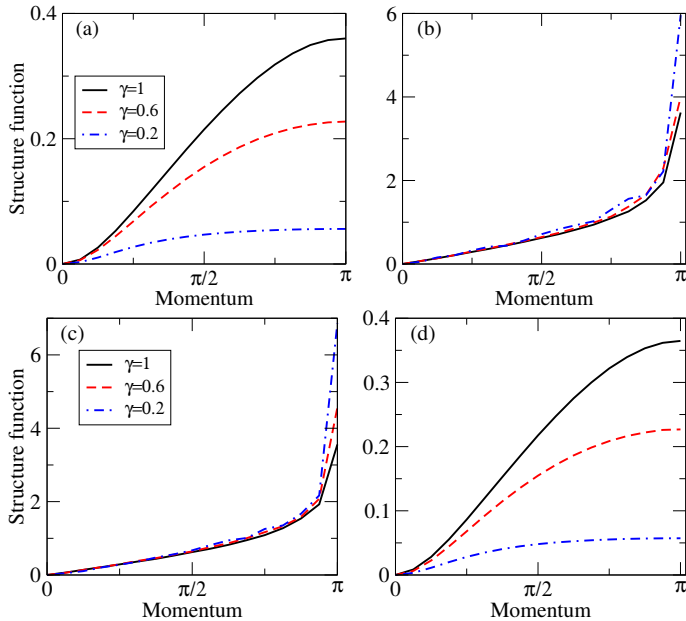
FIGURE 2.4: (a) Charge structure function for the half-filled model with $U = 4$. For $\gamma = 1$ there is a weak peak at $k = \pi$; as γ is reduced this peak is suppressed. (b) Spin structure function. For $\gamma = 1$ there is a strong peak at $k = \pi$ indicating strong antiferromagnetic ordering. This peak is enhanced as γ is reduced. (c) As above, but for $U = -4$. (d) As above, but for $U = -4$. The effect of changing the sign of U is to interchange the spin and charge degrees of freedom. Momentum is measured in units of the inverse lattice spacing.

Below these plots we show the corresponding structure functions for attractive interaction $U = -4$. It can be clearly seen that changing the sign of U simply has the effect of interchanging the spin and charge degrees of freedom, as noted in Par. 2.2. In this case we see that reducing γ now has the effect of suppressing the spin dynamics, while enhancing the staggered charge order (d, h, d, h). Similarly to before, deviation from the exact solution for $\gamma = 0$ opens channels for an alternating distribution of doublons and holons along the lattice i.e. a charge-density-wave (CDW) structure. Now the spin degrees of freedom are gapped, the charge excitations are gapless, and due to the charge-$SU(2)$ symmetry, the Luttinger-liquid parameter $K_\rho = 1$.

Results for $U = -2$ are given in Fig. 2.5. Looking first at the charge structure function, the result for the Hubbard model looks similar to that seen previously for $U = -4$. As γ is reduced, however, a new behavior emerges. When γ is reduced below 0.6, the charge structure function forms a peak at an *incommensurate* momentum, indicating the formation of an incommensurate CDW. At the same time an incommensurate SDW forms in the spin sector, at
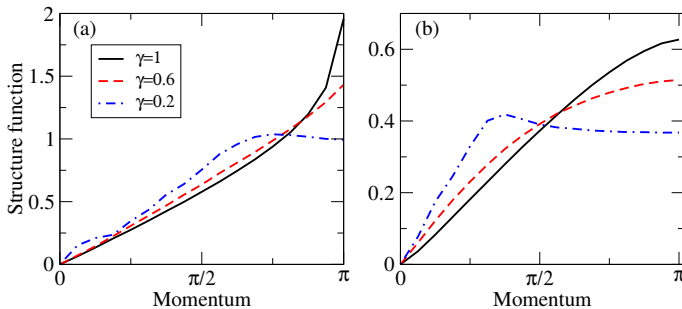
FIGURE 2.5: (a) Charge structure function for $U = -2$. As γ is reduced below 0.6, the system forms an incommensurate CDW. (b) Spin structure function for $U = -2$. For low γ the system also forms an incommensurate SDW. Momentum is measured in units of the inverse lattice spacing.

a smaller value of momentum. This incommensurate ordering is reminiscent of the behavior known for stripes in the 2D conventional Hubbard model upon doping [124].

The incommensurate order occurs generally for low values of γ for $|U| < 4$ (region III of the phase diagram Fig. 2.1). Reducing $|U|$ further to $U = 0$ shows the effect of γ on a non-interacting system. For $\gamma = 1$ the system consists of free fermions, and as can be seen in Fig. 2.6 the charge and spin correlators are identical to each other and are featureless. At $\gamma = 0.6$ the dynamics of the system is again slightly suppressed, but at a $\gamma = 0.2$ the system again manifests incommensurate charge and spin order, with the structure functions peaking at $k = k_F$.

Let us try to understand how these results connect to the exact solution for $|U| \leq 4$. In this case the ground state consists of a finite number of doublons and holons, separated by singly occupied sites to ensure their maximal delocalization along the lattice. Thus, in this sector a rather special ordering, characterized by coexistence of CDW and SDW order on different lattice sites, is possible. For a more detailed description let us consider few particular cases.

Let us start from the $U = 0$ case, where $n_d = 0.25$. The ground state configuration at $X \simeq 1$ consists of an alternating distribution of doublons and holons, separated by single occupied sites with alternating spins on these sites. A possible configuration would be

$$(d \uparrow h \downarrow d \uparrow h \downarrow d \uparrow h \downarrow \,...)$$

showing the coexistence of period-4 charge and spin density modulations, as observed in Fig. 2.6.

At $U = -2$, where $n_d = 0.3(3)$, a possible configuration would be

$$(d \uparrow h \, d \downarrow h \, d \uparrow h \, d \downarrow h \,...)$$
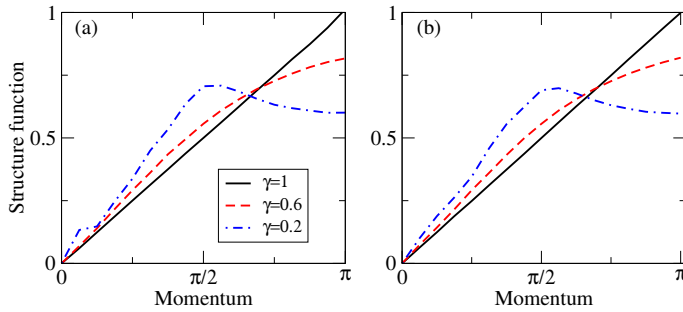
FIGURE 2.6: (a) Charge structure function for $U = 0$. (b) Spin structure function for $U = 0$. For the non-interacting case the charge and spin degrees of freedom behave identically. At $\gamma = 1$ they show no structure (free fermions), but form incommensurate ordered phases for low γ. Momentum is measured in units of the inverse lattice spacing.

showing the coexistence of a period-3 charge modulation with a period-6 spin density modulation.

For other values of U, the number of doublons (and singly occupied sites) will be in general incommensurate. The structure of the coexisting charge and spin density waves must reflect this incommensurability, and will consequently be much more complicated.

For $0 < U < 4$, the behavior is the same as for $-4 < U < 0$, but with the spin and charge structure functions inverted. For instance, for $U = 2$ Fig. 2.5(a) would hold for spin and Fig. 2.5(b) would hold for charge, indicating an incommensurate spin-charge-density wave.

To ensure that the behavior we have seen is not an artifact of the finite system size, we have repeated our simulations for $U = 2.5$ for lattice sizes between 16 sites and 100 sites. We show the results in Fig. 2.7, and it is clear that the incommensurate structure seen in the structure functions hardly alters as the lattice size is increased. We can thus be confident that our standard size of $L = 32$ is sufficiently large for finite size effects to be neglected.

From the simulation we have also evaluated the Luttinger parameter K_ρ, using Eq. (2.20). As shown in Fig. 2.8, for $\gamma = 1$ K_ρ is equal to 1 for negative values of U (the 10% deviation is within the numerical error of our calculation), indicating the coexistence of superconductivity and charge wave ordering. As U becomes positive, a gap opens in the charge sector and K_ρ can no longer strictly be defined for the half-filled case. This is marked in Fig. 2.8 by the calculated value of this parameter abruptly dropping, as the charge structure function is no longer linear at small momentum. For $\gamma = 0.6$ a similar behavior is seen, except that the opening of the charge gap now occurs at a higher value of $U \simeq 1.8$. As γ is reduced further this trend continues, and for
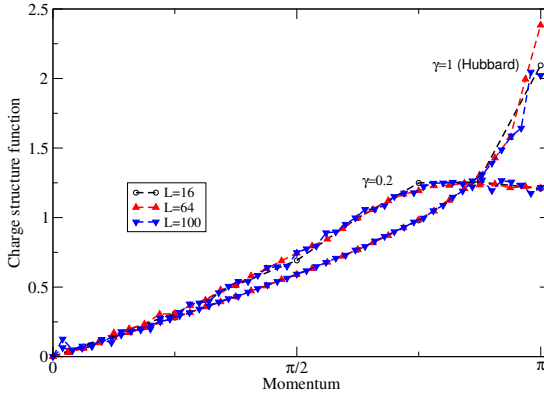
FIGURE 2.7: The charge structure function for $U = -2.5$ as the lattice size is increased. The results show little dependence on lattice size, indicating that finite size effects are not important in our analysis. Momentum is measured in units of the inverse lattice spacing.
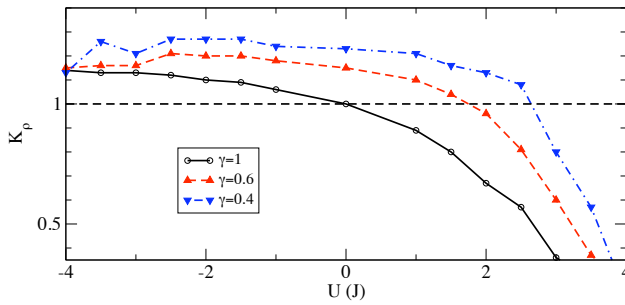

FIGURE 2.8: Luttinger-liquid parameter K_ρ. For $\gamma = 1$, K_ρ is approximately equal to 1 for negative U, then drops as U becomes positive, signaling the opening of the charge gap. As γ is decreased, this drop occurs at larger values of U. The dashed line is a guide to the eye, to assist in estimating where the drop occurs.

$\gamma = 0.2$ we find that the critical U has a value of approximately 3.5, in good agreement with the estimate given in Ref. [88].

Before closing this section, we want to mention that a model, similar to the one presented here, but without the three-body term, has been been previously investigated [125, 126]. For this so-called Hirsch model (see for instance Ref. [127]), the strongly-correlated regime at half-filling exhibits an incommensurate (singlet) superconducting phase that show many similarities with our findings. This phase has been captured using DMRG techniques, while bosonization and RG were unable to describe the transition [128].
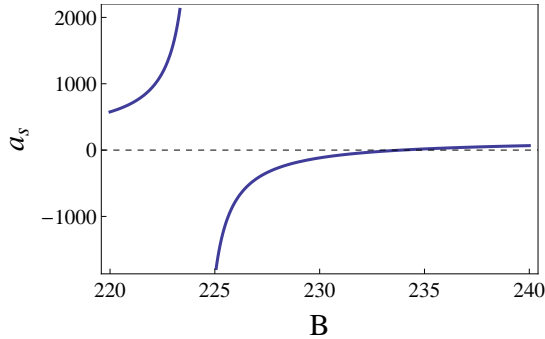
FIGURE 2.9: Feshbach resonance for ^{40}K with parameters $B_0(G) = 224.2$, $\Delta(G) = 9.7$ and $a_{bg}/a_0 = 174$.

At present, the phase diagram of the model (2.8) in 1D is only partially known; however, as we will show in the last section, the model can describe realistic experiments using cold atoms. This represents a good challenge for quantum simulations, as well as for new numerical calculations, as performed for instance in Ref. [89]. A fascinating possibility would be an emerging superconducting phase, with tightly bound pairs of momentum π, realizing the η-superconductivity first proposed by Yang [83].

2.6 EXPERIMENTAL PARAMETERS.

For the experimental realization of this model (in 1D for instance) we consider an optical lattice $V(\mathbf{r}) = V_x \sin^2(kx) + V_y \sin^2(ky) + V_z \sin^2(kz)$ with $k = 2\pi/\lambda$ generated by a laser with wavelength $\lambda = 1064$nm; we take the limit $V_x, V_y \gg V_z$ to allow dynamics only in one dimension. We studied the Feshbach resonance for ^{40}K at $B_0(G) = 224.2$, characterized by a width $\Delta(G) = 9.7$ and a background scattering length $a_{bg}/a_B = 174$, where a_B denotes the Bohr radius [10]. The dependence of the scattering length a_s on the magnetic field B is given near resonance by (see Fig. 2.9)

$$a_s = a_{bg}\left(1 - \frac{\Delta}{B - B_0}\right). \tag{2.22}$$

We choose a time dependent magnetic field of the form $B(t) = B_m + B_1 \cos(\omega t)$ and consider $|B_1| \ll |B_m - B_0|$. Therefore, at first order in $B_1/(B_m - B_0)$ we can write

$$\begin{aligned} a_s &\simeq a_{bg}\left[1 - \frac{\Delta}{B_m - B_0}\left(1 - \frac{B_1 \cos(\omega t)}{B_m - B_0}\right)\right] \\ &\equiv a_0 + a_1 \cos(\omega t), \end{aligned} \tag{2.23}$$
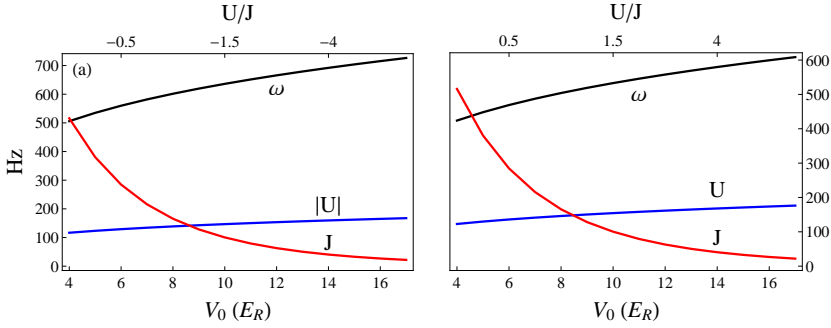
FIGURE 2.10: Comparison between frequency modulation ω of the magnetic field, hopping parameter J and Hubbard interaction U (all measured in Hz) at the zero of the Bessel function $\mathcal{J}_0(U_1/\hbar\omega)$ for ^{40}K close to a zero of a Feshbach resonance ($B_0(G) = 224.2$, $\Delta(G) = 9.7$ and $a_{bg}/a_0 = 174$). (a) In the attractive case $a_0 < 0$, we have chosen $B_m(G) = 233.5$ and $B_1(G) = 4$; (b) in the repulsive case $a_0 > 0$, we have chosen $B_m(G) = 234.36$ and $B_1(G) = 4$. The optical lattices parameters are $V_x = V_y = 25\,E_R$, $V_z = V_0$ and $\lambda = 1064$nm.

where we have defined $a_0 = a_{bg}[1 - \Delta/(B_m - B_0)]$ and $a_1 = -a_{bg}B_1\Delta/(B_m - B_0)^2$.

In Figs. 2.10(a) and (b), we plot the driving frequency values corresponding to the zero of the Bessel function $\mathcal{J}_0(U_1/\hbar\omega) = 0$ both in the attractive and repulsive case, respectively, in a particular range of parameters near the zero of the Feshbach resonance (so that we can reach the region of interest in the regime of strong coupling analyzed in this chapter) and compare with an estimate of U and J for the 1D case. We find that ω is in the sub-kilohertz regime $\omega \simeq 2\pi \times 500 - 600$Hz and we observe that such a choice of parameters fulfills the main approximations required from Floquet theory, *i.e.* $\omega \gg U$, J. Actually, in typical experiments [56] the kilohertz energy scale is far below the band gap and higher band contributions do not play a role, except for possible multiphoton processes. Moreover, one can see that the range where Floquet theory can be applied for this choice of parameters of the resonance allows us to explore the phase diagram in the main region of interest, where the correlated-hopping model should reveal interesting phenomena. Such a choice of parameters plotted in Fig. 2.10 can be considered as an example to show that the model described here can be realized in experiments; one would envisage that for different values or ranges of U/J, the optimal parameters will be chosen accordingly. We finally want to mention that to calculate the parameters U and J we have used the approximate formulas (given in terms of the recoil energy $E_R = \hbar^2(2\pi/\lambda)^2/2m$, with m denoting the atomic mass) [6]: $U/E_R = (2\pi/\lambda)a_s\sqrt{8/\pi}\,V_0^{1/4}V_{x,y}^{1/2}$ and $J/E_R = (4/\sqrt{\pi})\,V_0^{3/4}e^{-2\sqrt{V_0}}$, where we have introduced the potential depth $V_0 = V_z$ (assuming that the electron dynamics would be in the z direction),

and frozen the motion in the x and y directions taking $V_x = V_y = 25\,E_R$ such that we can consider one-dimensional effective systems.

2.7 CONCLUSIONS.

We have discussed a scheme for cold atoms to engineer an extension of the Hubbard model that includes nearest-neighbor correlations affecting the hopping processes for fermions in optical lattices. After imposing a time-dependent driving of the s-wave scattering length between atoms in two different hyperfine states (that we have modeled as a pseudo-spin 1/2 system assuming no spin imbalance), we have shown within Floquet theory that the system can be described by an effective Hamiltonian with correlated-hopping interactions. The model has an additional SU(2) symmetry, with respect to the usual spin-SU(2) symmetry of the Hubbard model, generated by the algebra of η operators. This fact opens the possibility of searching for a ground state characterized by the exotic η-pairing superconductivity proposed by Yang in 1989 as a metastable state of the Hubbard model. This model, for the particular case of $d = 1$ on which we focused in this work, has two integrable points as a function of the driving parameter X that tunes the coupling of the correlated-hopping interactions: one is the Hubbard model ($X = 0$) and the other one ($X = 1$) has been analyzed in Ref. [88] by Arrachea and Aligia. The integrable point discussed by them manifests η-pairing in the ground state. Unfortunately, the huge degeneracy of the ground state prevents the system from showing superconducting properties, like anomalous flux quantization [116]. Exploring this region of the phase diagram that extends over the whole filling axis (see Fig. 2.1, region III) can be quite challenging in general for experiments. Indeed, as discussed for the case of the supersymmetric model by Essler *et al.* [112], it is possible to draw the phase diagram of Fig. 2.1 using the grand canonical ensemble. Such representation is of fundamental importance because in typical cold atom systems the presence of the trap can be interpreted, in the local density approximation (LDA), as a local chemical potential such that different shells with different quantum phases would appear radially in the trapped gas. The consequence of this, however, is that the central "dome" (region III) would correspond to a single value of chemical potential $\mu = 0$, thus rendering its observation problematic.

We have focused on the study of the half-filled model, away from the integrable point $X = 1$, using the "world-line" algorithm to perform QMC simulations . We have explored the parameter space in the strong coupling regime, where known analytical methods like bosonization and RG techniques cannot be employed. We have found that an incommensurate order in the charge and the spin sector sets in for the ratio $|U/J| < 4$, where U and J are respectively the on-site interaction and the bare hopping amplitude. We have observed that the two kinds of orders manifests as a peak in the spin and charge structure functions at incommensurate (distinct) momenta. The two

orders exchange their behavior when $U \to -U$ as expected from the symmetries of the model. In particular, for the case $U = 0$ a peak appears exactly at $k_F = \pi/2$ in both structure functions.

A further investigation of the model would require the measurement of other types of orders, to see, for instance, what role is played by superconductivity when the incommensurate spin and charge order appears. These types of correlations cannot be computed with the QMC algorithm used in this work since it is based on a number-conserving representation of the fermionic Hilbert space; one would thus need to employ other techniques to look, for instance, at the 2-body density matrix. Moreover, deviations from half-filling are still to be studied in the strong coupling regime and the phase diagram has not been established yet, except for the case $X = 1/4$ [121] and $U = 0$ [89].

In dimensions $d \geq 2$, the physics of the model is almost all to be explored; weak-coupling Hartree-Fock calculations in $d = 2$ show that the model can exhibit d-wave superconductivity [129]. A very interesting possibility, deferred to further studies, would be the appearance of η-superconductivity in the ground state.

METAL-INSULATOR TRANSITIONS DRIVEN BY SHAKING

We theoretically investigate the behavior of a system of fermionic atoms loaded in a bipartite one-dimensional optical lattice that is under the action of an external time-periodic driving force. By using Floquet theory, an effective model is derived. The bare hopping coefficients are renormalized by zeroth order Bessel functions of the first kind with different arguments for the nearest-neighbor and next-nearest neighbor hopping. The insulating behavior characterizing the system at half-filling in the absence of driving is dynamically suppressed and for particular values of the driving parameter the system becomes either a standard metal or an unconventional metal with four Fermi points. The existence of the four Fermi-point metal relies on the fact that, as a consequence of the shaking procedure, the next-nearest-neighbor hopping coefficients become significant compared to the nearest-neighbor ones. We use the bosonization technique to investigate the effect of on-site Hubbard interactions on the four Fermi-point metal-insulator phase transition. Attractive interactions are expected to enlarge the regime of parameters where the unconventional metallic phase arises, whereas repulsive interactions reduce it. This metallic phase is known to be a Luther-Emery liquid (spin gapped metal) for both, repulsive and attractive interactions, contrarily to the usual Hubbard model which exhibits a Mott insulator phase for repulsive interactions. Ultracold fermions in driven one-dimensional bipartite optical lattices provide an interesting platform for the realization of this long studied four Fermi-point unconventional metal.

3.1 INTRODUCTION

In recent years, cold atoms in optical lattices have become a powerful tool for investigating quantum phase transitions and realizing new and unconventional states of matter [6, 15, 100]. Since the observation of the superfluid-Mott insulator (SF-MI) phase transition for the Bose-Hubbard model [16, 18], many models have been experimentally engineered and investigated with unprecedented control.

By introducing external time-dependent driving forces that dynamically suppress the hopping, namely by shaking the optical lattice [56, 130], the SF-MI phase transition has been achieved without the need of controlling the lattice potential depth [54, 55, 57]. Since then, the shaking technique has been employed in many other experimental setups to realize, for instance, classical magnetism [64], artificial gauge potentials in one [68] and two [72] dimen-

sions, extended ferromagnetic domains [131], to control photon-assisted [132] and correlated tunneling [133, 134], to generate super Bloch oscillations [135] and has inspired theoretical works that proposed schemes to realize doublon-holon condensates [82], non-Abelian gauge fields [73], density-dependent gauge potentials [136], and correlated-hopping models [137].

The high freedom available for generating optical lattices has also allowed one to play with the lattice geometry and to create bipartite lattices, which turned out to be a key ingredient to achieve higher-band condensates [35, 36, 138], coherence control [139], density-wave dynamics [42], graphene-like physics [75, 76], and to measure the Zak phase characterizing topological Bloch bands [140].

In condensed-matter systems, the model of correlated electrons in bipartite lattices with staggered on-site potential, known as the ionic-Hubbard model, has been the subject of intensive studies during the last decades [141–149]. Initially, the ionic-Hubbard model was proposed to study organic mixed-stack charge-transfer crystals [141] and later it has been used to describe the ferro-electric transition in perovskite materials [142]. Intensive interest in the study of the low-dimensional versions of the ionic-Hubbard model was motivated by the extremely rich phase diagram of this model revealing, at half-filling, the possibility for the realization of the band-insulator to Mott-insulator quantum phase transition with increasing on-site Hubbard coupling, via the sequence of unconventional insulating and/or metallic phases [143–149].

A similar, but different mechanism for the realization of the band-insulating state in the one-dimensional half-filled electron system has been proposed by Peierls in the early 30s of the last century, via the alternation in magnitude of the nearest-neighbor hopping amplitude [91]. However, contrary to the ionic-Hubbard model, the behavior of the Peierls model smoothly depends on the on-site Hubbard coupling and no quantum phase transitions are realized. Instead, one just finds a crossover from a band-insulating phase at weak coupling into the spin-Peierls phase at strong repulsive interaction [150–152]. Therefore, less attention has been given to the search of quantum phase transitions in the Peierls insulator.

In this chapter, we study a driven 1D bipartite optical lattice half-filled with fermionic atoms and show that it is possible to drive (band)-insulator to metal transitions by tuning the shaking parameter. Due to the presence of the $A - B$ sublattice characterized by nearest-neighbor hopping coefficients alternating in magnitude, the half-filled system is a Peierls insulator. Shaking the optical lattice at high-frequencies leads to a model with effective hopping parameters, where the bare value is multiplied by a Bessel function. Since the relevant hopping parameters are renormalized in different ways, the system realizes a large variety of quantum phases, such as several metals characterized by a Fermi surface with four Fermi points or two Fermi points, and Peierls insulators with direct or indirect gaps.

3.2 OPTICAL POTENTIAL

We consider a one-dimensional optical potential of the form [153]

$$V(x) = V_1 \sin^2(qx) + V_2 \sin^2(2qx + \pi/2), \tag{3.1}$$

where $V_1, V_2 > 0$ and $q = \pi/d$, so that the periodicity of the lattice is d. In Fig. 3.1 we show the shape of such a potential for the choice of parameters $V_1 = 1E_{\text{rec}}$ and $V_2 = 7E_{\text{rec}}$, where $E_{\text{rec}} = \hbar^2 \pi^2/2Md^2$ denotes the recoil energy of atoms with mass M. The choice of the phase $\pi/2$ in the optical potential ensures that the bottom of all the wells is at the same depth, while the maxima alternate in height, thus leading to a bipartite lattice. Therefore, the unit cell of the corresponding optical lattice contains two sites, that we denote by A and B. We introduce here a notation that will become useful later: since the spacing between neighboring wells is not constant, but is alternating in length, we call the shortest distance $2al$ and the largest distance $d - 2al$, where $a \equiv d/2$ is now the average distance between two neighboring wells.

The aim of this work is to study the optical potential (3.1) subject to an external driving that periodically shifts the full potential according to

$$x \rightarrow x + x_0 \cos(\omega \tau), \tag{3.2}$$

with x_0 the maximum displacement and ω the frequency of the shaking. Recently, such a problem has been studied for a single atom loaded in the lattice, focusing in particular on the phenomenon of dynamical localization and its consequences on the superfluid-Mott insulator transition for an interacting gas of bosons [154]. In our work, we will instead discuss the effect of the driving term on a system of fermions, for which the presence of a Fermi surface has dramatic consequences already at the non-interacting level. This time-periodic shift of the potential can be realized, for instance, by frequency modulation of the laser beams creating the optical potential [56].

We now focus our attention on the potential (3.1) in the absence of driving, and let the study of the time-dependent problem to the second part of the present work. To calculate the band structure, it is useful to rewrite the potential as

$$V(x) = -\frac{V_1}{4} \left(e^{i2qx} + e^{-i2qx} \right) + \frac{V_2}{4} \left(e^{i4qx} + e^{-i4qx} \right), \tag{3.3}$$

where we have dropped an overall constant. The Schrödinger equation for an atom in a space-periodic potential reads

$$\left[-\frac{\hbar^2}{2M} \frac{\partial^2}{\partial x^2} + V(x) \right] \psi_{nk}(x) = \epsilon_n(k) \psi_{nk}(x), \tag{3.4}$$

with $\psi_{nk}(x) = e^{ikx} u_{nk}(x)$, where n is the band index, k is quasi-momentum, and u_{nk} are Bloch functions. Since the Bloch functions are periodic with the
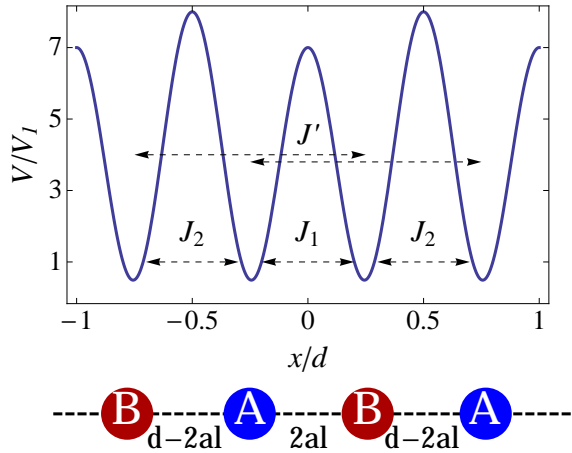
FIGURE 3.1: Potential profile for $V_1 = 1E_{rec}$ and $V_2 = 7E_{rec}$. The main hopping coefficients used in the tight-binding model are also displayed (see text). For this potential profile, one finds $l = 0.2443$.

periodicity d of the lattice, we can perform a Fourier expansion and finally express the wave function as

$$\psi_{kn}(x) = \sum_m c_m^{(n)} e^{i(k+\frac{2\pi}{d}m)x},$$ (3.5)

where $m \in \mathbb{Z}$. By substituting Eq. (3.3) and Eq. (3.5) in Eq. (3.4), one can cast the Schrödinger equation into the form

$$4(k+m)^2 c_m^{(n)} + \left[-\frac{V_1}{4} \left(c_{m-1}^{(n)} + c_{m+1}^{(n)} \right) + \frac{V_2}{4} \left(c_{m-2}^{(n)} + c_{m+2}^{(n)} \right) \right] = \epsilon_n(k) c_m^{(n)},$$ (3.6)

where we renamed $ka/\pi \to k$, so that $-1/2 \le k \le 1/2$ and V_1, V_2, and ϵ_n are now expressed in units of E_{rec}. This equation defines a linear system for the unknown coefficients $c_m^{(n)}$ that can be easily solved with standard libraries.

We have truncated the Fourier expansion retaining m from -5 to 5, corresponding to 11 bands. The result for $V_1 = 1E_{rec}$ and $V_2 = 7E_{rec}$ is shown in Fig. 3.2.

3.3 TIGHT-BINDING MODEL

The single-particle Hamiltonian in second quantization reads

$$H_0 = \int dx\, \psi^\dagger(x) \left[-\frac{\hbar^2}{2M} \frac{\partial^2}{\partial x^2} + V(x) \right] \psi(x).$$ (3.7)
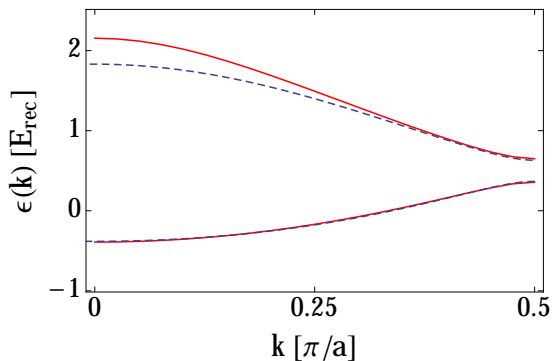
FIGURE 3.2: Lowest two bands for $V_1 = 1E_{rec}$ and $V_2 = 7E_{rec}$. The red solid line is the result from the numerical solution of the Schrödinger equation; the blue dashed line is the tight-binding spectrum, where the parameters have been chosen by fitting the lowest band.

We restrict ourselves to a zero-temperature analysis and thus we retain the lowest two bands only, which is a reasonable assumption for sufficiently deep optical lattices, i.e. when $\max\{V_1, V_2\} \gtrsim 5\, E_{rec}$, and when the interactions are weak compared to the energy separation between these two bands and higher ones. One can introduce a set of maximally-localized Wannier functions [155] centered around the minimum of each well which form a complete single-particle orthonormal basis (further details of how to construct these single-particle states for a bipartite lattice are given in Refs. [153, 156]). Thus, we can expand the field operators (retaining only the lowest bands states) as

$$\psi(x) = \sum_{j\nu} a_{j\nu} \mathcal{W}_0(x - R_{j\nu}), \tag{3.8}$$

where $a_{j\nu}^{(\dagger)}$ destroys (creates) an atom in the Wannier state $\mathcal{W}_0(x - R_{j\nu})$ localized at the minimum $\nu = A, B$ in the cell j. From now on, we will suppress the double-index notation to identify the lattice sites, in favor of a single-index notation and use the convention that A sites are mapped to even sites. The single-particle tight-binding Hamiltonian is therefore

$$H_0 = -J_1 \sum_j (a_{2j}^\dagger a_{2j+1} + \text{h.c.}) - J_2 \sum_j (a_{2j}^\dagger a_{2j-1} + \text{h.c.}) - J' \sum_j (a_j^\dagger a_{j+2} + \text{h.c.}) \tag{3.9}$$

The definition of the parameters of the tight-binding Hamiltonian can be written as

$$J_1 = -\int dx\, \mathcal{W}_0^*(x - R_{jA})\, \hat{H}_0\, \mathcal{W}_0(x - R_{jB}) \tag{3.10}$$

$$J_2 = -\int dx\, \mathcal{W}_0^*(x - R_{jA})\, \hat{H}_0\, \mathcal{W}_0(x - R_{(j-1)B}) \tag{3.11}$$

$$J' = -\int dx\, \mathcal{W}_0^*(x - R_{j\nu})\, \hat{H}_0\, \mathcal{W}_0(x - R_{(j+1)\nu}) \tag{3.12}$$

We dropped a term $\sum_j E_j n_j$ because it only leads to an energy shift, given that one can assume the on-site energies in each well to be equal, i.e. $E_A = E_B$ (the wells have the same depth and the same curvature). However, the on-site energy has been determined when fitting the bands (see Table 1). Moreover, because of the symmetries of the potential, we assumed the next-nearest-neighbor hopping $A \to A$ to be equal to $B \to B$ and we called it J'. The Hamiltonian can be diagonalized in momentum space, yielding the spectrum (in units where we take the lattice spacing $a = 1$)

$$\epsilon_\pm(k) = -2J' \cos 2k \pm \sqrt{\Delta(k)}, \tag{3.13}$$

where

$$\Delta(k) = J_1^2 + J_2^2 + 2J_1 J_2 \cos 2k. \tag{3.14}$$

We see that the spectrum is invariant under the following two transformations:

$$J_1 \to -J_1, \quad J_2 \to -J_2, \tag{3.15}$$

and

$$J_1 \to J_2, \quad J_2 \to J_1. \tag{3.16}$$

Moreover, one notices that the gap at $k = \pi/2$ is directly connected to the fact that $J_1 \neq J_2$. Indeed, were this not the case, i.e. $J_1 = J_2$, one would recover the monopartite limit and the gap would close.

The hopping coefficients of the tight-binding model have been estimated by fitting the lowest branch of the spectrum $\epsilon_-(k)$ in Eq. (3.13) to the numerical results from the band structure calculation. The results for the case $V_1 = 1E_{\mathrm{rec}}$ and $V_2 = 7E_{\mathrm{rec}}$ are summarized in Table 1 and the comparison with the exact band structure calculation is shown in Fig. 3.2. A more accurate estimate of these parameters would require the calculation of the Wannier functions or the use of the method described in Ref. [153], which is beyond the scope of this work.

Parameter	Fit
$E_{A,B}$	0.612
J_1	0.6195
J_2	0.4870
J'	-0.0564

TABLE 1: Fitting parameters of the tight-binding model for $V_1 = 1\,E_{rec}$ and $V_2 = 7\,E_{rec}$. All the parameters are given in units of recoil energy E_{rec}.

3.4 FLOQUET THEORY

Let us now turn to the time-dependent problem and consider a shaken optical potential according to $x \rightarrow x + x_0 \cos(\omega\tau)$. In the reference frame of the lattice, the single-particle Hamiltonian can thus be written as [54, 157]

$$H(\tau) = H_0 + W(\tau), \tag{3.17}$$

where the driven part is the dipole term

$$W(\tau) = x F_\omega \cos(\omega\tau), \qquad F_\omega = M x_0 \omega^2. \tag{3.18}$$

In second quantization, the driven part has the form

$$W(\tau) = F_\omega \cos(\omega\tau) \sum_{i,j} \langle R_i | x | R_j \rangle a_i^\dagger a_j, \tag{3.19}$$

where we defined

$$\langle R_i | x | R_j \rangle = \int dx\, \mathcal{W}_0^*(x - R_i)\, x\, \mathcal{W}_0(x - R_j). \tag{3.20}$$

Performing the shift $x \rightarrow x + (R_i + R_j)/2$ and assuming that the Wannier functions can be chosen real and with a well defined parity (in the present case they can be taken as even functions), one finds that the matrix elements (3.20) are vanishing unless $i = j$. Since the Wannier functions are exponentially localized [153, 156], one obtains

$$\int dx\, \mathcal{W}_0^*(x - R_i)\, x\, \mathcal{W}_0(x - R_i) \simeq R_i. \tag{3.21}$$

We choose now the zero of coordinates as in Fig. 3.1 and we thus rewrite the positions of the lattice sites R_j as $R_j = a(j + l_j)$, where $l_j = -l - j/2$ for j even and $l_j = l - (j+1)/2$ for j odd. This leads to a time-dependent term

$$W(\tau) = K \cos(\omega\tau) \sum_j (j + l_j) n_{j\nu}, \qquad K = a M x_0 \omega^2. \tag{3.22}$$

To treat the full time-dependent problem, we use the Floquet theory, valid for Hamiltonians that are periodic in time [103, 104, 158]. We introduce a composite Hilbert space $\mathcal{H}' = \mathcal{H} \otimes \mathcal{H}_T$, where $\mathcal{H}$ is the original Hilbert space and $\mathcal{H}_T$ is the Hilbert space of T-periodic complex-valued functions. We then define the scalar product in $\mathcal{H}'$ as

$$\langle\langle \cdot | \cdot \rangle\rangle = \frac{1}{T} \int_0^T d\tau \langle \cdot | \cdot \rangle, \tag{3.23}$$

where $\langle \cdot | \cdot \rangle$ is the scalar product in $\mathcal{H}$. According to Floquet theorem, the solutions of the Schrödinger equation have the form $|\psi_n(\tau)\rangle = e^{-iE_n\tau}|u_n(\tau)\rangle$. The quasienergies E_n and the Floquet modes $|u_n(\tau)\rangle$ satisfy the eigenvalue problem $\mathfrak{H}(\tau)|u_n(\tau)\rangle = E_n|u_n(\tau)\rangle$, where $\mathfrak{H}(\tau) \equiv H(\tau) - i\hbar\partial_\tau$ is the so-called Floquet Hamiltonian. Moreover, quasienergies that differ by $m\hbar\omega$, with $m \in \mathbb{Z}$, identify the same solution of the Schrödinger equation, leading to a Brillouin zone structure. The next aim is to calculate the eigenvalues of the Floquet Hamiltonian. We choose Fock-like states $|\{n_j\}\rangle$ as a basis of $\mathcal{H}$, whereas we consider plane waves as a basis of $\mathcal{H}_T$. The basis vectors in $\mathcal{H}'$ are therefore defined as

$$|\{n_j\}, m\rangle\rangle = |\{n_j\}\rangle \exp(im\omega\tau). \tag{3.24}$$

It is now convenient to perform a unitary transformation [54] that changes the basis vectors into

$$|\{n_j\}\rangle \exp\left[-i\frac{K}{\hbar\omega}\sin(\omega\tau)\sum_j(j+l_j)n_j + im\omega\tau\right], \tag{3.25}$$

which is useful to compute the matrix elements of the Floquet Hamiltonian,

$$\langle\langle\{n_j'\}, m'|H_0 + W(\tau) - i\hbar\partial_\tau|\{n_j\}, m\rangle\rangle. \tag{3.26}$$

We now focus the attention on the hopping terms, i.e H_0. They are all of the form

$$\langle\langle\{n_j'\}, m'|a_i^\dagger a_{i'}|\{n_j\}, m\rangle\rangle = \langle\{n_j'\}|a_i^\dagger a_{i'}|\{n_j\}\rangle g(T), \tag{3.27}$$

with

$$g(T) = \frac{1}{T}\int_0^T d\tau \exp\left\{i\frac{K}{\hbar\omega}s\sin(\omega\tau) - i(m'-m)\omega\tau\right\},$$

where we defined $s = \sum_j(j+l_j)(n_j'-n_j)$. By using the integral representation of the Bessel functions of the first kind

$$\mathcal{J}_n(x) = \frac{1}{2\pi}\int_0^{2\pi} d\tau e^{ix\sin\tau - in\tau}, \tag{3.28}$$
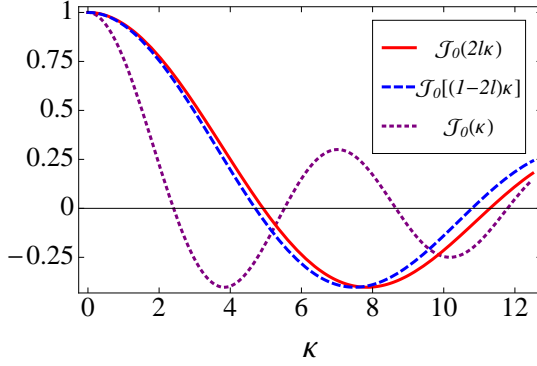
FIGURE 3.3: Relevant Bessel functions renormalizing the hopping coefficients as a function of $\kappa \equiv K/\hbar\omega$. As in Fig. 3.1, we have considered $l = 0.2443$.

we can rewrite Eq. (3.27) as

$$\langle \{n'_j\} | a_i^\dagger a_{i'} | \{n_j\} \rangle \, \mathcal{J}_{m'-m} \left(\frac{K}{\hbar\omega} s \right) . \tag{3.29}$$

Only a limited set of matrix elements (3.27) is needed, because the tight-binding Hamiltonian includes three main hopping processes. Let us consider, as an example, the case $i = 2p$ and $i' = 2p + 1$ with p an integer, which corresponds to the hopping term with amplitude J_1. The Fock-state configurations that give non-zero matrix elements are

$$\{n_j\} = \{n_1, n_2, \ldots, n_{2p}, n_{2p+1}, \ldots\}, \tag{3.30}$$

$$\{n'_j\} = \{n_1, n_2, \ldots, n_{2p} \pm 1, n_{2p+1} \mp 1, \ldots\}, \tag{3.31}$$

yielding

$$s = (2p + l_{2p})(n_{2p} \pm 1 - n_{2p}) + (2p + 1 + l_{2p+1})(n_{2p+1} \mp 1 - n_{2p+1}) = \mp 2l . \tag{3.32}$$

By using the property that Bessel functions of the first kind with odd index are odd and Bessel functions with even index are even, one can finally write

$$\mathcal{J}_{m'-m} \left(\frac{K}{\hbar\omega} s \right) = (\mp 1)^{m'-m} \mathcal{J}_{m'-m} \left(2l \frac{K}{\hbar\omega} \right) . \tag{3.33}$$

Similar arguments can be applied when $i = 2p - 1$, $i' = 2p$ (hopping term J_2) and when $|i - i'| = 2$ (hopping terms J'), leading respectively to $s = \mp(1 - 2l)$ and $s = \mp 1$. For the matrix elements of the density operator, namely $i = i'$, one finds that $s = 0$ and thus $g(T) = \delta_{m,m'}$.

The term $W(\tau)$ in the matrix elements now drops because the time derivative term $-i\hbar\partial_\tau$ cancels it. In the limit $\hbar\omega \gg J_1, J_2, J'$ one can perturbatively

neglect the off-diagonal elements of the Floquet Hamiltonian with $m \neq m'$ and therefore write the matrix elements in block-diagonal form

$$\langle\langle\{n'_j\}, m'|\mathfrak{H}|\{n_j\}, m\rangle\rangle \approx \delta_{m,m'}\langle\{n'_j\}|H_0^{\text{eff}} + m\hbar\omega|\{n_j\}\rangle, \tag{3.34}$$

where the operator H_0^{eff} has the same functional form as H_0 [see Eq. (3.9)], but with renormalized hopping coefficients

$$J_1 \quad \rightarrow \quad \bar{J}_1 \equiv \mathcal{J}_0\left(2l\frac{K}{\hbar\omega}\right)J_1, \tag{3.35}$$

$$J_2 \quad \rightarrow \quad \bar{J}_2 \equiv \mathcal{J}_0\left[(1-2l)\frac{K}{\hbar\omega}\right]J_2, \tag{3.36}$$

$$J' \quad \rightarrow \quad \bar{J}' \equiv \mathcal{J}_0\left(\frac{K}{\hbar\omega}\right)J'. \tag{3.37}$$

The behavior of the Bessel functions is shown in Fig. 3.3. From now on we take $m = 0$ in Eq. (3.34), thus choosing one specific Brillouin zone for the quasienergies.

3.5 SPECTRUM OF THE EFFECTIVE HAMILTONIAN

The dependence of the renormalized hopping coefficients on the driving parameter $\kappa \equiv K/\hbar\omega$ allows for the realization of several regimes, due to fundamental changes in the shape of the quasienergy spectrum of the effective Hamiltonian H_0^{eff}. Since for each hopping coefficient the regimes where the Bessel function changes sign occur for different values of the argument κ, a very rich behavior is expected, with various realizations of band structure configurations. Let us consider the different scenarios and discuss the changes of the spectrum as a function of κ. We concentrate on the half-filled case and investigate the influence of the spectrum on the transport properties of the different ground states realized.

For relatively small values of κ, the nearest-neighbor hopping coefficients J_1 and J_2 simultaneously reduce in magnitude, but the shape of the bands is not much affected, as long as these coefficients are large compared with $\bar{J}'$ (see Fig. 3.4(a)). Around $\kappa \approx 4.5$, the second band is inverted and the system displays an indirect gap, as shown in Fig. 3.4(b): the minimum at $k = 0$ of the second band is larger in energy than the maximum at $k = \pi/2$ of the lowest band. In Fig. 3.4(c) we show the case where the minimum at $k = 0$ of the second band lowers in energy and the indirect gap now vanishes. This scenario makes possible the realization of a four Fermi-point metallic state. In Fig. 3.4(d), the limiting case where the two bands touch at $k = 0$ is shown. This requires, from Eq. (3.14), that $\Delta(0) = (\bar{J}_1 + \bar{J}_2)^2 = 0$, i.e. $\bar{J}_1 = -\bar{J}_2$, as can be observed by a simple inspection of Fig. 3.5(a). This scenario is only realizable because the Bessel functions that renormalize the nearest-neighbor hopping coefficients have different arguments, so that $\bar{J}_2$ can change
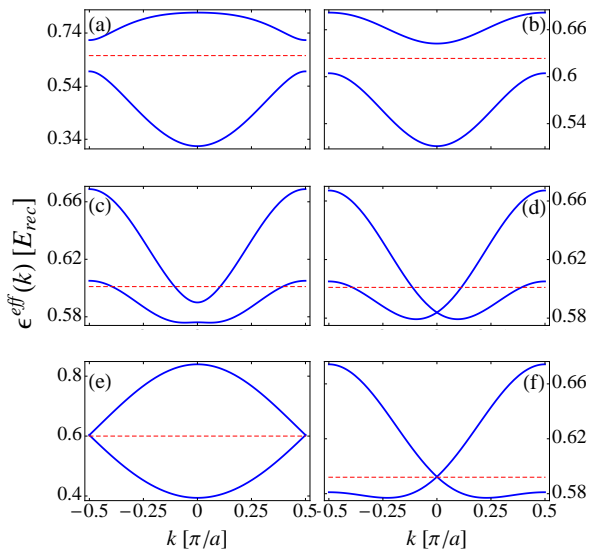
FIGURE 3.4: Quasienergy spectra of H_0^{eff} in units of E_{rec} for (a) $K/\hbar\omega = 4$, (b) $K/\hbar\omega = 4.6$, (c) $K/\hbar\omega = 4.8$, (d) $K/\hbar\omega = 4.824$, (e) $K/\hbar\omega = 5.7$, (f) $K/\hbar\omega = 11.074$. The red dashed line is the Fermi level at half-filling.
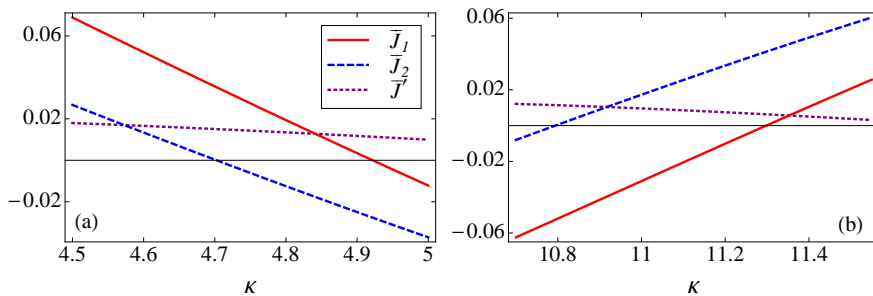

FIGURE 3.5: Renormalized hopping coefficients near the (a) first and (b) second zero of the Bessel functions $\mathcal{J}_0\,(2l\kappa)$ and $\mathcal{J}_0\,[(1-2l)\kappa]$, respectively.
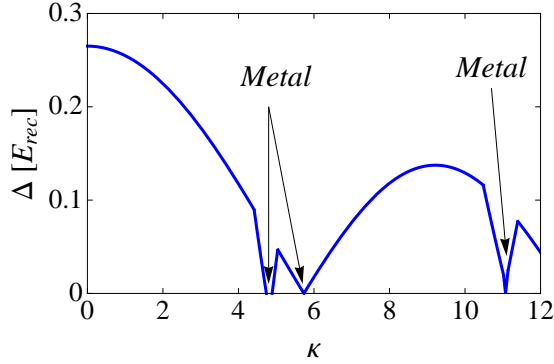
FIGURE 3.6: Band gap as a function of the shaking parameter κ showing several metal-insulator transitions.

sign before $\bar{J}_1$ does. Since the renormalized hopping coefficients $\bar{J}_1$ and $\bar{J}_2$ change with different slope as functions of κ, they can therefore become equal, despite the fact that their bare value was different in the undriven case. This happens at $\kappa \approx 5.7$, and causes the closing of the gap at $k = \pi/2$ since $\Delta(\pi/2) = (\bar{J}_1 - \bar{J}_2)^2$ [see Fig. 3.4(e)]. Another case appears for larger values of κ. For $\kappa = 11.074$, near the points where $\mathcal{J}_0(2l\kappa)$ and $\mathcal{J}_0[(1-2l)\kappa]$ vanish, one finds once again that $\bar{J}_1 = -\bar{J}_2$. The band touching point at $k = 0$ is shown in Fig. 3.4(f).

3.6 PHASE DIAGRAM AT HALF-FILLING

By using the band analysis presented in the previous paragraph, we can now describe the behavior of the system in the half-filled case (one particle per site and total (pseudo)spin $S_{\text{tot}}^z = 0$) in the absence of interactions. In Fig. 3.6 we show how the band gap Δ changes as a function of $\kappa = K/\hbar\omega$. In the regimes where $\Delta \neq 0$ (which include the undriven case with $\kappa = 0$), the Fermi energy lies inside the gap and the system is a Peierls insulator.

One notices that near $\kappa = 4.5$, the gap function is not smooth and starts dropping rapidly to zero. The reason for this non-smooth behavior is the inversion of the second band, leading to a change of the gap from direct to indirect. These features in the gap behavior appear for many values of κ, and are always related to band inversion (either the first or the second band).

The system undergoes two metal-insulator transitions around $\kappa \approx 4.8$. One can easily prove that the metal phase appears for $\bar{J}' \geq (|\bar{J}_1 + \bar{J}_2| - |\bar{J}_1 - \bar{J}_2|)/4$. For the parameters chosen here, this yields $4.74 < \kappa < 4.89$. In this metal phase, the Fermi surface exhibits four Fermi points as shown in Fig. 3.4(c)-(d).

For $\kappa > 4.89$, a gap opens again and leads to a (Peierls) insulating behavior. Eventually, the gap at $k = \pi/2$ vanishes at $\kappa = 5.7$ where $\bar{J}_1 = \bar{J}_2$ and one

finds again a metal (see Fig. 3.4(e)). Moreover, since the nearest-neighbor hopping coefficients are now equal, the unit cell consists of only one lattice site and the Brillouin zone is doubled. Therefore, the spectrum of Fig. 3.4(e) corresponds to a folded cosine-like band and the metallic phase in this case is the standard two Fermi-point gapless phase of a 1D half-filled electron system in absence of lattice dimerization.

A remarkable behavior seems to occur at $\kappa = 11.074$. At this point, the bands approach each other linearly at $k = 0$ because the gap closes since $\bar{J}_1 = -\bar{J}_2$ (see Fig. 3.4(f)). However, this dispersion that apparently exhibits one single Fermi point does not lead to a new metallic phase but to a conventional Luttinger liquid with two Fermi points. One can easily reach this conclusion by performing a canonical transformation on the fermionic operators $a_n \to e^{i\alpha_n} a_n$, where $\{\alpha_n\} \equiv \{\ldots, \pi, \pi, 0, 0, \pi, \pi, 0, 0, \ldots\}$. Such a transformation flips the sign of the hopping coefficient every second bond and therefore maps the model with alternating hopping to the typical model with uniform hopping and a cosine-like band, thus leading to a conventional metal with two Fermi points. The price to pay is that the next-nearest neighbor hopping coefficient will also change sign, but since it is quite small in magnitude compared to the nearest-neighbor one, it will have no consequences on the metallic properties.

3.7 EFFECT OF INTERACTIONS

Let us now add to the Hamiltonian (3.9) a Hubbard interaction term, commonly realized in experimental setups at low temperatures [47],

$$H_U = U \sum_i n_{i\uparrow} n_{i\downarrow}, \tag{3.38}$$

where

$$U = \frac{1}{2} \times \frac{4\pi\hbar^2 a_s^{\text{eff}}}{M} \int dx \, |\mathcal{W}_0(x - R_{j\nu})|^4, \tag{3.39}$$

and a_s^{eff} is the effective s-wave scattering length for the 1D system, therefore containing also the contribution of the harmonic confinement in the two orthogonal spatial directions. The Hubbard parameter U, depends on the s-wave scattering length a_s, and can therefore be tuned by using Feshbach resonances (for example for ^{40}K atoms), thus spanning the repulsive regime $U > 0$, the attractive regime $U < 0$ and the non-interacting limit $U = 0$. Since this term has a density-density form, it is not affected by the shaking scheme previously discussed and therefore appears also in the effective Hamiltonian H_0^{eff}, under the supplementary condition that $\hbar\omega \gg U$. Moreover, one can understand the reason why the Hubbard parameter U does not carry a sublattice index by considering the harmonic approximation. Since the two wells have the same curvature, the corresponding harmonic oscillator states (*i.e.* the

Wannier functions) have the same form in the two wells and the integral in
Eq. (3.39) will be independent on which well is referred to.

We will focus in the rest of this section on the fate of the region where
the unconventional metal with four-Fermi points is found, once the Hubbard
interaction is turned on. As we will show, a central role is played by the
next-nearest neighbor hopping $\bar{J}'$. On the other hand, interactions will not
affect the positions where the two Fermi-point metals are realized because
this involves only a relation between $\bar{J}_1$ and $\bar{J}_2$, namely $\bar{J}_1 = \pm\bar{J}_2$.

To study the effect of interactions, we first write the non-interacting part in
the Peierls form

$$H_0 = -t\sum_n (1 + (-1)^n\delta)\left(a_n^\dagger a_{n+1} + \text{h.c.}\right) + t'\sum_n \left(a_n^\dagger a_{n+2} + \text{h.c.}\right) + \mu N$$

$$= H_t + H_{t\delta} + H_{t'} + \mu N, \tag{3.40}$$

where we have defined

$$t(1+\delta) = \bar{J}_1, \quad t(1-\delta) = \bar{J}_2, \quad t' = -\bar{J}', \tag{3.41}$$

and a chemical potential has been introduced to control the filling. In the case
discussed in this work, the indirect gap is due to the band inversion of the
upper band, given by the condition

$$\bar{J}' > \bar{J}'_{c1} = \frac{1}{4}(|\bar{J}_1 + \bar{J}_2| - |\bar{J}_1 - \bar{J}_2|) = \frac{1}{2}(|t| - |t\delta|). \tag{3.42}$$

The transition in the single particle spectrum from a Peierls insulator to a
metal with four Fermi points appears when the indirect gap closes, *i.e.*

$$\bar{J}' > \bar{J}'_{c2} = \frac{1}{4}(|\bar{J}_1 + \bar{J}_2| + |\bar{J}_1 - \bar{J}_2|) = \frac{1}{2}(|t| + |t\delta|). \tag{3.43}$$

These critical values are renamed for t' as $t'_{c1} = -\bar{J}'_{c1}$ and $t'_{c2} = -\bar{J}'_{c2}$. The
transition therefore occurs for $t' < t'_{c2}$. The chemical potential in the Peierls
insulator at half-filling is chosen to lie in the center of the (direct or indirect)
gap. This defines the chemical potential

$$\mu = \begin{cases} |t\delta| - |t| & t'_{c2} < t' < t'_{c1}, \\ 2t' & t' > t'_{c1}. \end{cases} \tag{3.44}$$

3.7.1 *Bosonization*

The theory is bosonized in a similar way as in Ref. [149]. One considers the
terms $H_{t'}$, $H_{t\delta}$ and H_U as perturbations. The "unperturbed" spectrum given
by H_t is linearized around the Fermi points, that are given at half-filling by
$k_F = \pm\pi/2a$; the corresponding Fermi velocity is $v_F = \pm 2ta$.

In the continuum limit, one substitutes

$$a_{n,\sigma} \rightarrow \sqrt{a}\, e^{ik_F x} \psi_{R\sigma}(x) + \sqrt{a}\, e^{-ik_F x} \psi_{L\sigma}(x), \tag{3.45}$$

where $x = na$ and $\psi_{L\sigma}(x)$, $\psi_{R\sigma}(x)$ denote, respectively, left and right movers. The fermionic fields are then bosonized according to

$$\psi_{R(L)\sigma}(x) = \frac{1}{\sqrt{2\pi a}} e^{\pm i \sqrt{\pi} [\phi_\sigma(x) \pm \theta_\sigma(x)]}. \tag{3.46}$$

A change of basis for the bosonic fields $\phi_\sigma(x)$ and $\theta_\sigma(x)$ (from now on we drop the hat on the operators) is performed to describe the charge and spin degrees of freedom:

$$\phi_c = \frac{1}{\sqrt{2}}(\phi_\uparrow + \phi_\downarrow), \quad \phi_s = \frac{1}{\sqrt{2}}(\phi_\uparrow - \phi_\downarrow) \tag{3.47}$$

$$\theta_c = \frac{1}{\sqrt{2}}(\theta_\uparrow + \theta_\downarrow), \quad \theta_s = \frac{1}{\sqrt{2}}(\theta_\uparrow - \theta_\downarrow). \tag{3.48}$$

The Hamiltonian can thus be cast into the following form

$$H = H_c + H_s + H_{cs}, \tag{3.49}$$

where

$$H_c = \int dx \left\{ \frac{u_c}{2K_c} [\partial_x \phi_c(x)]^2 + \frac{u_c K_c}{2} [\partial_x \theta_c(x)]^2 \right.$$
$$\left. - \mu_{\text{eff}} \sqrt{\frac{2}{\pi}} \partial_x \phi_c(x) - \frac{U}{2\pi^2 a^2} \cos[\sqrt{8\pi}\phi_c(x)] \right\},$$

$$H_s = \int dx \left\{ \frac{u_s}{2K_s} [\partial_x \phi_s(x)]^2 + \frac{u_s K_s}{2} [\partial_x \theta_s(x)]^2 + \frac{U}{2\pi^2 a^2} \cos[\sqrt{8\pi}\phi_s(x)] \right\},$$

$$H_{cs} = -\frac{4t\delta}{\pi a} \int dx \, \cos[\sqrt{2\pi}\phi_c(x)] \cos[\sqrt{2\pi}\phi_s(x)], \tag{3.50}$$

and we defined $\mu_{\text{eff}} \equiv \mu - 2t'$, $u_c K_c = u_s K_s = v_F$, $u_c/K_c = 1 + U/\pi v_F$ and $u_s/K_s = 1 - U/\pi v_F$. The bosonic model just derived couples charge and spin degrees of freedom because of the term H_{cs}. For this reason, the exact solution of this model is not known and one has to resort to approximation methods or numerical calculations [149].

3.7.2 *Phase diagram analysis*

In the non-interacting limit $U = 0$ studied in the previous sections, the half-filled system shows a transition from a band insulator to a metal with four Fermi points. Such a transition, that happens when $t' < t'_{c2}$, can be also predicted in the bosonized model written in terms of ϕ_σ and θ_σ. The condition is

that the effective chemical potential μ_{eff} exceeds the mass gap $2t\delta$, which in turn yields $t' < t'_{c2}$ [149]. In the charge and spin representation, the model becomes rather more complicated but one can obtain a qualitative understanding (also of the interacting case) by performing a mean-field decoupling of the H_{cs} term, along the same lines as in Ref. [149].

One introduces the expectations values

$$m_c = 4t\delta\langle\cos[\sqrt{2\pi}\phi_s(x)]\rangle\,, \tag{3.51}$$

$$m_s = 4t\delta\langle\cos[\sqrt{2\pi}\phi_c(x)]\rangle\,, \tag{3.52}$$

and writes $H = \tilde{H}_c + \tilde{H}_s$ with

$$\tilde{H}_c = H_c - \frac{m_c}{\pi a}\int dx\,\cos[\sqrt{2\pi}\phi_c(x)]\,, \tag{3.53}$$

$$\tilde{H}_s = H_c - \frac{m_s}{\pi a}\int dx\,\cos[\sqrt{2\pi}\phi_s(x)]\,, \tag{3.54}$$

which now displays a clear decoupling between charge and spin degrees of freedom. However, the new mass terms still couple the two sectors thanks to the mean-field equations (3.51)-(3.52). There is an asymmetry in the charge sector due to the presence of the effective chemical potential μ_{eff}, which is responsible for the phase transition from metal to insulator as previously argued for the non-interacting case. In the weak coupling limit $U \ll t$, where $K_{c,s} \approx 1$, the terms proportional to $\cos[\sqrt{8\pi}\phi_{c,s}(x)]$ can be neglected because they are irrelevant and the new terms $\cos[\sqrt{2\pi}\phi_{c,s}(x)]$ dominate the physics of this system. One can therefore analyze the model in the form (3.53)-(3.54) by using the exact solution found by Zamolodchikov [159] for the sine-Gordon Hamiltonian with $\beta^2 = 2\pi$

$$H_\alpha^{SG} = \int dx\left\{\frac{u_\alpha}{2}[(\partial_x\phi_\alpha)^2 + (\partial_x\theta_\alpha)^2] - \frac{m_\alpha}{\pi a}\cos[\sqrt{2\pi K_\alpha}\phi_\alpha]\right\}\,,$$

when $0 < K_\alpha < 2$ and $\alpha = c, s$. Here the Luttinger parameter K_α has been reabsorbed into newly defined bosonic fields $\phi_\alpha \to \sqrt{K_\alpha}\phi_\alpha$ and $\theta_\alpha \to \theta_\alpha/\sqrt{K_\alpha}$. The excitation spectrum consists of solitons, antisolitons and breathers (soliton-antisoliton bound states). The lowest-energy excitations in this range of K_α are given by the breathers. The lightest breather mass Δ_α (which is twice the energy gap of the system) is related to the soliton mass M_α via

$$\Delta_\alpha = 2M_\alpha\sin\left(\frac{\pi}{2}\frac{K_\alpha}{4 - K_\alpha}\right)\,. \tag{3.55}$$

The soliton mass M_α can be calculated from the bare mass m_α using the relation

$$M_\alpha/\Lambda = C(K_\alpha)\,(m_\alpha/\Lambda)^{2/(4-K_\alpha)}\,, \tag{3.56}$$

where Λ is a high-energy cut-off. Finally, to solve the mean-field equations one needs [160]

$$\langle\cos(\sqrt{2\pi K_\alpha}\phi_\alpha)\rangle = B(K_\alpha)(M_\alpha/\Lambda)^{K_\alpha/2}\,. \tag{3.57}$$

The coefficients $C(K_\alpha)$ and $B(K_\alpha)$ are given by

$$C(K_\alpha) = \frac{2\Gamma(\frac{K_\alpha}{8-2K_\alpha})}{\sqrt{\pi}\Gamma(\frac{2}{4-K_\alpha})} \cdot \left[\frac{\Gamma(1-K_\alpha/4)}{2\Gamma(K_\alpha/4)}\right]^{\frac{2}{4-K_\alpha}} \tag{3.58}$$

and

$$B(K_\alpha) = [\Gamma(1/2+\xi/2)\Gamma(1-\xi/2)]^{(K_\alpha/2)-2} \times$$
$$\times \left[\frac{2\sin(\pi\xi/2)}{4\sqrt{\pi}}\right]^{K_\alpha/2} \left[\frac{(1+\xi)\pi^2\Gamma(1-K_\alpha/4)}{\sin(\pi\xi)\Gamma(K_\alpha/4)}\right] \tag{3.59}$$

where $\xi = K_\alpha/(4-K_\alpha)$ and $\Gamma(x)$ is Euler's gamma function.

Based on this approach, one can solve the self-consistent equations for the charge and spin gaps, Δ_c and Δ_s respectively, and obtain a qualitative understanding of the role of interactions. For $\mu_{\text{eff}} = 0$ the two gaps are equal when $U = 0$. The charge gap increases as a function of U, while the spin gap decreases. Therefore, repulsive interactions lead to a larger charge gap, while they reduce the spin gap. This picture is confirmed by numerical simulations [146], but a quantitative agreement would require a careful estimate of the Luttinger parameters, which is beyond the scope of the present work.

Let us now consider the effect of the chemical potential μ_{eff} on the four Fermi-point phase. Such a phase appears for $\kappa_A < \kappa < \kappa_B$, where $\kappa_A \approx 4.74$ and $\kappa_B \approx 4.89$. In the non-interacting picture, the transition occurs when μ_{eff} exceeds the band gap. One can assume an analogous criterion to hold in the interacting case, *i.e.* $\mu_{\text{eff}} > \Delta_c/2$, where Δ_c is the lowest breather mass in the charge sector, as discussed above. In the presence of the interactions the charge gap is renormalized and increases as a function of U, as concluded already at the mean-field level. Therefore, the critical value of t' for the metal transition changes because the effective gap to overcome now depends on U, and for repulsive interactions it is larger than for $U = 0$. One thus expects that the interval $[\kappa_A, \kappa_B]$ shrinks because the charge gap that t' needs to overcome has now increased. In the limit of strong Hubbard coupling ($U \gg t, t'$) the charge gap $\Delta_c \sim U$ and the range of κ where the metallic phase is reached vanishes above a critical value U_c, i.e. when the charge gap is large enough, such that the effect of t' is no longer sufficient to close it. On the other hand, attractive interactions $U < 0$ have the opposite effect. In the limit of strong Hubbard coupling ($|U| \gg t, t'$) the charge gap $\Delta_c \sim \delta t^2/|U|$ and therefore the region where the metallic phase is realized enlarges.

As it follows from the performed mean-field analysis, in the case of weak repulsive interaction and in close proximity to the metal-insulator transition ($t' \lesssim t'_{c2}$), the charge gapless phase is also spin gapless and thus shows properties of a Luttinger liquid. However, deeply inside the metallic phase ($t' \ll t'_{c2}$), where the properties of the system are determined by the four Fermi points and the effect of the direct single-particle gap is negligible, the system becomes similar to the one-dimensional half-filled $t - t'$ Hubbard model. This

model has been studied in detail, both analytically and numerically [161–171], and it is known to give rise to a Luther-Emery liquid for attractive and repulsive on-site interactions, i.e. a spin gapped metal.

In the repulsive case, the dominant instability is the charge-density-wave, which exhibits the slowest power-law decay of the corresponding correlations. Notice that this behavior is different from the conventional Hubbard model, for which the charge gap is open, the spin gap is zero and the dominant correlation is the spin-density-wave. In the opposite case of attractive on-site coupling, the spin gap is present for arbitrary $t' < t'_{c2}$ and the system behaves as a spin gapped metal with dominant singlet-superconducting instability, characterized by a power-law decay of the corresponding correlations.

3.8 CONCLUSIONS

In this chapter, we have investigated how to realize metal-insulator transitions for a system of fermionic atoms loaded in a bipartite one-dimensional optical lattice at half-filling. The bipartite character of the optical lattice is essential because it ensures that the nearest-neighbor hopping coefficients alternate in magnitude, opening a gap at the edge of the Brillouin zone ($k = \pi/2$). The Fermi level lies inside the gap at half-filling and therefore the system behaves as a band insulator (Peierls insulator).

By introducing an external high-frequency driving force that shakes the lattice, we have shown that the hopping coefficients are all renormalized by Bessel functions that depend on the shaking parameter κ with different arguments. This feature allows for a competition of the different hopping coefficients, which can reduce in magnitude and change sign, severely altering the shape of the bands. We have observed that the system can exhibit band inversion, generating an indirect gap, as well as band touching and band crossing.

The different regimes reached by this scheme show several possible transitions from Peierls insulators with direct or indirect gap to metallic states with two or four Fermi points. The scheme that we have discussed in this chapter represents, to the best of our knowledge, the first method that has been proposed to experimentally realize such an unconventional four Fermi-point metallic state, the properties of which have been theoretically discussed in the literature in the past decades [161–171]. Notice that this cannot be realized in conventional lattices, the bipartite nature of the lattice being an essential requirement.

Finally, we have qualitatively investigated the effect of on-site interactions on the metallic phases. The two Fermi-point metallic phase, appearing only at some discrete values of the driving parameter κ, behaves as an ordinary Luttinger liquid and therefore is expected to be analogous to the conventional Hubbard model. Concerning the four Fermi-point metallic phase, we have argued, based on a mean-field analysis supported by former numerical calcu-

lations, that the region in κ where such a phase appears would shrink (and eventually disappear) for repulsive interactions, whereas it would widen for attractive ones. A quantitative estimate of this process is left for future investigations.

CONTROLLING COHERENCE IN A BIPARTITE OPTICAL LATTICE

The control of transport properties is a key tool at the basis of many technologically relevant effects in condensed matter. The clean and precisely controlled environment of ultracold atoms in optical lattices allows one to prepare simplified but instructive models, which can help to better understand the underlying physical mechanisms. Here we show that by tuning a structural deformation of the unit cell in a bipartite optical lattice, one can induce a phase transition from a superfluid into various Mott insulating phases forming a shell structure in the superimposed harmonic trap. The Mott shells are identified via characteristic features in the visibility of Bragg maxima in momentum spectra. The experimental findings are explained by Gutzwiller mean-field and quantum Monte Carlo calculations. Our system bears similarities with the loss of coherence in cuprate superconductors, known to be associated with the doping induced buckling of the oxygen octahedra surrounding the copper sites.

4.1 INTRODUCTION

Rapid and precise control of transport properties are at the heart of many intriguing and technologically relevant effects in condensed matter. Small changes of some external parameter, for example, an electric or a magnetic field, may be used to significantly alter the mobility of electrons. Prominent examples are field effect transistors [172] and systems showing colossal magneto-resistance [173]. Often, the control is achieved via structural changes of the unit cell, leading to an opening of a band gap. In iron-based superconductors, the variation of pressure is a well-known technique to control their transport properties [174]. In certain high-T_c superconductors, pulses of infrared radiation, which excite a mechanical vibration of the unit cell, can for short periods of time switch these systems into the superconducting state at temperatures where they actually are insulators [175]. In La-based high-T_c cuprates, the drastic reduction of T_c at the doping value of $x = 1/8$, known as "the 1/8 mystery", is connected to a structural transition that changes the lattice unit cell [176].

Ultra-cold atoms in optical lattices provide a particularly clean and well controlled experimental platform for exploring many-body lattice physics [15]. Schemes for efficient manipulation of transport properties can be readily implemented and studied with great precision. In conventional optical lattices, tuning between a superfluid and a Mott insulating phase has been
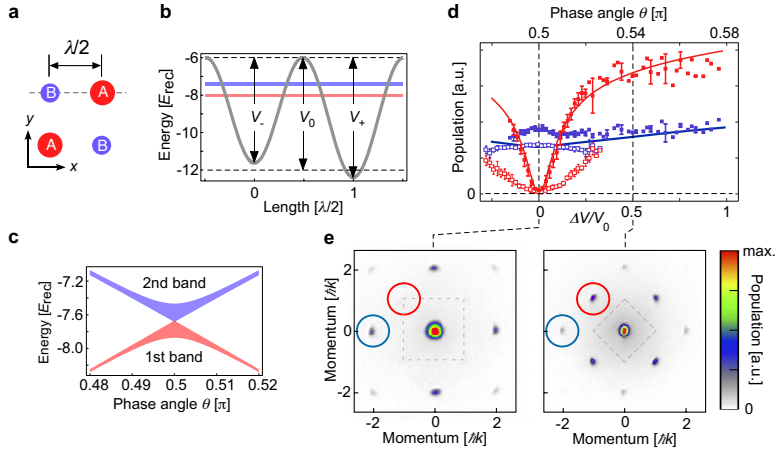
FIGURE 4.1: Lattice potential. (a) Sketch of the lattice geometry within the xy-plane. $\lambda = 1064$ nm denotes the wavelength of the laser light. (b) The potential along the dashed trajectory in (a) is plotted for $\theta = 0.51\,\pi$ and $V_0 = 6\,E_{\mathrm{rec}}$ (thick grey line) with the first and second bands represented, respectively, by the red and blue horizontal bars. (c) The first two bands are plotted versus θ for $V_0 = 6\,E_{\mathrm{rec}}$. (d) The red and blue squares show the relative number of atoms (normalized to the total particle number and plotted versus $\Delta V/V_0$) associated with the Bragg peaks enclosed by red and blue circles in (e), respectively. The filled (open) squares are recorded for $V_{\mathrm{z},0} = 0$ ($V_{\mathrm{z},0} = 22\,E_{\mathrm{rec}}$). The error bars indicate the statistical errors for 5 measurements. The solid lines are determined by a full band calculation (neglecting interaction) with no adjustable parameters. (e) Momentum spectra ($V_0 = 6E_{\mathrm{rec}}$, $V_{\mathrm{z},0} = 0$) are shown with $\Delta V = 0$ (left) and $\Delta V/V_0 = 0.5$ (right) with the respective FBZs imprinted as dashed rectangles.

achieved by varying the overall lattice depth V_0, with the consequence of changing the height of the tunneling barriers and the on-site contact interaction energy [18]. The equivalent is not easily possible in condensed matter systems, since the lattice depth is practically fixed.

In this chapter, we present an ultracold atom paradigm, where tuning the system between a superfluid and a Mott insulator becomes possible via controlled distortion of the unit cell. This distortion acts to adjust the relative depth ΔV between two classes of sites (denoted by A and B) forming the unit cell and allows us to drive a superfluid to Mott insulator transition without altering the average lattice depth. We can access a rich variety of Mott-insulating states with different integer populations of the A- and B-sites, which give rise to a shell structure in the finite harmonic trap potential, leading to characteristic features in the visibility of Bragg maxima in momentum spectra. We compare our observations with quantum Monte Carlo (QMC) and Gutzwiller mean field calculations, thus obtaining a detailed quantitative understanding of the system. In the following, we first describe the experi-

mental set-up; then, we theoretically investigate the behavior of the visibility for two different cases: first, for fixed barrier height V_0, by varying ΔV (bipartite lattice), and second, for $\Delta V = 0$ (monopartite lattice), by tuning the lattice depth V_0. Although monopartite lattices have been previously studied in great detail, and QMC calculations have provided a good fitting of the visibility curve measured experimentally [177], here we show more accurate data and argue that the main features of the curve can be understood in terms of a precise determination of the onset of new Mott lobes in the phase diagram.

4.2 DESCRIPTION OF THE EXPERIMENTAL SET-UP

In the experiment, performed by the group of Prof. Hemmerich in Hamburg, an optical lattice of ^{87}Rb atoms is prepared using an interferometric lattice set-up [34, 36, 93, 178]. A two-dimensional (2D) optical potential is produced, comprising deep and shallow wells (A and B in Fig. 4.1(a)) arranged as the black and white fields of a chequerboard. In the xy-plane, the optical potential is given by

$$V(x, y) = -V_0 \left[\cos^2(kx) + \cos^2(ky) + 2\cos(\theta)\cos(kx)\cos(ky) \right] , \quad (4.1)$$

with the tunable well depth parameter V_0 and the lattice distortion angle θ. An additional lattice potential $V_z(z) \equiv -V_{z,0}\cos^2(kz)$ is applied along the z-direction. In order to study an effectively 2D scenario, $V_{z,0}$ is adjusted to 29 E_{rec}, such that the motion in the z-direction is frozen out. Here, $k \equiv 2\pi/\lambda$, $E_{rec} \equiv \hbar^2 k^2/2m$, m denotes the atomic mass, and $\lambda = 1064$ nm is the wave length of the lattice beams. Apart from the lattice, the atoms experience a nearly isotropic harmonic trap potential. Adjustment of θ permits controlled tuning of the effective well depths of the deep and shallow wells $V_\pm \equiv V_0 (1 \pm \cos(\theta))^2$ and their difference $\Delta V \equiv V_+ - V_- = 4 V_0 \cos(\theta)$ (see Fig. 4.1(b)). The effective mean well depth $\bar{V}_0 = (V_+ + V_-)/2 = V_0 \left[1 + \cos^2(\theta) \right]$ is only weakly dependent on θ. For example, within the interval $0.46 < \theta/\pi < 0.54$ one has $\cos^2(\theta) < 0.015$ and hence $\bar{V}_0 \approx V_0$. Tuning of θ significantly affects the effective band width, as shown in Fig. 4.1 (c). At $\theta = \pi/2$, the A- and B-wells become equal, which facilitates tunneling as compared to values $\theta \neq \pi/2$, where the broad lowest band of the $\theta = \pi/2$-lattice splits into two more narrow bands.

The experimental procedure begins with the production of a nearly pure Bose-Einstein condensate of typically 5×10^4 rubidium atoms (^{87}Rb) in the $F = 2, m_F = 2$ state confined in a nearly isotropic magnetic trap with about 30 Hz trap frequency. The adjusted values of the lattice depth V_0 are determined with a precision of about 2 percent by carefully measuring the resonance frequencies with respect to excitations into the third band along the x- and y-directions. The adjustment of θ is achieved with a precision exceeding $\pi/300$ by an active stabilization with about 10 kHz bandwidth. In a typical

experimental run, the lattice potentials $V(x, y)$ and $V_z(z)$ are increased to the desired values by an exponential ramp of 160 ms duration. After holding the atoms in the lattice for 20 ms, momentum spectra are obtained by rapidly ($< 1\,\mu$s) extinguishing the lattice and trap potentials, permitting a free expansion of the atomic sample during 30 ms, and subsequently recording an absorption image. The magnetic trap and the finite Gaussian profile of the lattice beams (beam radius = 100 μm) give rise to a combined trap potential. For $V_{z,0} = 29\,E_{rec}$ and $V_0 = 18\,E_{rec}$ this yields trap frequencies of 73 Hz in the xy-plane and 65 Hz along the z-direction. The observed momentum spectra comprise pronounced Bragg maxima with a visibility depending on the parameters V_0 and ΔV. These spectra are analyzed by counting the atoms ($n_{d,0}$) in a disk with 5 pixel radius around some higher order Bragg peak and within a disk of the same radius but rotated with respect to the origin by $45°$ ($n_{d,45}$). The visibility is obtained as $\mathcal{V} = (n_{d,0} - n_{d,45})/(n_{d,0} + n_{d,45})$ [94].

The distribution of Bragg peaks reflects the shape of the underlying first Brillouin zone (FBZ), which changes size and orientation as ΔV is detuned from zero. This is illustrated in Fig. 4.1(d) and (e). In (e) two spectra recorded for $\Delta V = 0$ (left) and $\Delta V / V_0 = 0.5$ (right) are shown. For $\Delta V = 0$ (the special case of a monopartite square lattice), the increased size of the FBZ gives rise to destructive interference, such that the $\pm(1, \pm 1)\hbar k$-Bragg peaks indicated by the red circle vanish. As ΔV is detuned from zero, a corresponding imbalance of the A- and B-populations yields a retrieval of the $\pm(1, \pm 1)\hbar k$-Bragg peaks. This is shown in Fig. 4.1(d) for the case of approximately vanishing interaction energy per particle $U \approx 0$ ($V_{z,0} = 0$) by the filled red squares and for $U \approx 0.3\,E_{rec}$ ($V_{z,0} = 22\,E_{rec}$) by the open red squares, respectively. It is seen that the interaction energy significantly suppresses the formation of a population imbalance and corresponding $\pm(1, \pm 1)\hbar k$-Bragg peaks.

4.3 MODEL

For low temperatures and for large lattice depths V_0, the system is described by the inhomogeneous Bose-Hubbard model [16, 17]

$$H = -J \sum_{\langle i,j \rangle} (a_i^\dagger a_j + \text{h.c.}) - \sum_i \tilde{\mu}_i n_i + \frac{U}{2} \sum_i n_i (n_i - 1), \qquad (4.2)$$

where J is the coefficient describing hopping between nearest-neighbor sites, U accounts for the on-site repulsion, and $\tilde{\mu}_i$ is a local chemical potential, which depends on the frequency ω of the trap and on the sublattice: $\tilde{\mu}_i = \mu_{A,B} - m\,\omega^2 \mathbf{r}_i^2 / 2$. The ratio U/J is a monotonously increasing function of V_0 / E_{rec}.
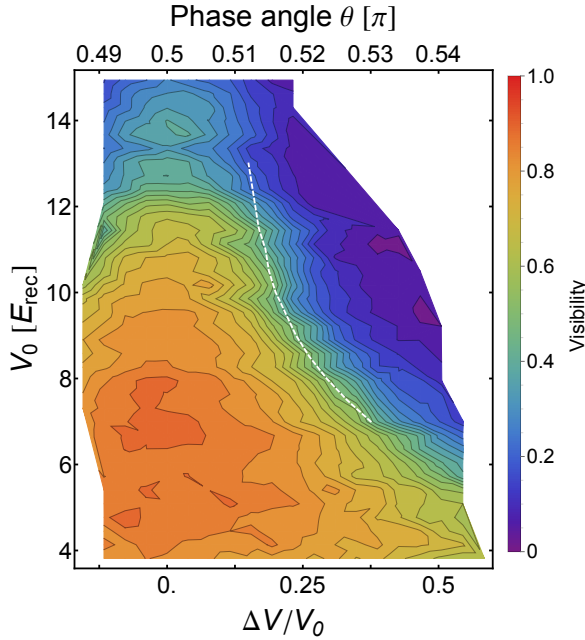
FIGURE 4.2: Visibility measurements in the bipartite lattice. The visibility (parametrized by the color code shown on the right edge) is plotted as a function of the well depth parameter V_0 (measured in units of the recoil energy E_{rec}) and the potential energy off-set difference ΔV between shallow and deep wells in the bipartite lattice. The dashed line corresponds to the theoretical calculation of the points where the fraction of particles $n_B = \sum_{i \in B} n_i / N$ of the B sublattice vanishes ($n_B < 5.5 \times 10^{-3}$).

4.3.1 Band-structure and tight-binding model

Using the potential of Eq. (4.1), we have numerically solved the Schrödinger equation for the single particle problem to obtain the exact band structure, including 14 bands in the plane-wave matrix representation of the Hamiltonian [179].

The single-particle problem is reformulated in terms of a tight-binding model Hamiltonian,

$$H_{SP} = -J \sum_{\langle i,j \rangle} (a_i^\dagger a_j + \text{h.c.}) - J_A \sum_{\langle i,j \rangle_A} (a_i^\dagger a_j + \text{h.c.}) - J_B \sum_{\langle i,j \rangle_B} (a_i^\dagger a_j + \text{h.c.})$$
$$+ E_A \sum_{i \in A} n_i + E_B \sum_{i \in B} n_i , \tag{4.3}$$

where J is the hopping between neighboring sites of different sublattices, J_A (J_B) is the hopping coefficient between neighboring sites of sublattice A (B) (see Fig. 4.3), and E_A (E_B) is the on-site energy of sites belonging to sublattice A (B). We neglect the $A \to A$ hopping (henceforth indicated as J'_A) along the
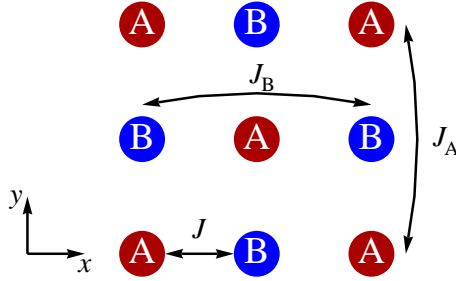
FIGURE 4.3: Hopping processes included in the tight-binding model.

diagonal lines of the lattice (same for $B \rightarrow B$), because for the monopartite lattice ($\theta = \pi/2$ or $\Delta V = 0$) these hopping coefficients are exactly zero as a consequence of the symmetry of the Wannier functions. For sufficiently small deviations from $\theta = \pi/2$, we expect that these coefficients are still negligible compared to J_A or J_B; this assumption is supported by the full band structure calculation. For $\theta \gtrsim 0.53\,\pi$, this assumption becomes less reliable (see Fig. 4.4).

We are going to show below that J is the dominant term and we will therefore drop the coefficients J_A and J_B as shown in the model (4.2). Moreover, the onsite energies E_A and E_B will be included in the chemical potential $\tilde{\mu}_i$, namely $\mu_A \equiv -E_A$ and $\mu_B \equiv -E_B$.

By diagonalizing the Hamiltonian in Eq. (4.3) in momentum space and taking the lattice constant to unity, an analytic expression for the corresponding band structure (depending on the parameters E_A, E_B, J, J_A, J_B) can be derived,

$$H_{SP}(\mathbf{k}) = \begin{pmatrix} E_A - 4J_A \cos(2k_x)\cos(2k_y) & -4J\cos(k_x)\cos(k_y) \\ -4J\cos(k_x)\cos(k_y) & E_B - 4J_B \cos(2k_x)\cos(2k_y) \end{pmatrix}. \quad (4.4)$$

When θ is tuned away from zero a gap opens, splitting the lowest band. We denote the two resulting bands by "1" and "2", with the corresponding energies $E_1(k_x, k_y)$ and $E_2(k_x, k_y)$. It is straightforward to verify that

$$E_A = E_1(\pi/2, \pi/4),$$
$$E_B = E_2(\pi/2, \pi/4),$$
$$J = \frac{1}{4}\sqrt{(E_1(\pi/4, \pi/4) - E_2(\pi/4, \pi/4))^2 - (E_A - E_B)^2},$$
$$J_A = \frac{1}{8}(E_1(\pi/2, 0) - E_1(\pi/2, \pi/2)),$$
$$J_B = \frac{1}{8}(E_2(\pi/2, 0) - E_2(\pi/2, \pi/2)). \quad (4.5)$$

In order to determine the parameters of the model Hamiltonian (4.3), instead of calculating Wannier functions, we use these equations to adjust the
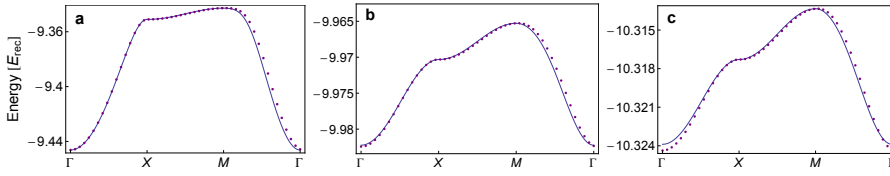
FIGURE 4.4: Lowest band in the bipartite optical potential. The lowest energy band for $V_0 = 7\,E_{rec}$ and (a) $\theta = 0.502\,\pi$, (b) $\theta = 0.52\,\pi$, and (c) $\theta = 0.53\,\pi$ is plotted versus k, along the high-symmetry lines of the first Brillouin zone. The dots are the results of the exact diagonalization, the solid line is calculated according to the tight-binding Hamiltonian (4.3) with parameter values determined according to Eq. (4.5).
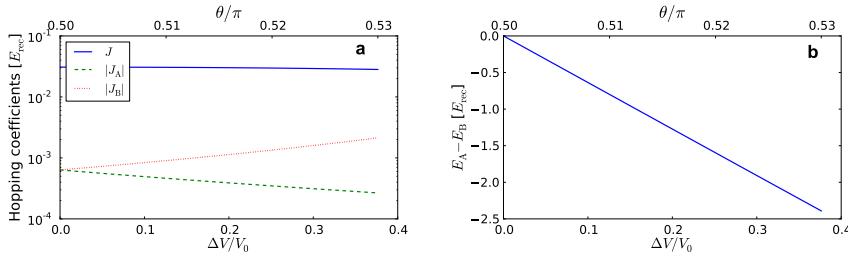

FIGURE 4.5: Tight-binding parameters. (a) Hopping coefficients and (b) energy difference $E_A - E_B$ versus ΔV (or equivalently θ) according to Eq. (4.5) for $V_0 = 8\,E_{rec}$.

tight-binding bands to the exact band structure calculation, finding reasonable agreement up to $\theta = 0.53\,\pi$, as shown in Fig. 4.4. The resulting values of the hopping coefficients and the energy difference $E_A - E_B$ are plotted in Fig. 4.5. Since $|J_A|$ and $|J_B|$ are nearly two orders of magnitude smaller than J, we will neglect them in what follows, as long as $J \neq 0$.

4.3.2 *Mean-field phase diagram of the bipartite lattice model*

In this section, we discuss the mean-field phase diagram of the bosonic model (4.2) in the absence of the trapping potential. We also consider the possibility that the interaction on A and B sites are different and we therefore introduce two interaction parameters U_A and U_B. The model is therefore

$$H = -J \sum_{\langle i,j \rangle} (a_i^\dagger a_j + \text{h.c.}) - \mu_A \sum_{i \in A} n_i - \mu_B \sum_{i \in B} n_i$$
$$+ \frac{U_A}{2} \sum_{i \in A} n_i(n_i - 1) + \frac{U_B}{2} \sum_{i \in B} n_i(n_i - 1). \tag{4.6}$$

We restrict ourselves to nearest-neighbor hopping coefficients, which are the only relevant ones, as shown in Fig. 4.5. The Hamiltonian in Eq. (4.6) describes a bipartite lattice, in which one allows for different densities in the

two sublattices since there are two (in principle) independent chemical potentials. We know already that the chemical potentials are fixed by the onsite energies found from the exact band structure calculation. However, we keep the treatment completely general at the moment and we will specify the values of the parameters when we will apply these findings to the experiments. A similar problem has been discussed also in Ref. [180]. Extending a standard approach [20, 181], we apply a mean-field decoupling of the hopping term [first term in Eq. (4.6)],

$$a_{i(A)} \to \psi_A + \delta a_{i(A)}, \qquad a_{i(B)} \to \psi_B + \delta a_{i(B)} \tag{4.7}$$

with the order parameters $\psi_{A,B} \equiv \langle a_{i(A,B)} \rangle$ and the fluctuations $\delta a_{i(A,B)}$. Neglecting the second order fluctuations of the fields, one finds

$$H_J \simeq - 4J \sum_{i \in A} \left(\psi_B a_i + \psi_B^* a_i^\dagger \right) - 4J \sum_{i \in B} \left(\psi_A a_i + \psi_A^* a_i^\dagger \right)$$
$$+ 4N_A J(\psi_A^* \psi_B + \psi_A \psi_B^*) \equiv H_{J0} + 4N_A J(\psi_A^* \psi_B + \psi_A \psi_B^*), \tag{4.8}$$

where N_A denotes the number of sites in the sublattice A. We use H_{J0} as a perturbation to the interaction part of the Hamiltonian (4.6), and neglect for the moment the irrelevant constant shift given by the last term in Eq. (4.8). Since H_{J0} is local, the total Hamiltonian contains only local terms and we can apply perturbation theory in each unit cell. The unperturbed Hamiltonian $H(J = 0)$ is diagonal with respect to the number operators and, hence, the eigenstates of $H(J = 0)$ in each unit cell are $|n_A, n_B\rangle$, where n_A and n_B are the occupation numbers of the sites A and B, respectively. The energy per unit cell is given by

$$E(n_A, n_B) = \frac{U_A}{2} n_A (n_A - 1) + \frac{U_B}{2} n_B (n_B - 1) - \mu_A n_A - \mu_B n_B. \tag{4.9}$$

The ground state corresponds to occupations g_A and g_B determined by the relations $U_\nu (g_\nu - 1) < \mu_\nu < U_\nu g_\nu$, with $\nu = A, B$. The first order contribution of the perturbation H_{J0} vanishes because H_{J0} does not conserve the number of particles, whereas the second order is found to be

$$E^{(2)} = \sum_{(n_A, n_B) \neq (g_A, g_B)} \frac{|\langle g_A, g_B | H_{J0} | n_A, n_B \rangle|^2}{E(g_A, g_B) - E(n_A, n_B)}$$
$$= (4J)^2 \left[\frac{|\psi_B|^2 g_A}{U_A(g_A - 1) - \mu_A} + \frac{|\psi_B|^2 (g_A + 1)}{\mu_A - U_A g_A} + \frac{|\psi_A|^2 g_B}{U_B(g_B - 1) - \mu_B} \right.$$
$$\left. + \frac{|\psi_A|^2 (g_B + 1)}{\mu_B - U_B g_B} \right]. \tag{4.10}$$

Including the previously ignored constant shift and using the fact that at zero temperature the calculated energy is the same as the Helmholtz free energy F, we can write

$$F[\psi_A, \psi_B] = F^{(0)} + \sum_{\mu, \nu = A, B} \psi_\mu^* M_{\mu\nu} \psi_\nu \tag{4.11}$$
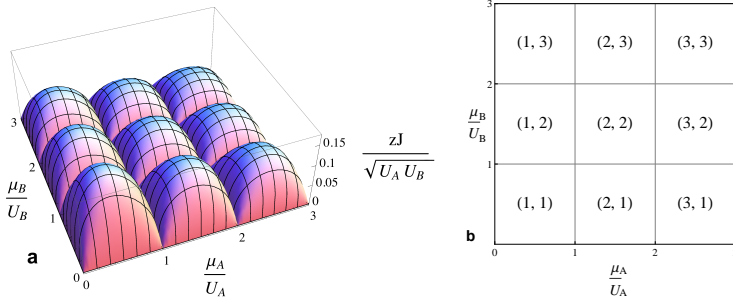
FIGURE 4.6: Mean-field phase diagram in the bipartite lattice. (a) Phase boundaries: inside each lobe there is a Mott insulator phase with occupations that can differ in the two sublattices according to the chemical potentials, above the lobes the gas is superfluid. (b) Configurations of the occupation numbers (g_A, g_B) inside each lobe.

with

$$F^{(0)} = \frac{U_A}{2} g_A(g_A - 1) + \frac{U_B}{2} g_B(g_B - 1) - \mu_A g_A - \mu_B g_B \qquad (4.12)$$

and

$$\mathbf{M} = \begin{pmatrix} \left(\frac{g_B}{U_B(g_B-1)-\mu_B} + \frac{g_B+1}{\mu_B-U_B g_B} \right) J^2 z^2 & zJ \\ zJ & \left(\frac{g_A}{U_A(g_A-1)-\mu_A} + \frac{g_A+1}{\mu_A-U_A g_A} \right) J^2 z^2 \end{pmatrix}. \qquad (4.13)$$

Here, $z = 2d$ is the coordination number of the lattice; in our case $d = 2$ and $z = 4$. According to the (generalized) Landau criterion for continuous phase transitions, the phase boundaries are given by the condition $\text{Det}[\mathbf{M}] = 0$. In the phase diagram shown in Fig. 4.6(a), one observes a series of lobes corresponding to Mott-insulator phases with occupation numbers that can vary in the two sublattices according to the value of the chemical potentials (see also Fig. 4.6(b), where the (g_A, g_B) filling of the Mott lobes is explicitly given). Outside the lobes the system is superfluid.

We now discuss the effect of the additional harmonic trap potential. We set $U_A = U_B = U$, which is a very good approximation for $\theta \lesssim 0.53\, \pi$. In Fig. 4.7, horizontal sections through the mean-field phase diagram are plotted for fixed values of V_0. The lobes for $\mu_B < 0$ correspond to Mott phases with occupations $(g_A, g_B) = (g, 0)$, with g integer. For different values of θ, we also plot the lines $\mathcal{L}(\theta)$ given by

$$\mu_B - \mu_A = \Delta\mu(\theta), \qquad (4.14)$$

where $\Delta\mu(\theta) = E_A - E_B$ is the difference of the local energies E_A and E_B determined through Eq. (4.5). According to the local density approximation,
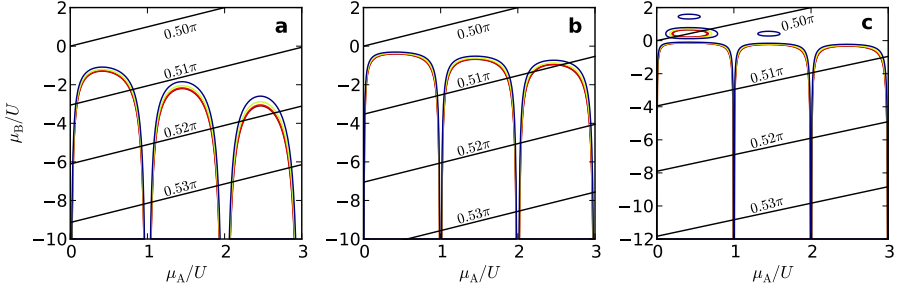
FIGURE 4.7: Sections through the mean-field phase diagram of the bipartite lattice. For (a) $V_0 = 8E_{rec}$, (b) $V_0 = 10E_{rec}$, and (c) $V_0 = 12E_{rec}$, sections through the phase diagram in Fig. 4.6 at fixed values of J/U are shown. In each panel, the small change of the Mott lobe boundaries with θ is indicated by contours of different colors; the largest lobe corresponds to the largest value of θ, i.e. the lowest value of J/U (see Fig. 4.5(a)). The diagonal lines are given by Eq. (4.14), for different values of θ (or equivalently, different values of $\Delta V / V_0$).

one can define a local chemical potential $\tilde{\mu}_i = \mu_{A,B} - m\omega^2 \mathbf{r}_i^2 / 2$ with a maximal value in the center of the trap fixed by the total particle number, which decreases towards the edge of the trap. Hence, the phases encountered locally along a radial path pointing outwards from the trap center are given by the homogeneous phase diagram, when following the lines $\mathcal{L}(\theta)$ towards decreasing values of μ_A / U. The lines $\mathcal{L}(\theta)$ shift to large, negative values of μ_B / U as θ increases. Since the particle density is a monotonous function of the chemical potential, the population of the B sites decreases as θ increases and eventually vanishes. Hence, the density profile evolves into a wedding cake structure where only the A sites are populated, i.e., most atoms contribute to pure A-site Mott shells $(g, 0)$ separated by narrow superfluid films, also with negligible B population (see Fig. 4.8 for an example of density profiles calculated with the Gutzwiller ansatz). The plot also shows that for increasing V_0 the Mott lobes $(g, 0)$ cover an increasing area in the phase diagram, while at the same time the lines $\mathcal{L}(\theta)$ shift towards lower values of μ_B / U.

4.3.3 *Gutzwiller method*

The Gutzwiller ansatz approximation used in this chapter is an extension of the well-known procedure employed for the Bose-Hubbard model in conventional monopartite lattices [182, 183] that takes into account the different local energies for the sites of type A and B. The wave-function is assumed to be a product of single-site wave-functions $|\phi\rangle = \prod_i |\phi_i\rangle$. On each site the ansatz reads

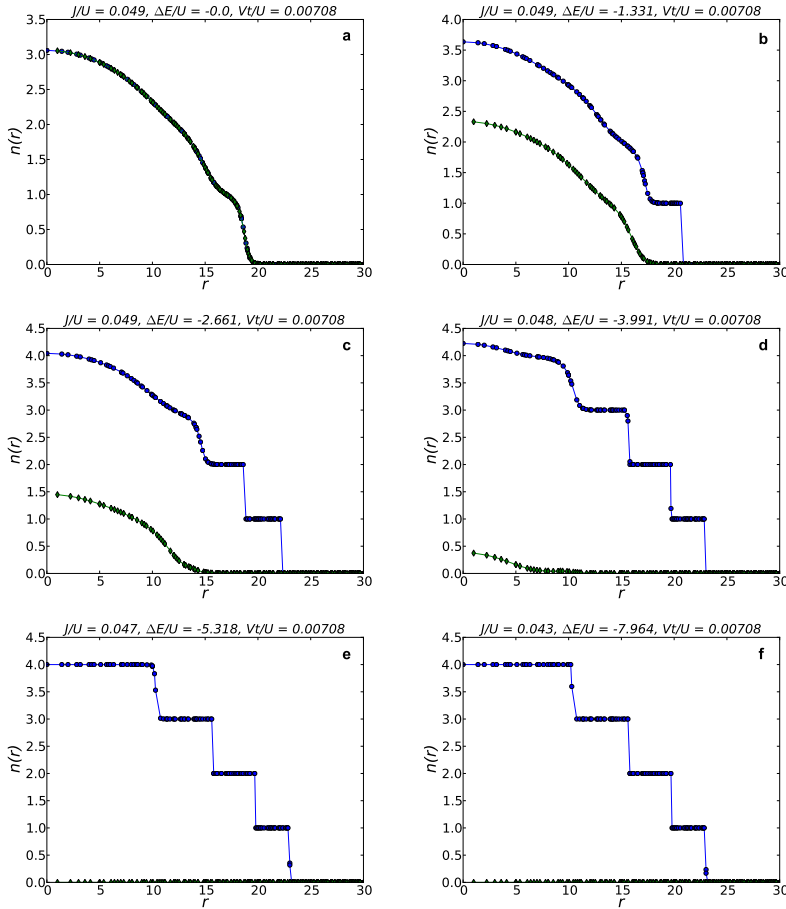$$|\phi_i\rangle = \sum_{n=0}^{\infty} f_n^{(i)} |n\rangle. \tag{4.15}$$

FIGURE 4.8: Density profiles obtained using the Gutzwiller ansatz for an extended 69×69 lattice in the presence of an harmonic trap for (a) $\theta = 0.5$, (b) $\theta = 0.505$, (c) $\theta = 0.51$, (d) $\theta = 0.515$, (e) $\theta = 0.52$, (f) $\theta = 0.53$ at $V_0 = 10E_{rec}$. Circles (diamonds) denote A (B) sites.

We have included states up to $n = 7$ and considered real Gutzwiller coefficients for an extended 69×69 lattice, which is allowed because of the U(1) symmetry and the fact that the ground state cannot have nodes, according to Feynman's no-node theorem.

As shown in the previous section, the mean-field Hamiltonian can be written as a sum of site decoupled local Hamiltonians represented in the local Fock basis, $H_{\mathrm{MF}} = \sum_i H_i$. This statement is true also in the presence of the trapping harmonic potential, since the latter can be represented as a local chemical potential. Each local Hamiltonian needs, as an input, the order parameters of the neighbor sites (ψ_B for the local Hamiltonian on sites

of type A and vice versa). One can thus use the following iterative proce-
dure to determine the ground state at a given value of J/U and $\tilde{\mu}_i/U$: start
with a random guess of the order parameters $\psi_{A,B}$, diagonalize the local
Hamiltonians H_i, take the eigenvectors of the lowest energy state (i.e., the
Gutzwiller coefficients $f_n^{(i)}$), calculate the new order parameters $\psi_i = \langle a_i^\dagger \rangle =$
$\sum_n \sqrt{n+1} f_n^{(i)} f_{n+1}^{(i)}$ and repeat the procedure until convergence. In this way,
we have obtained Fig. 4.8 for the density profiles and Fig. 4.9 to be discussed
in the next section.

4.4   BIPARTITE LATTICE $\Delta V \neq 0$

The visibility measured for fixed V_0 as a function of ΔV (see Fig. 4.2) exhibits
a region of rapid decrease. When the lattice barrier is large, e.g. $V_0 = 12\, E_{rec}$,
a modest detuning $\Delta V \sim 0.25\, V_0$ is able to completely destroy phase coher-
ence with the consequence of a vanishing visibility. At smaller barrier heights,
e.g. $V_0 = 6 E_{rec}$, superfluidity remains robust up to significantly larger val-
ues of ΔV. To explain this behavior, we performed a mean-field calculation
using the Gutzwiller technique outlined in the previous section for the Bose-
Hubbard model given by Eq. (4.2). The values of J and $\Delta\mu = \mu_A - \mu_B$ have
been estimated from the exact band structure and U has been calculated
within the harmonic approximation. The total number of particles has been
fixed to $N = 2 \times 10^3$ and the trap frequency takes into account the waist of
the laser beam. We performed large-scale Gutzwiller calculations in presence
of a trap, thus going beyond Local Density Approximation [182, 183].

In Fig. 4.9(a), we show the evolution of the fraction of particles in the B sites
(which we assumed to be the shallow wells). As ΔV increases, the number of
bosons in the B sites decreases because of the excess potential energy required
for their population. Within the tight-binding description, this is captured by
the increased chemical potential difference between A and B sites as ΔV
grows. Our calculations predict a critical value ΔV_c for which the population
of the B sublattice vanishes. As shown in Fig. 4.9(a), ΔV_c becomes smaller as
V_0 increases. This corresponds to the observation in the phase diagram shown
in Fig. 4.7 that the area covered by the Mott insulating regions with vanishing
B-populations (filling $g_B = 0$) increases as the hopping amplitude is reduced.
The critical values ΔV_c for different values of V_0 are also shown in Fig. 4.2 as
a dashed white line on top of the experimental data for the visibility. This line
consistently lies on experimental points corresponding to constant visibility
($\mathcal{V} \approx 0.5$), where phase coherence is rapidly lost, and suggests the onset of a
new regime.

In Fig. 4.9(b) it is shown that, in addition to the population of the B sites,
also the condensate fraction at the A sites approaches zero beyond the critical
value ΔV_c (see the inset in Fig. 4.9(a) for the total condensed fraction); in this
regime, the density profile displays only sharp concentric Mott shells of the
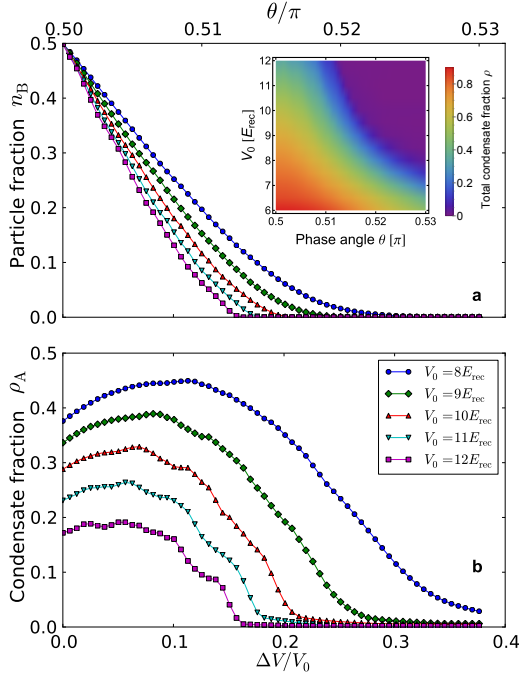
FIGURE 4.9: Gutzwiller results in the trap. (a) Particle number fraction on the B sites (n_B). The inset shows the total condensed fraction $\rho = \sum_i \rho_i / N$. (b) Condensate fraction on the A sites ($\rho_A = \sum_{i \in A} \rho_i / N$, where $\rho_i = |\psi_i|^2$, with ψ_i the mean-field order parameter) as a function of ΔV for increasing values of V_0 and fixed total number of particles $N = 2 \times 10^3$, calculated with the Gutzwiller ansatz. The key shows the color code for both, the curves in (a) and (b).

form $(g_A, g_B) = (g, 0)$ where the integer filling g of the Mott regions can reach $g = 4$ (see Fig. 4.8). This can be understood by considering that in the new regime where B sites are empty, the particles populating A sites can only delocalize (and thus establish phase coherence) by hopping through the intermediate B sites. Since these are second order processes, they are highly suppressed when $\Delta \mu$ is large enough and the system has to become an imbalanced Mott insulator.

In the new Mott-insulating regime, particle-hole pairs are responsible for a non-vanishing visibility, as in the conventional case in absence of imbalance [94]. By performing perturbation theory on top of the ideal Mott-insulating
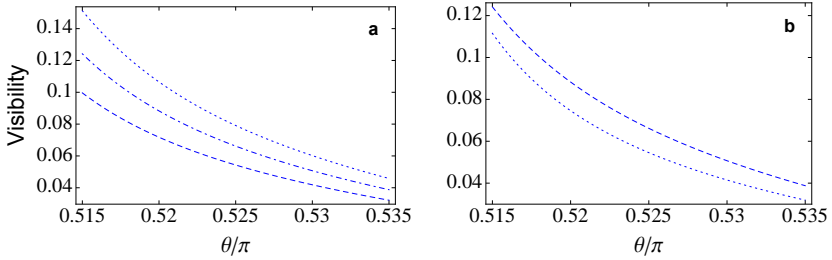
FIGURE 4.10: Visibility curves calculated within perturbation theory for $V_0 = 10.8\,E_{rec}$. (a) Visibility up to second order for average filling $\bar{g} = 2$ (dashed), $\bar{g} = 2.5$ (dash-dotted), $\bar{g} = 3$ (dotted). (b) Comparison of the visibility curves including contributions up to first order (dotted) and up to second order (dashed) for average filling $\bar{g} = 2.5$.

state $|MI\rangle = \prod_{i \in A} |g\rangle_i \prod_{j \in B} |0\rangle_j$, the ground state can therefore be written as (see Appendix C)

$$|\psi_G\rangle = \left(1 - \frac{J^2}{2\Delta^2}\right) |MI\rangle - \frac{J}{\Delta} \sum_{\langle i,j \rangle} a_i^\dagger a_j |MI\rangle \tag{4.16}$$

$$- \frac{2J^2}{U\Delta} \sum_{\langle i,j \rangle_A} a_i^\dagger a_j |MI\rangle - \frac{J^2}{U\Delta} \sum_{\langle\langle i,j \rangle\rangle_A} a_i^\dagger a_j |MI\rangle \,,$$

where $\Delta \equiv U(g-1) + \Delta\mu$. The first term is simply the unperturbed term with a wave function renormalization, whereas the linear term in J describes particle-hole pairs with the particle sitting on the A site and the hole in the neighbor B site, or vice-versa. The last two terms are second order processes that involve intermediate B sites and describe particle-hole pairs within the A sublattice only. This ground state leads to the visibility

$$\mathcal{V} = c_1 J/\Delta + c_2 J^2/U\Delta + c_3 J^2/\Delta^2, \tag{4.17}$$

where $c_1 = -2(\bar{g}+1)(1-r_1)$, $c_2 = 4(\bar{g}+1)(2r_1 + r_2 - 3)$, $c_3 = -4(\bar{g}+1)^2(r_1+3)(1-r_1)$, with $r_1 \equiv \cos(\sqrt{2}\pi) \approx -0.266$ and $r_2 \equiv \cos(\sqrt{8}\pi) \approx -0.858$. The visibility obtained in Eq. (4.17) is of the order 10^{-1} in the highly imbalanced regime for filling between 2 and 3 (see Fig. 4.10(a)). The second order processes contribute significantly, as can be observed in Fig. 4.10(b). In the theory just discussed, we did not include the contributions given by the bare next-nearest-neighbor hopping processes (J_A), despite the fact that the ground state (4.16) effectively includes this type of hopping contributions through virtual transitions. The reason is that the effective hopping processes contribute more substantially to the visibility than the bare ones (not displayed here).

In Fig. 4.11, the experimental data for the visibility (extracted from Fig. 4.2) are plotted for $V_0 = 10.8\,E_{rec}$ and $V_0 = 11.44\,E_{rec}$. By using the average filling
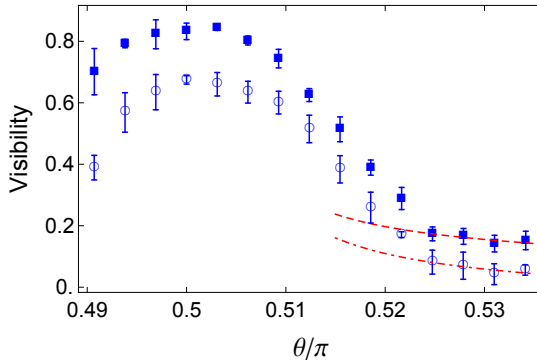
FIGURE 4.11: Comparison of the measured visibility with the theory at large imbalance. The data shown are for $V_0 = 10.8\,E_{rec}$ (squares) and $V_0 = 11.44\,E_{rec}$ (circles). The dashed (dash-dotted) line is obtained by fitting the last four data points with Eq. (4.17) using the average filling $\bar{g}$ as a fitting parameter. We obtain respectively $\bar{g} = 2.75 \pm 0.23$ and $\bar{g} = 3.77 \pm 0.31$. The data for $V_0 = 10.8\,E_{rec}$ are shifted along the vertical axis by 0.1. The error bars represent the statistical variance of typically 4-5 independent measurements.

$\bar{g}$ in the trap as a fitting parameter, we found that the theoretical visibility curve compares reasonably well with the experimental data both in magnitude and scaling behavior, with an average filling of the order $\bar{g} \approx 3$ (see Fig. 4.11). A perturbative description of the visibility data for large θ by means of Eq. (4.17) is only possible in a window $V_0 \approx 11 \pm 1\,E_{rec}$, where sufficient data points are available in the low visibility tail with values of the visibility large enough to be measured with sufficient precision to allow fitting.

4.5 MONOPARTITE LATTICE $\Delta V = 0$

Adjustment of $\Delta V = 0$ produces the special case of a conventional monopartite square lattice, extensively studied in the literature during the past decade [18, 94, 184, 185]. Experiments in 3D cubic lattices have suggested that the formation of Mott shells within the external trap could be associated to the appearance of kinks in the visibility [94, 184], whereas experiments in 2D triangular lattices have rather detected an instantaneous decrease [186]. Arguable attempts were made to interpret small irregularities in the observed visibility in this respect. On the theoretical front, a quantum Monte Carlo study of the 1D trapped Bose-Hubbard model [187] has shown the appearance of kinks in $\mathcal{V}$ as a function of U / J. Unfortunately, this study, employing a trap curvature proportional to J rather than V_0, appears to have limited relevance for experiments. More realistic QMC simulations of 2D and 3D confined systems have been able to quantitatively describe the momentum
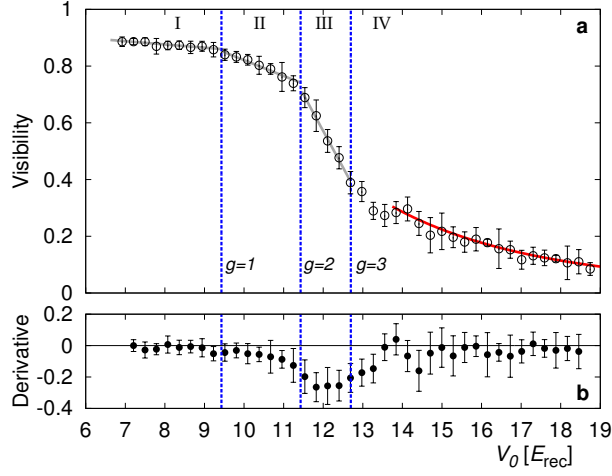
FIGURE 4.12: Visibility measurement in the monopartite lattice. (a) Visibility of ^{87}Rb, plotted as a function of the well depth V_0, for $\Delta V = 0$ and $V_{z,0} = 29\,E_{rec}$. Vertical dashed lines: values of V_0/E_{rec} corresponding to the tips of the Mott lobes with different filling g, as computed through QMC. Grey solid lines in regions I - III are a guide to the eyes, whereas the red line in region IV displays a fit to the function $A(U/zJ)^\alpha$ with $A = 4.0 \pm 0.7$ and $\alpha = -1.00 \pm 0.06$, showing good agreement with the theoretical prediction [94]. The error bars represent the statistical variance of typically 4-5 independent measurements. (b) Numerical derivative of the visibility data; vertical lines as in (a). The error bars are derived from the ones in (a).

distribution [188] and the experimental visibility [177, 189], however with no indications for distinct features associated to Mott shells. To clarify this long standing discussion, we have analyzed the visibility of Fig. 4.2 along the $\Delta V = 0$ trajectory versus V_0 with increased resolution in Fig. 4.12. Guided by an inhomogeneous mean-field calculation indicating that the local filling g is lower than 4, we computed the critical J/U values for the tips of Mott lobes with $g = 1, 2$ and 3, by making use of the worm algorithm as implemented in the ALPS libraries [190–192] (the simulations have been run by Tommaso Comparin). Superimposed upon the experimental data, we mark in Fig. 4.12 with (blue) dashed lines the values of V_0/E_{rec} corresponding to the values of J/U at the tip of the Mott lobes obtained by QMC. As V_0 is increased in Fig. 4.12, four different regimes are crossed. For small values of V_0 (regime I), most of the system is in a superfluid phase. Increasing V_0 yields only little loss of coherence due to increasing depletion, and hence the visibility remains nearly constant. When the first Mott ring with $g = 1$ particle per site is formed, the system enters regime II, where the visibility decreases slowly but notably as the $g = 1$-Mott shell grows. When the second Mott-insulating ring with $g = 2$ arises (regime III), a sharp drop of the visibility

occurs indicating a significantly increased growth of the Mott-insulating part of the system with V_0. Finally, when the third Mott ring with $g = 3$ forms or closes in the center of the trap, only a small superfluid fraction remains in the system, such that the visibility cannot further rapidly decrease with V_0 (regime IV), i.e., a quasi-plateau arises in Fig. 4.12. The red solid line shows that for large V_0 the visibility acquires a $(U/J)^{-1}$ dependence, in agreement with a result obtained by first-order perturbation theory in J/U [94].

4.6 CONCLUSIONS

Several conclusions can be drawn from our experimental and theoretical investigations: for monopartite lattices the visibility comprises characteristic signatures, which can be connected to the position of the tips of the Mott-insulator lobes in a μ/U versus J/U phase diagram calculated by QMC. Mean-field calculations are insufficient, even when the inhomogeneity due to the trap is taken into account. Deforming the unit cell of a bipartite lattice is a means to efficiently tune a transition from a superfluid to a Mott-insulating state. The visibility displays distinct regions with explicitly different slope, as a function of the detuning between the A and B sublattices. A pronounced loss of coherence occurs at the critical value of the detuning ΔV_c, at which the population of the shallow wells vanish. Our work may shed some light also on the behavior of condensed-matter systems, where loss of phase coherence occurs due to a structural modification of the lattice. For example, in $La_{2-x}Ba_xCuO_4$ high-T_c cuprate, superconductivity is weakened at the structural transition from a low-temperature orthorhombic (LTO) into a low-temperature tetragonal (LTT) phase [193]. The same occurs for $La_{2-x-y}Nd_ySr_xCuO_4$ [176]. This structural transition corresponds to a buckling of the oxygen octahedra surrounding the copper sites, which changes the nature of the copper-oxygen lattice unit cell [193]. The critical buckling angle $\theta_c = 3.6 \deg$ for the destruction of superconductivity [194] bears similarities with the critical deformation angle θ_c (or equivalently ΔV_c) found here. Most of the present theoretical studies of high-T_c superconductivity concentrate only on the copper lattice. We hope that our results will inspire further investigations of the specific role played by the oxygen lattice, and its importance in preserving phase coherence.

VARMA PHASES WITH HIGHER-BANDS BECS

We investigate superfluid phases of bosonic atoms in optical lattices with Lieb geometry, which is the well-known 2D Cu-O lattice of high-T_c cuprates. By tuning the difference in the lattice depth between neighboring sites, we design several scenarios with alternating s and p orbitals hybridizing into bands that are gapped from the lowest one. We study the possible condensates arising and show which are the conditions to realize a bosonic analog of the Varma phases. These electronic states of matter that break time-reversal symmetry but preserve the translational symmetry of the lattice were originally proposed by Chandra Varma to explain the pseudo-gap phase of high-T_c cuprates. In particular, we show how one can realize the bosonic analog of Varma's loop state, known to display the anomalous Hall effect for a fermionic system.

5.1 INTRODUCTION

The understanding of the elusive high-temperature supeconductors phase diagram is one of the major challenges of modern physics, which has defeated theoreticians for almost 30 years [26]. Paradoxically, the most mysterious regime in this phase diagram (see Fig. 5.1) is not the superconducting phase itself but the so-called pseudo-gap phase. The understanding of this phase, which precedes the superconducting one and exhibits also a gap, has been longly debated and many proposals have been put forward. Without going into detail, let us just mention the π-flux phase [195] and the Varma phases [95], which were proposed as possible candidates for the ground state in the pseudo-gap regime.

Although both phases break time-reversal symmetry, a fundamental difference between them is that the latter preserves translational symmetry in the lattice while the former breaks it. Within mean-field theory, Varma phases emerge from nearest-neighbor interactions that lead to spontaneous currents in the bonds of the lattice of cuprates, the geometry of which is also known as Lieb lattice. There are many possible current patterns that can arise under these conditions, and one of them (represented in Fig. 5.2(a)) has been used to explain the pseudogap phase of cuprates. This phase breaks time-reversal and inversion symmetry, but mirror symmetry is preserved with respect to the diagonal axis with positive slope. Another possibility (not realized in cuprates) is shown in Fig. 5.2(b). This last state is quite remarkable because it is known to exhibit the quantum anomalous Hall effect (QAHE) [37, 96].
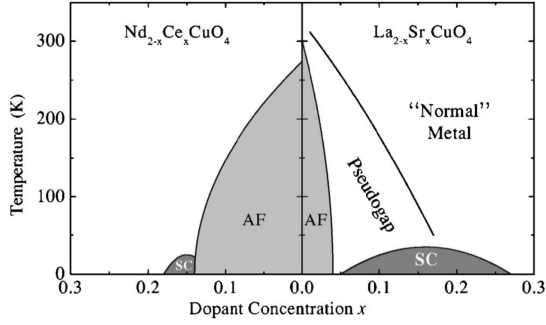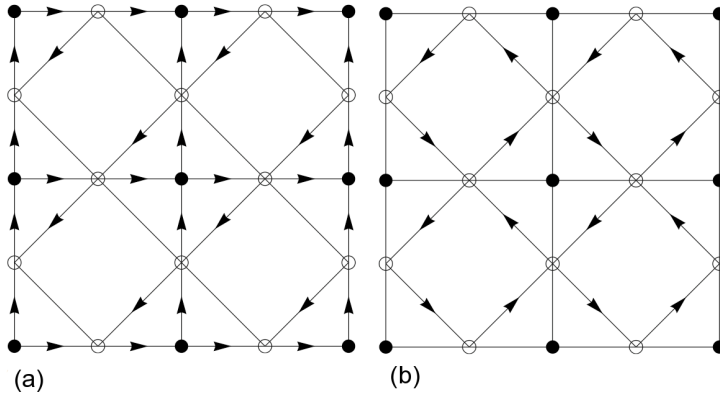
73

FIGURE 5.1: Cuprate phase diagram [26].

FIGURE 5.2: (a) Θ_{II}-loop phase proposed by Varma for the pseudogap phase of cuprates [95]; (b) loop state which has anomalous Hall effect. Figures are adapted from Ref. [37].

The word "anomalous" here is used because no magnetic field is applied and nevertheless the system displays a quantized transverse conductivity.

Indeed, as shown by Haldane [29], quantum Hall phenomena do not require a net magnetic field, but simply broken time-reversal symmetry. This result has been proven at the single-particle level for the case of a honeycomb lattice, where a staggered flux is engineered in such a way that the net flux per plaquette is zero and translational symmetry is preserved. Haldane model describes a topological insulator with quantized transverse conductivity. The state shown in Fig. 5.2(b) is equivalent to Haldane model but on the Lieb lattice: it breaks time-reversal symmetry but does not break translational symmetry. As pointed out by Sun and Fradkin [37], breaking time-reversal symmetry and mirror symmetry while keeping inversion unbroken is a sufficient condition to obtain AHE for a fermionic system.
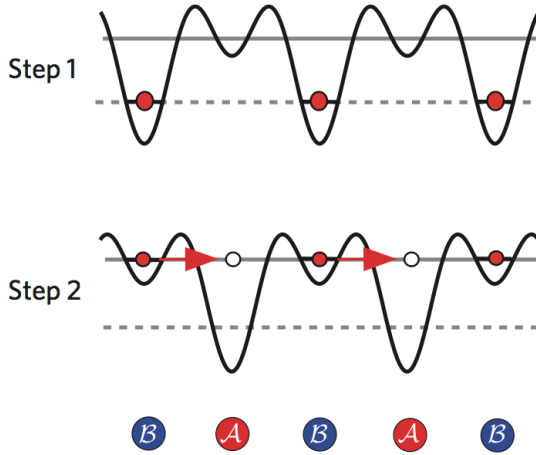
FIGURE 5.3: Swapping procedure to achieve condensation in the second band of an optical lattice. Figure adapted from Ref. [34].

States with broken time-reversal symmetry have been recently discovered in cold-atom systems by forming metastable condensates in higher bands of bipartite optical lattices [34–36]. Since excited states can have a short lifetime, the challenge of establishing phase coherence in the lowest energy state of an excited band has been circumvented by employing a swapping procedure that exploits the bipartite character of a chequerboard square lattice (see Fig. 5.3). In this lattice, there are two classes of sites, $\mathcal{A}$ and $\mathcal{B}$, that alternate as in a chequerboard. The atoms are prepared in the s-like orbitals of the deeper wells (let us call it $\mathcal{B}$), where they are localized. After the swap, which involves a quick change of the optical potential profile such that the $\mathcal{A}$ sites become the deep ones, atoms will be in excited s-like orbitals. To prevent the decay to the lowest states caused by collisions, the swap is performed such that the s-orbitals on the $\mathcal{B}$ sites are energetically resonant with p-orbitals on the neighbor $\mathcal{A}$ sites. Therefore, the atoms start jumping into the p-orbitals, where they establish phase coherence and condense before decaying to the lowest band.

In this chapter, we consider bosons on the Lieb lattice[1]. The geometrical structure of the lattice allows us to discuss bosonic models with alternating s and p orbitals. The time-reversal symmetry breaking occurring in the models that we are going to analyze leads to condensates that share similarities with the Varma phases introduced above. We investigate several scenarios and show under which conditions a bosonic superfluid phase equivalent to Fig. 5.2(b) can be obtained. We discuss a model with four bands that requires

---

[1] At present, the Lieb lattice has not been realized in cold atoms yet. However, some schemes to engineer this lattice currently exist [196].
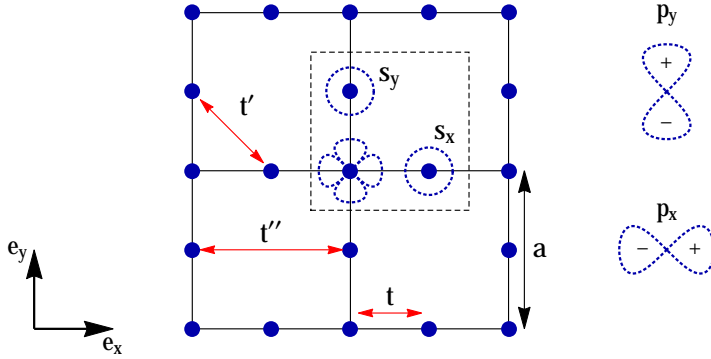
FIGURE 5.4: Lieb lattice with p_x and p_y orbitals on the corners, s orbitals on the edges. The nodal structure of the p_x and p_y orbitals is also shown.

an analysis of the effect of interactions to fix all the free parameters of the ground-state wave function.

5.2   4-BAND MODEL

5.2.1   *Tight-binding Hamiltonian*

In this section, we consider a model with p_x and p_y orbitals on the corners, and s orbitals on each site along the edges that we call respectively s_x and s_y, as shown in Fig. 5.4. Now, there are in total 4 orbitals in the unit cell. The Hamiltonian is

$$H^0 = t \sum_i \sum_{\alpha=x,y} \sum_{\sigma=\pm 1} \sigma\, p_\alpha^\dagger(\mathbf{r}_i) s(\mathbf{r}_i + \sigma\mathbf{e}_\alpha) + \text{h.c.} \tag{5.1}$$
$$- t' \sum_i \sum_{\rho,\sigma=\pm 1} s^\dagger(\mathbf{r}_i + \sigma\mathbf{e}_x) s(\mathbf{r}_i + \rho\mathbf{e}_y) + \text{h.c.}$$
$$- t'' \sum_i \sum_{\sigma=\pm 1} s^\dagger(\mathbf{r}_i + \mathbf{e}_x) s(\mathbf{r}_i + \mathbf{e}_x + 2\sigma\mathbf{e}_y) + \text{h.c.}$$
$$- t'' \sum_i \sum_{\sigma=\pm 1} s^\dagger(\mathbf{r}_i + \mathbf{e}_y) s(\mathbf{r}_i + \mathbf{e}_y + 2\sigma\mathbf{e}_x) + \text{h.c.}.$$

Notice that there is no hopping between s and p_y orbitals along the x axis, namely terms like $p_y^\dagger(\mathbf{r}_i) s(\mathbf{r}_i + \mathbf{e}_x)$ do not appear in the Hamiltonian. This is due to the fact that the s orbitals are even while the p orbitals can be even or odd, depending on which symmetry axis it is considered. The same reasoning applies to the hopping between s and p_x orbitals along the y axis. To simplify the notation, we define $s(\mathbf{r}_i + \mathbf{e}_\alpha) \equiv s_\alpha(\mathbf{r}_i)$. After going to Fourier space, we

introduce the vector $\Psi_{\mathbf{k}} \equiv \left(p_x(\mathbf{k}), p_y(\mathbf{k}), s_x(\mathbf{k}), s_y(\mathbf{k})\right)$ and we thus write the Hamiltonian in the form

$$H^0 = \sum_{\mathbf{k}} \Psi_{\mathbf{k}}^\dagger H_{\mathbf{k}} \Psi_{\mathbf{k}} , \tag{5.2}$$

where

$$H_{\mathbf{k}}^0 = \begin{pmatrix} 0 & 0 & 2it\tilde{s}_x & 0 \\ 0 & 0 & 0 & 2it\tilde{s}_y \\ -2it\tilde{s}_x & 0 & -2t''\tilde{c}_y & -4t'\tilde{c}_x\tilde{c}_y \\ 0 & -2it\tilde{s}_y & -4t'\tilde{c}_x\tilde{c}_y & -2t''\tilde{c}_x \end{pmatrix} . \tag{5.3}$$

We have defined $\tilde{c}_{x,y} \equiv \cos(k_{x,y}/2)$, $\tilde{s}_{x,y} \equiv \sin(k_{x,y}/2)$. One can easily show that the spectrum of the Hamiltonian does not depend on the sign of t or t', i.e. the spectrum is invariant with respect to $t \to -t$ or $t' \to -t'$; the sign of t'' instead matters and will be relevant. From now on we consider units of energy in which $t = 1$.

The band structure of the model (5.3) can be very rich as shown in Fig. 5.5 and several scenarios are possible depending on the value of the hopping parameter t''. The sign of t'' determines whether the minimum of the band is at the X point $(\pi, 0)$ (and equivalently $(0, \pi)$) or at the M point (π, π) (see Fig. 5.5(a)-(b)). When t'' is assumed to be negligible, a degeneracy connecting the X and M points arises (see Fig. 5.5(c)). In Fig. 5.5(d), we show a fitting of our model with a realistic band structure obtained from an optical lattice with Lieb geometry (courtesy of A. Hemmerich). At the moment, regime (b) cannot be realized because it requires the sign inversion of t''.

In the rest of this chapter, we focus on a system of bosons for cases (a) and (b), which can be treated in the weak-coupling limit within mean-field theory. We defer case (c) to future investigation. Nevertheless, it is worth mentioning that case (c) is particularly interesting because the high-degeneracy of the ground state enhances the role of interactions and can lead to non-trivial ground states depending on the filling factors [197].

To analyse the condensation of a gas of bosons for cases (a) and (b), we first compute the eigenstates of the lowest band at the high-symmetry points X (X') and M:

- X point $(\pi, 0)$

$$\left(\frac{i}{2}\left(t'' + \sqrt{4 + t''^2}\right), 0, 1, 0\right) , \tag{5.4}$$

- X' point $(0, \pi)$

$$\left(0, \frac{i}{2}\left(t'' + \sqrt{4 + t''^2}\right), 0, 1\right) , \tag{5.5}$$
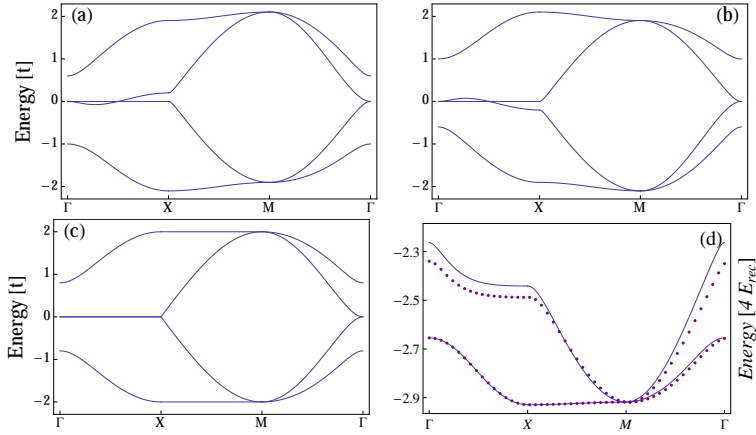
FIGURE 5.5: Energy spectrum of the Hamiltonian (5.3) in units of t for (a) $t' = 0.2$, $t'' = 0.1$, (b) $t' = 0.2$, $t'' = -0.1$, (c) $t' = 0.2$, $t'' = 0$. In (d) we fit the tight-binding model parameters providing the energy spectrum (continuous lines) to the exact band structure of a Lieb optical potential (dots) (courtesy of A. Hemmerich) with values $t = 0.3$, $t' = 0.049$, $t'' = 0.004$ in units of $4E_{rec}$. The fit requires an energy off-set $\xi_p = 0.289$ for the p orbitals. The optical potential provides a band structure of the type (a) (or (c) when t'' can be neglected), while the band structure (b) requires the sign inversion of t'' and is, at present, out of reach.

- M point (π,π)

$$\left(\frac{i}{2}\left(-t'' + \sqrt{4 + t''^2}\right), 0, 1, 0\right)\left(0, \frac{i}{2}\left(-t'' + \sqrt{4 + t''^2}\right), 0, 1\right). \quad (5.6)$$

5.2.2 *Interactions*

Let us now consider onsite interactions for the system of bosons discussed here. To simplify the notation, we indicate the sublattice where the s and p orbitals are as $\mathcal{S}$ and $\mathcal{P}$, respectively. The interaction part of the Hamiltonian can be written in general as [31]

$$H_{\text{int}} = \frac{U_s}{2}\sum_{i\in\mathcal{S}} n_{s,i}(n_{s,i} - 1) + \frac{U_p}{2}\sum_{i\in\mathcal{P}}\left(n_{p,i}^2 - \frac{L_{z,i}^2}{3} - \frac{2}{3}n_{p,i}\right), \quad (5.7)$$

where we defined the total density on the p orbitals

$$n_{p,i} \equiv n_{p_x}(\mathbf{r}_i) + n_{p_y}(\mathbf{r}_i) \quad (5.8)$$

and the angular momentum

$$L_{z,i} = -i\left[p_x^\dagger(\mathbf{r}_i)p_y(\mathbf{r}_i) - p_y^\dagger(\mathbf{r}_i)p_x(\mathbf{r}_i)\right]. \quad (5.9)$$

We have assumed that we can approximate the orbitals with the isotropic harmonic oscillator states:

$$W_{p_x}(\mathbf{r}) = \frac{\sqrt{2\pi}m\omega}{\pi\hbar}\, x\, e^{-\frac{m\omega}{2\hbar}(x^2+y^2)}\,, \tag{5.10}$$

$$W_{p_y}(\mathbf{r}) = \frac{\sqrt{2\pi}m\omega}{\pi\hbar}\, y\, e^{-\frac{m\omega}{2\hbar}(x^2+y^2)}\,, \tag{5.11}$$

$$W_s(\mathbf{r}) = \sqrt{\frac{m\omega}{\hbar\pi}}\, e^{-\frac{m\omega}{2\hbar}(x^2+y^2)}\,. \tag{5.12}$$

Therefore, we may evaluate the interaction parameters

$$U_{p_x} \equiv \int d\mathbf{r}\, |W_{p_x}(\mathbf{r})|^4 = \frac{3}{8}\frac{m\omega}{\hbar\pi}\,,$$

$$U_{p_x p_y} \equiv \int d\mathbf{r}\, |W_{p_x}(x,y)|^2 |W_{p_y}(y,x)|^2 = \frac{1}{8}\frac{m\omega}{\hbar\pi}\,,$$

$$U_s \equiv \int d\mathbf{r}\, |W_s(\mathbf{r})|^4 = \frac{1}{2}\frac{m\omega}{\hbar\pi}\,,$$

$$U_p \equiv U_{p_x} = U_{p_y} = 3U_{p_x p_y}\,,$$

$$U_s = \frac{4}{3}U_p\,. \tag{5.13}$$

The interaction Hamiltonian shows that the states with angular momentum different from zero $L_z = \pm 1$ lower the energy, which is a sort of Hund's rule, therefore fixing the relative phase between p_x and p_y orbitals and leading to a $p_x \pm ip_y$ order that breaks time-reversal symmetry. We will see below in more detail how this happens.

5.2.3   Mean-field solution

The form of the eigenstates at the minima of the spectrum allows us to take an ansatz for the condensate wave function of the form

$$\langle p_\alpha(\mathbf{r}_i)\rangle = \sqrt{\rho_p}e^{i\mathbf{k}_\alpha\cdot\mathbf{r}_i}e^{i\theta_\alpha} \equiv \sqrt{\rho_p}e^{i\theta_\alpha(\mathbf{r}_i)} \tag{5.14}$$

$$\langle s_\alpha(\mathbf{r}_i + \mathbf{e}_\alpha)\rangle = \sqrt{\rho_s}e^{i\mathbf{k}_\alpha\cdot(\mathbf{r}_i+\mathbf{e}_\alpha)}e^{i\phi_\alpha} \equiv \sqrt{\rho_s}e^{i\phi_\alpha(\mathbf{r}_i)}\,, \tag{5.15}$$

where we let the condensate density on p and s orbitals be different in the general case and we introduced global phases to be fixed by minimizing the mean-field energy. For the condensate at the M point one trivially has that $\mathbf{k}_x = \mathbf{k}_y = (\pi, \pi)$, namely all the orbitals will take a contribution from the condensation at M. For the condensate at X and X' the ansatz requires $\mathbf{k}_x = (\pi, 0)$ and $\mathbf{k}_y = (0, \pi)$. This is justified from the fact that the eigenstate at the X point has non-vanishing components only for p_x and s_x orbitals, while the eigenstate at the X' point analogously has non-vanishing components only for p_y and s_y orbitals.

The angular momentum, in the mean-field approximation, takes the simple form

$$\langle L_z(\mathbf{r}_i) \rangle = 2\rho_p \sin[\theta_y(\mathbf{r}_i) - \theta_x(\mathbf{r}_i)]. \tag{5.16}$$

Therefore, the mean-field energy contribution coming from the interaction is

$$E_{\text{int}}^{\text{MF}} \simeq \frac{\rho_p^2 U_p}{3} \{5 + \cos[2\Delta\theta(\mathbf{r}_i)]\} + U_s \rho_s^2, \tag{5.17}$$

where we defined $\Delta\theta(\mathbf{r}_i) = \theta_x(\mathbf{r}_i) - \theta_y(\mathbf{r}_i)$. One immediately notices that interactions are minimized when $\Delta\theta(\mathbf{r}_i) = \pm\pi/2$, which in turn implies that the expectation value of the angular momentum operator $\langle L_z(\mathbf{r}_i) \rangle$ is non-vanishing, a consequence of the time-reversal symmetry breaking.

Let us now define the condensation points as $\mathbf{k}_\alpha \equiv (k_{\alpha x}, k_{\alpha y})$. The mean-field energy contribution coming from the hopping terms reads

$$E_{\text{kin}}^{\text{MF}} = - 4t \sin(k_{xx}/2)\sqrt{\rho_s \rho_p} \sin(\phi_x - \theta_x) \tag{5.18}$$
$$- 4t \sin(k_{yy}/2)\sqrt{\rho_s \rho_p} \sin(\phi_y - \theta_y) - 2t''\rho_s \left[\cos(k_{xy}) + \cos(k_{yx})\right].$$

Notice that there is no contribution from the hopping term t'. This term will however be present in the study of the excitations. Moreover, for the two kind of condensates considered here, we have $\sin(k_{xx}/2) = \sin(k_{yy}/2) = 1$.

Assuming $t > 0$, the minimization of the kinetic energy requires

$$\phi_\alpha - \theta_\alpha = \pi/2. \tag{5.19}$$

In the rest of the chapter we will adopt the gauge choice $\phi_y = \pi/2$.

5.2.4   Condensate in $M = (\pi, \pi)$

In this case, since $\mathbf{k}_x = \mathbf{k}_y = (\pi, \pi)$, one has $\theta_x(\mathbf{r}_i) - \theta_y(\mathbf{r}_i) = \theta_x - \theta_y = \pm\pi/2$. Let us consider the solution with the plus sign (the other solution is the time reversal conjugate) and obtain for the phases

$$\theta_x = \pi/2, \quad \theta_y = 0, \quad \phi_x = \pi, \quad \phi_y = \pi/2. \tag{5.20}$$

The mean-field free energy is

$$E^{\text{MF}} \simeq -8t\sqrt{\rho_s \rho_p} + 4t''\rho_s + \frac{4}{3}\rho_p^2 U_p + U_s \rho_s^2, \tag{5.21}$$

and the order parameters can be written as

$$\langle p_x(\mathbf{r}_i) \rangle = i\sqrt{\rho_p}e^{i\pi\cdot\mathbf{r}_i},$$
$$\langle p_y(\mathbf{r}_i) \rangle = \sqrt{\rho_p}e^{i\pi\cdot\mathbf{r}_i},$$
$$\langle s_x(\mathbf{r}_i) \rangle = -i\sqrt{\rho_s}e^{i\pi\cdot\mathbf{r}_i},$$
$$\langle s_y(\mathbf{r}_i) \rangle = -\sqrt{\rho_s}e^{i\pi\cdot\mathbf{r}_i}. \tag{5.22}$$
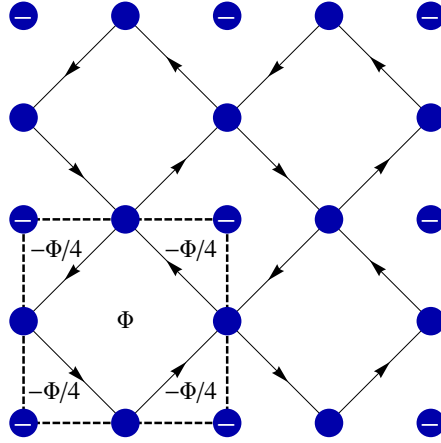
FIGURE 5.6: Superfluid-currents pattern for the condensate in M with rectified angular momenta. The minus signs represents the angular momenta on the sites with p-orbitals pointing all in the same direction. The inner path inside the plaquette corresponds to a flux $\Phi = 2\pi$ threading the surface.

The angular momenta on the $\mathcal{P}$ sites are non-vanishing and have a ferromagnetic structure

$$\langle L_z(\mathbf{r}_i)\rangle = -2\rho_p \,. \tag{5.23}$$

We introduce a bond-current operator $J^{\mu\nu}(i,j)$ that describes the superfluid current between site i (flavor μ) and site j (flavor ν)

$$J^{\mu\nu}(i,j) = -it_{ij}(c_{\mu i}^\dagger c_{\nu j} - c_{\nu j}^\dagger c_{\mu i})\,. \tag{5.24}$$

The expectation value of this operator appears, for instance, in the continuity equation obtained from the Gross-Pitaevskii equation on the lattice. We will therefore calculate the average superfluid current of each bond using the mean-field ansatz $c_{\nu j} \to \langle c_{\nu j}\rangle$. We start from the $p_x - s_x$ bond

$$\langle J^{p_x s_x}(\mathbf{r}_i, \mathbf{r}_i + \mathbf{e}_x)\rangle = -it\sqrt{\rho_s\rho_p}\,(-1+1) = 0\,. \tag{5.25}$$

The same holds for the bonds $p_y - s_y$, so there are no currents running along the edges of the squares. The currents can only be among the $s - s$ bonds, and there are 4 of these bonds in each plaquette,

$$\langle J^{s_x s_y}(\mathbf{r}_i + \mathbf{e}_x, \mathbf{r}_i + \mathbf{e}_y)\rangle = it'\rho_s(-i-i) = 2t'\rho_s\,. \tag{5.26}$$

This is the current that goes from $\mathbf{r}_i + \mathbf{e}_x$ to $\mathbf{r}_i + \mathbf{e}_y$, the direction of which depends on the sign of t'. The other currents in the plaquette read

$$\langle J^{s_x s_y}(\mathbf{r}_i + \mathbf{e}_x, \mathbf{r}_i + 2\mathbf{e}_x + \mathbf{e}_y)\rangle = it'\rho_s(i+i) = -2t'\rho_s,$$
$$\langle J^{s_y s_x}(\mathbf{r}_i + \mathbf{e}_y, \mathbf{r}_i + 2\mathbf{e}_y + \mathbf{e}_x)\rangle = it'\rho_s(-i-i) = 2t'\rho_s,$$
$$\langle J^{s_y s_x}(\mathbf{r}_i + 2\mathbf{e}_x + \mathbf{e}_y, \mathbf{r}_i + 2\mathbf{e}_y + \mathbf{e}_x)\rangle = it'\rho_s(i+i) = -2t'\rho_s. \tag{5.27}$$

In Fig. 5.6, the pattern of superfluid currents and angular momenta (represented by a minus sign) is shown. This ground state breaks time-reversal and mirror symmetry but does not break translational and inversion symmetry [37]. Moreover, if you consider the portion of the plaquette delimited by the bond currents, there is a net flux piercing the surface, while the total flux per plaquette is zero (see Fig. 5.6). The global phase in $\mathbf{r}_i + \mathbf{e}_x$ is $-\pi/2$, whereas in $\mathbf{r}_i + \mathbf{e}_y$ it is π. Therefore, the phase difference across each bond is $\Delta\phi_{\text{bond}} = \pi/2$ and the total phase picked up in a closed path (corresponding to the flux) is $\Phi = 2\pi$.

5.2.5 *Condensate in $X = (\pi, 0)$ and $X' = (0, \pi)$*

In this case, since $\mathbf{k}_x = (\pi, 0)$ and $\mathbf{k}_y = (0, \pi)$, one has $2\left[\theta_x(\mathbf{r}_i) - \theta_y(\mathbf{r}_i)\right] = 2(\mathbf{k}_x \cdot \mathbf{r}_i - \mathbf{k}_y \cdot \mathbf{r}_i + \theta_x - \theta_y) = 2\pi(m-n) + 2(\theta_x - \theta_y) = \pm\pi$, where we defined $\mathbf{r}_i \equiv (m, n)$ with m, n integers. Since the shift $2\pi(m-n)$ does not change the value of the interaction term (proportional to $\cos[2\Delta\theta(\mathbf{r}_i)]$), we find the same solution for the global phases as before

$$\theta_x = \pi/2, \quad \theta_y = 0, \quad \phi_x = \pi, \quad \phi_y = \pi/2. \tag{5.28}$$

The mean-field free energy is

$$E^{\text{MF}} \simeq -8t\sqrt{\rho_s\rho_p} - 4t''\rho_s + \frac{4}{3}\rho_p^2 U_p + U_s\rho_s^2, \tag{5.29}$$

where one has to notice the difference in sign in the term proportional to t'', and the order parameters can be written as

$$\langle p_x(\mathbf{r}_i)\rangle = i\sqrt{\rho_p}e^{i\mathbf{k}_x \cdot \mathbf{r}_i},$$
$$\langle p_y(\mathbf{r}_i)\rangle = \sqrt{\rho_p}e^{i\mathbf{k}_y \cdot \mathbf{r}_i},$$
$$\langle s_x(\mathbf{r}_i)\rangle = -i\sqrt{\rho_s}e^{i\mathbf{k}_x \cdot \mathbf{r}_i},$$
$$\langle s_y(\mathbf{r}_i)\rangle = -\sqrt{\rho_s}e^{i\mathbf{k}_y \cdot \mathbf{r}_i}. \tag{5.30}$$

The angular momenta on the $\mathcal{P}$ sites are non-vanishing and have an anti-ferromagnetic structure

$$\langle L_z(\mathbf{r}_i)\rangle = -2\rho_p \sin[\pi(m-n) + \pi/2] = -2\rho_p(-1)^{m+n}. \tag{5.31}$$

In this ground state, because of the staggered structure, translational sym-
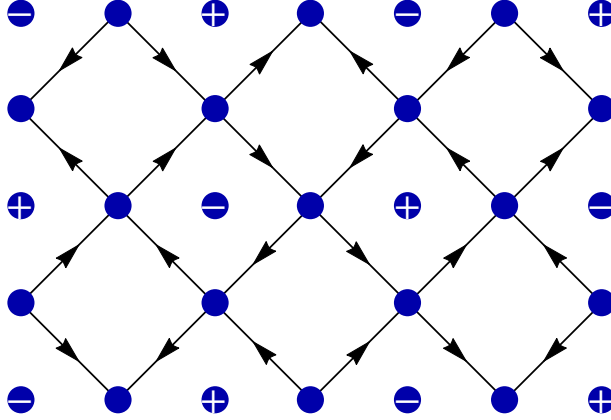
FIGURE 5.7: Superfluid-currents pattern for the condensate in $X - X'$ with staggered angular momenta.

metry is broken. Let us now check the pattern of currents. As before, the currents along the edges will be vanishing. Instead, the currents along the diagonal $s - s$ bonds are finite and read

$$
\begin{aligned}
\langle J^{s_x s_y}(\mathbf{r}_i + \mathbf{e}_x, \mathbf{r}_i + \mathbf{e}_y)\rangle &= it'\rho_s(-i-i)(-1)^{m+n} = 2t'\rho_s(-1)^{m+n} \\
\langle J^{s_x s_y}(\mathbf{r}_i + \mathbf{e}_x, \mathbf{r}_i + 2\mathbf{e}_x + \mathbf{e}_y)\rangle &= it'\rho_s(i+i)(-1)^{m+n} = -2t'\rho_s(-1)^{m+n}, \\
\langle J^{s_y s_x}(\mathbf{r}_i + \mathbf{e}_y, \mathbf{r}_i + 2\mathbf{e}_y + \mathbf{e}_x)\rangle &= it'\rho_s(-i-i)(-1)^{m+n} = 2t'\rho_s(-1)^{m+n}, \\
\langle J^{s_y s_x}(\mathbf{r}_i + 2\mathbf{e}_x + \mathbf{e}_y, \mathbf{r}_i + 2\mathbf{e}_y + \mathbf{e}_x)\rangle &= it'\rho_s(i+i)(-1)^{m+n} = -2t'\rho_s(-1)^{m+n}.
\end{aligned}
\tag{5.32}
$$

The pattern is shown in Fig. 5.7. In the enlarged unit cell one can see that inversion symmetry (with respect to any $\mathcal{P}$ site) is not broken but mirror symmetry is. The difference between this phase and the one found previously is the fact that translation symmetry is now broken while it was not before.

5.2.6 *Bogolyubov theory and topological excitations*

Until now, we have analyzed the possible ground states that the model can have depending on the sign of the hopping coefficient t''. In this section, we are instead interested in calculating the excitation spectrum within Bogolyubov theory. To this intent, each bosonic operator is split into its mean-field expectation value and the fluctuations around it, namely $\phi_i \to \langle \phi_i \rangle + \delta\phi_i$. Only terms up to quadratic order in the fluctuations are retained. Imposing that the terms linear in the fluctuations vanish gives a constraint for the chemical potential.

The quadratic terms coming from the interactions on the $\mathcal{S}$ sites are

$$
\frac{U_s}{2} \sum_{i \in \mathcal{S}} \left(\langle s_i \rangle^2 \delta s_i^\dagger \delta s_i^\dagger + \text{h.c.} + 4|\langle s_i \rangle|^2 \delta s_i^\dagger \delta s_i \right) . \tag{5.33}
$$

On the $\mathcal{P}$ sites there are more possibilities and one finds

$$
\begin{aligned}
\frac{U_p}{2} \sum_{i \in \mathcal{P}} & \left\{ \left[\left(\langle p_{x,i}^\dagger \rangle^2 + \frac{1}{3} \langle p_{y,i}^\dagger \rangle^2 \right) \delta p_{x,i} \delta p_{x,i} + \left(\langle p_{y,i}^\dagger \rangle^2 + \frac{1}{3} \langle p_{x,i}^\dagger \rangle^2 \right) \delta p_{y,i} \delta p_{y,i} \right. \right. \\
& + \frac{4}{3} \langle p_{x,i}^\dagger \rangle \langle p_{y,i}^\dagger \rangle \delta p_{x,i} \delta p_{y,i} + \frac{4}{3} \left. \left(\langle p_{x,i}^\dagger \rangle \langle p_{y,i} \rangle + \langle p_{y,i}^\dagger \rangle \langle p_{x,i} \rangle \right) \delta p_{x,i} \delta p_{y,i}^\dagger \right] + \text{h.c.} \\
& + \left(4 \langle p_{x,i}^\dagger \rangle \langle p_{x,i} \rangle + \frac{4}{3} \langle p_{y,i}^\dagger \rangle \langle p_{y,i} \rangle \right) \delta p_{x,i}^\dagger \delta p_{x,i} \\
& + \left. \left(4 \langle p_{y,i}^\dagger \rangle \langle p_{y,i} \rangle + \frac{4}{3} \langle p_{x,i}^\dagger \rangle \langle p_{x,i} \rangle \right) \delta p_{y,i}^\dagger \delta p_{y,i} \right\} . \tag{5.34}
\end{aligned}
$$

The Hamiltonian is now quadratic in the fluctuations and can be Fourier transformed in the Nambu basis. For the condensate in M we introduce the vector $\delta\psi_{\mathbf{k}} = (\delta p_{x,\mathbf{k}}, \delta p_{y,\mathbf{k}}, \delta s_{x,\mathbf{k}}, \delta s_{y,\mathbf{k}}, \delta p_{x,-\mathbf{k}}^\dagger, \delta p_{y,-\mathbf{k}}^\dagger, \delta s_{x,-\mathbf{k}}^\dagger, \delta s_{y,-\mathbf{k}}^\dagger)$ and obtain

$$
H^{\text{Bog}} = \frac{1}{2} \sum_{\mathbf{k}} \delta\psi_{\mathbf{k}} H_{\mathbf{k}}^{\text{Bog}} \delta\psi_{\mathbf{k}} , \qquad H_{\mathbf{k}}^{\text{Bog}} = \begin{pmatrix} H_{\mathbf{k}}^0 + H^1 & \Delta \\ \Delta^\dagger & H_{-\mathbf{k}}^0 + H^1 \end{pmatrix} , \tag{5.35}
$$

where we defined $H_{\mathbf{k}}^0$ in Eq. (5.3) and

$$
H^1 = \begin{pmatrix} \frac{8}{3} U \rho_p - \mu & 0 & 0 & 0 \\ 0 & \frac{8}{3} U \rho_p - \mu & 0 & 0 \\ 0 & 0 & \frac{8}{3} U \rho_s - \mu & 0 \\ 0 & 0 & 0 & \frac{8}{3} U \rho_s - \mu \end{pmatrix} , \tag{5.36}
$$

$$
\Delta = \begin{pmatrix} -\frac{2}{3} U \rho_p & \frac{2}{3} i U \rho_p & 0 & 0 \\ \frac{2}{3} i U \rho_p & \frac{2}{3} U \rho_p & 0 & 0 \\ 0 & 0 & -\frac{4}{3} U \rho_s & 0 \\ 0 & 0 & 0 & \frac{4}{3} U \rho_s \end{pmatrix} . \tag{5.37}
$$

Notice that we have introduce the chemical potential μ and we defined $U \equiv U_p = \frac{3}{4} U_s$ (see (5.13)). We are going to calculate the chemical potential assuming that $2(\rho_s + \rho_p) = n$, where n is the fixed total density of condensed particles per plaquette and $\mu = \delta E^{\text{MF}}/\delta n$. The non-linearity of the mean-field energy functional (5.21) requires that the chemical potential has to be found numerically. The excitation spectrum is found by diagonalizing the non-Hermitian operator $\sigma_z H_{\mathbf{k}}^{\text{Bog}}$, where $\sigma_z = \text{diag}(1,1,1,1,-1,-1,-1,-1)$,
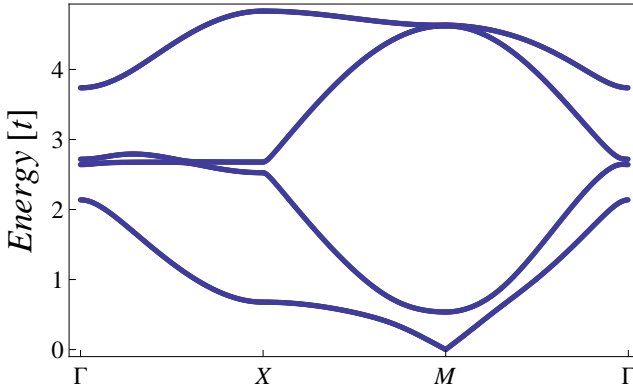
FIGURE 5.8: Bogolyubov spectrum for a model of bosons condensing at the M point. Parameters are chosen in units where $t = 1$: $t' = 0.2$, $t'' = -0.1$, $U = 0.01$. Minimization of the mean-field free energy with the constraint that $\rho_s + \rho_p = 100$ gives $\mu = -1.4347$ and $\rho_s U = 0.5187$.

as discussed in standard textbooks [1]. The eigenvalue problem has therefore the form $\sigma_z H_{\mathbf{k}}^{\text{Bog}} W_{\mathbf{k}}^i = \omega_{\mathbf{k}}^i W_{\mathbf{k}}^i$. The normalization of the eigenvectors is such that $W_{\mathbf{k}}^\dagger \sigma_z W_{\mathbf{k}} = \sigma_z$ and $W_{\mathbf{k}} \sigma_z W_{\mathbf{k}}^\dagger = \sigma_z$, where $W_{\mathbf{k}}$ is the matrix having the eigenvectors $W_{\mathbf{k}}^i$ in its columns. These normalization conditions guarantee that the new operators in which the Hamiltonian is diagonal $\delta\psi'_{\mathbf{k}} = W_{\mathbf{k}} \delta\psi_{\mathbf{k}}$ satisfy bosonic commutation relations.

The excitation spectrum in Fig. 5.8 shows that the degeneracy at the M point is lifted, as it should be since only one continuous symmetry is broken, namely U(1), and therefore there will be only one gapless mode, according to Goldstone's theorem. Moreover, the lowest branch of the spectrum has no degeneracy with respect to the other branches. This makes possible to investigate the existence of a Chern number associated to it [67]

$$c_n = \frac{1}{2\pi} \int \mathrm{d}\mathbf{k}\, F_{xy}(\mathbf{k})\,, \tag{5.38}$$

where the Berry curvature $F_{xy}(\mathbf{k})$ is defined as

$$F_{xy}(\mathbf{k}) = \partial_{k_x} A_y(\mathbf{k}) - \partial_{k_y} A_x(\mathbf{k})\,, \qquad A_\alpha = -i\langle W_{\mathbf{k}}^i | \partial_{k_\alpha} | W_{\mathbf{k}}^i \rangle\,. \tag{5.39}$$

The scalar product used in the definition of the Berry potential A_α has a signature given by the metric σ_z [198]. The computation is performed using the method by Hatsugai [199] and we find a non-zero Chern number $c_n = 1$ for the lowest branch of the Bogolyubov spectrum. The Berry curvature is shown in Fig. 5.9. The system just described proves that a weakly interacting bosonic superfluid can have excitations which possess topological properties, as a non-vanishing Berry curvature, generated by a time-reversal symmetry-
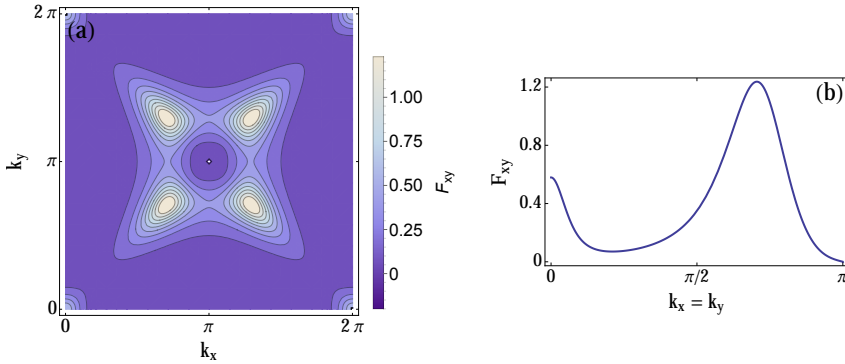
FIGURE 5.9: Berry curvature F_{xy} of the lowest branch of the Bogolyubov spectrum for the condensate at the M point. (a) Berry curvature in the full Brillouin zone. (b) Berry curvature for $k_x = k_y$.

breaking mechanism. To the best of our knowledge, it provides the first ex- ample where such phenomenon occurs. It is known that the dynamics of the excited modes of a condensed gas are influenced by a non-trivial Berry curvature [200, 201], which is a way to reveal the effects of the topological properties.

An interesting question to be addressed is whether for the superfluid in the strongly-interacting limit one could split the excitation branches in a way that a gap between the first and second branch appears for all values of the momenta. In that case, one can expect the presence of edge states inside the gap. Moreover, at low filling and strong interactions the system becomes a Mott insulator with a gap in the excitation spectrum [16, 30, 202]. Also in this case one might wonder whether edge states will appear in the newly formed gap together with persistent currents [97].

We have also analyzed the Bogolyubov spectrum for the $X - X'$ condensate and we have found that there is not a separated lower branch for which a Chern number can be defined. Moreover, the Berry curvature is locally zero and this system does not display topological excitations. The reasons behind the difference between the two condensates is at the moment still not clarified but is expected to be characterized by the symmetries of the Bogolyubov Hamiltonian.

5.3 CONCLUSIONS

In this chapter, we discussed the possibility to realize Varma phases in a two-dimensional Lieb lattice with bosons in the weak-coupling limit. We con- sidered a four-band model with hybridized s and p orbitals sitting on neigh- boring sites, namely s orbitals on the edges of the lattice and p_x, p_y orbitals

on the corners. We found that two ground states are possible depending on whether the minima of the bands are at the $X - X'$ points or at the M point. The ground state for the condensate at the M point is the analogous of the Varma loop state, which shows anomalous Hall effect. The p orbitals display a ferromagnetic order given by rectified angular momenta of the form $p_x + ip_y$ (or its time-reversal state $p_x - ip_y$). Loop currents connect the $s - s$ bonds in each plaquette, such that translational and inversion symmetry are not broken but mirror symmetry is. The other ground state instead breaks translational symmetry and the angular momenta are staggered. The first scenario has a non-trivial excitation spectrum with non-vanishing Berry curvature. These topological features would become observable when probing the collective modes of the gas.

In future, it would be interesting to investigate the strongly-correlated regime, in particular the Mott-insulating phase, where one can expect the appearance of a bosonic Mott insulator with persistent currents and topological excitations.

PROOF OF ODLRO FOR ETA-PAIRING STATES

The existence of off-diagonal long-trange order (ODLRO) and therefore superconductivity requires that some matrix elements of the reduced two-body density matrix ρ_2 are non-vanishing at large distances [107, 109]. To apply this concept to η-superconductivity, let us assume that an eigenstate of the Hamiltonian $|\psi\rangle$ that is of highest-weight of the SU(2) algebra (2.12) exists, i.e.

$$\eta|\psi\rangle = 0, \qquad \eta_z|\psi\rangle = \frac{1}{2}(L-N)|\psi\rangle. \tag{A.1}$$

Such a state must therefore contain a fixed number of doublons and in particular, the first of Eqs. (A.1) reveals that this number is exactly zero. Because of the relations (2.12), we see that the corresponding angular momentum operators for such an SU(2) algebra are

$$\eta \;\rightarrow\; J_+, \qquad \eta^\dagger \rightarrow\; J_-, \qquad \eta_z \rightarrow\; J_z, \tag{A.2}$$

where J_+ and J_- are, respectively, raising and lowering operators of a generic SU(2) algebra and $J_\pm \equiv J_x \pm J_y$. From (A.1) it follows that we are considering a representation of the SU(2) algebra with $j = (L-N)/2$ and the state $|\psi\rangle$ has $m = j$. What about the state with $m = -j$? One can obtain it by several applications of the operator $\eta^\dagger$, i.e. J_-. This happens upon applying the $\eta^\dagger$ operator $L-N$ times. Indeed, the number of holes in $|\psi\rangle$ is precisely $L-N$ and thus $L-N$ is the maximum number of times that one can apply $\eta^\dagger$ to the state $|\psi\rangle$.

Let us recall that in general the following relation holds:

$$J_-|j,m\rangle = \sqrt{j(j+1)-m(m-1)}|j,m-1\rangle, \tag{A.3}$$

where the states $|j,m\rangle$ and $|j,m-1\rangle$ have norm one. We can now define the state $|\psi_n\rangle = (\eta^\dagger)^n|\psi\rangle$, which contains n doublons, and focus on the matrix elements of the density matrix for the state $|\psi_n\rangle$,

$$\langle j\downarrow, j\uparrow |\rho_2| i\downarrow, i\uparrow\rangle \equiv (\rho_2)_{ji} = \frac{\langle\psi|\eta^n c^\dagger_{i\uparrow} c^\dagger_{i\downarrow} c_{j\downarrow} c_{j\uparrow} (\eta^\dagger)^n|\psi\rangle}{\langle\psi|\eta^n (\eta^\dagger)^n|\psi\rangle}. \tag{A.4}$$

To have ODLRO is sufficient to require[1]

$$(\rho_2)_{ji} \xrightarrow{|j-i|\to\infty} A, \tag{A.5}$$

---

[1] Here we are assuming for simplicity that the $\eta^\dagger$ operator is creating doublons with momentum zero. In the η_π case discussed by Yang and that applies to the correlated-hopping model discussed in Chapter 2, one has to substitute $A \to A\, e^{i\pi\cdot(r_i-r_j)}$ and the proof holds as well.

in the thermodynamic limit, with $A \neq 0$. To calculate such a constant, we set [112]

$$A = \lim_{L \to \infty} \frac{1}{L^2} \sum_{i,j} (\rho_2)_{ji}, \tag{A.6}$$

and thus

$$\sum_{i,j} (\rho_2)_{ji} = \frac{\langle \psi_n | \eta^\dagger \eta | \psi_n \rangle}{\langle \psi_n | \psi_n \rangle} = \frac{\langle \psi_{n+1} | \psi_{n+1} \rangle}{\langle \psi_n | \psi_n \rangle} - 2 \frac{\langle \psi_n | \eta_z | \psi_n \rangle}{\langle \psi_n | \psi_n \rangle}. \tag{A.7}$$

You can prove by induction that

$$[\eta_z, (\eta^\dagger)^n] = -n \, (\eta^\dagger)^n, \tag{A.8}$$

and then

$$\langle \psi_n | \eta_z | \psi_n \rangle = \langle \psi_n | \eta_z (\eta^\dagger)^n | \psi \rangle = -n \langle \psi_n | \psi_n \rangle + \langle \psi_n | (\eta^\dagger)^n \eta_z | \psi \rangle =$$
$$= \langle \psi_n | \psi_n \rangle \left[\frac{1}{2}(L - N) - n \right]. \tag{A.9}$$

The last task is to calculate the ratio $\langle \psi_{n+1} | \psi_{n+1} \rangle / \langle \psi_n | \psi_n \rangle$. This can be easily done because of the relation (A.3),

$$\langle \psi_{n+1} | \psi_{n+1} \rangle = ||(\eta^\dagger)^n | \psi \rangle||^2 = \left(\prod_{\alpha=0}^{n} \sqrt{j(j+1) - (m-\alpha)(m-\alpha-1)} \right)^2 \langle \psi | \psi \rangle. \tag{A.10}$$

The ratio yields

$$\frac{\langle \psi_{n+1} | \psi_{n+1} \rangle}{\langle \psi_n | \psi_n \rangle} = j(j+1) - (m-n)(m-n-1). \tag{A.11}$$

After some straightforward algebra in which one must use $j = m = (L - N)/2$, you find

$$\frac{1}{L^2} \sum_{i,j} (\rho_2)_{ji} = \frac{1}{L^2} \left[n(L-N) - n^2 + n \right] = \frac{n}{L} \left(1 - \frac{N}{L} - \frac{n}{L} + \frac{1}{L} \right). \tag{A.12}$$

Calling the doublon density n_d, in the thermodynamic limit $L \to \infty$, with all densities finite, we recover

$$A = n_d(1 - \nu - n_d), \tag{A.13}$$

where we have denoted by ν the electron density of the state $|\psi\rangle$, which is the result by Essler *et al.* [112]. We are interested in the possibility of having ODLRO for the state $|\psi_n\rangle$. Hence, under the assumption that there were no

doublons in the state $|\psi\rangle$, we can consider that ν is the density of single electrons n_f of the state $|\psi_n\rangle$. Thus, using the relation $n_d + n_h + n_f = 1$, we find

$$A = n_d \, n_h \, . \tag{A.14}$$

We can therefore conclude that to have ODLRO we need a finite density of either doublons and holons. This is why, for instance, the upper part of the phase diagram shown in Chapter 2 does cannot contain such state. Moreover, as shown in Ref. [88], the ground-state manifold in the central part of the phase diagram (namely what we called region III in Chapter 2) contains states of the form $|\psi_n\rangle$ which therefore possess ODLRO, as we have just proven in detail.

DERIVATION OF THE EFFECTIVE MODEL

The Hamiltonian of the Hubbard model with a time-dependent interaction reads:

$$
\begin{aligned}
H &= -J \sum_{\langle i,j \rangle, \sigma} (c_{i\sigma}^\dagger c_{j\sigma} + \text{h.c.}) + \bar{U}(t) \sum_i n_{i\uparrow} n_{i\downarrow} \\
&= -J \sum_{\langle i,j \rangle, \sigma} (c_{i\sigma}^\dagger c_{j\sigma} + \text{h.c.}) + U \sum_i n_{i\uparrow} n_{i\downarrow} + U_1 \cos(\omega t) \sum_i n_{i\uparrow} n_{i\downarrow} \\
&\equiv H_J + H_U + H_{\text{d}}(t).
\end{aligned}
\tag{B.1}
$$

Let us define the following Floquet basis

$$
| \{n_{j\sigma}\}, m \rangle = | \{n_{j\sigma}\} \rangle \exp\left(-i\frac{U_1}{\hbar\omega} \sin(\omega t) \sum_j n_{j\uparrow} n_{j\downarrow} + im\omega t \right),
\tag{B.2}
$$

where $| \{n_{j\sigma}\} \rangle$ stands for a Fock state, and compute the Floquet Hamiltonian matrix elements using this basis (the double brackets indicates the time average)

$$
\langle\langle \{n'_{j\sigma}\}, m' | H - i\hbar\partial_t | \{n_{j\sigma}\}, m \rangle\rangle.
\tag{B.3}
$$

The derivative $-i\hbar\partial_t | \{n_{j\sigma}\}, m \rangle$ cancels with $H_{\text{d}}(t) | \{n_{j\sigma}\}, m \rangle$. Let us now examine H_U: we have to calculate the following term

$$
\frac{1}{T} \int_0^T dt\, e^{i\omega t(m-m')} \langle \{n'_{j\sigma}\} | H_U | \{n_{j\sigma}\} \rangle \exp\left[-i\frac{U_1}{\hbar\omega} \sin(\omega t) \sum_j (n_{j\uparrow} n_{j\downarrow} - n'_{j\uparrow} n'_{j\downarrow}) \right].
\tag{B.4}
$$

$| \{n_{j\sigma}\} \rangle$ are eigenstates of H_U, hence $n_{j\sigma} = n'_{j\sigma}$, $\forall j$, and we find

$$
\frac{1}{T} \int_0^T dt\, e^{i\omega t(m-m')} \langle \{n'_{j\sigma}\} | H_U | \{n_{j\sigma}\} \rangle = \langle \{n'_{j\sigma}\} | H_U | \{n_{j\sigma}\} \rangle \delta_{m,m'}.
\tag{B.5}
$$

For the hopping part, we have to calculate

$$
\frac{1}{T} \int_0^T dt\, e^{i\omega t(m-m')} \langle \{n'_{j\sigma}\} | H_J | \{n_{j\sigma}\} \rangle \exp\left[-i\frac{U_1}{\hbar\omega} \sin(\omega t) \sum_j (n_{j\uparrow} n_{j\downarrow} - n'_{j\uparrow} n'_{j\downarrow}) \right].
\tag{B.6}
$$

It is crucial now to evaluate the term $\langle\{n'_{j\sigma}\}|H_J|\{n_{j\sigma}\}\rangle$. The typical form of this quantity is

$$\langle\{n'_{j\sigma}\}|c^\dagger_{i\sigma}c_{k\sigma}|\{n_{j\sigma}\}\rangle\,. \tag{B.7}$$

If $\sigma=\uparrow$ (and correspondingly $\bar{\sigma}\equiv\downarrow$), it implies that $n'_{i\sigma}=n_{i\sigma}+1$, $n'_{i\bar{\sigma}}=n_{i\bar{\sigma}}$, $n'_{k\sigma}=n_{k\sigma}-1$, $n'_{k\bar{\sigma}}=n_{k\bar{\sigma}}$ and $n'_{j\rho}=n_{j\rho}$ for $j\neq i,k$. As a consequence, the density dependent part in the exponential becomes

$$\begin{aligned}
\hat{s} &\equiv \sum_j(n_{j\uparrow}n_{j\downarrow}-n'_{j\uparrow}n'_{j\downarrow}) = n_{i\uparrow}n_{i\downarrow}+n_{k\uparrow}n_{k\downarrow}-(n_{i\uparrow}+1)n_{i\downarrow}-(n_{k\uparrow}-1)n_{k\downarrow}\\
&= -n_{i\downarrow}+n_{k\downarrow}\,.
\end{aligned} \tag{B.8}$$

An analogous result holds for $\sigma=\downarrow$. We now use the integral representation of Bessel functions of first kind:

$$\mathcal{J}_n(x)=\frac{1}{2\pi}\int_{-\pi}^{\pi}dt\,e^{i(x\sin t-nt)}\,, \tag{B.9}$$

define $\tau=\omega t$ and then shift $\tau\to\tau+\pi$. The integral then becomes

$$\frac{1}{2\pi}\int_{-\pi}^{\pi}d\tau\,e^{i(\tau+\pi)(m-m')-i\frac{U_1}{\hbar\omega}\hat{s}\sin(\tau+\pi)}=\frac{(-1)^{m-m'}}{2\pi}\int_{-\pi}^{\pi}d\tau\,e^{i\tau(m-m')+i\frac{U_1}{\hbar\omega}\hat{s}\sin\tau}\,, \tag{B.10}$$

which yields

$$(-1)^{m-m'}\mathcal{J}_{m'-m}\left(\frac{U_1}{\hbar\omega}\hat{s}\right)\,, \tag{B.11}$$

that can be reabsorbed in H_J. In the large frequency limit $\hbar\omega\gg J,U$, the off-diagonal elements of the Floquet Hamiltonian can be (perturbatively) neglected and we can then consider only $m=m'$ and choose $m=0$ in the first Floquet Brillouin zone. Therefore, the approximate form of the Floquet Hamiltonian is

$$H_{\text{eff}}=-J\sum_{\langle i,j\rangle,\sigma}(c^\dagger_{i\sigma}c_{j\sigma}+\text{h.c.})\mathcal{J}_0\left[K(n_{i\bar{\sigma}}-n_{j\bar{\sigma}})\right]+U\sum_i n_{i\uparrow}n_{i\downarrow}\,, \tag{B.12}$$

where we defined $K\equiv U_1/\hbar\omega$.

PERTURBATIVE APPROACH FOR THE VISIBILITY IN THE ASYMPTOTIC LIMIT.

The regime where the imbalance between A and B sites is large can be studied using perturbation theory up to second order [203], when the filling is chosen to be integer in the homogeneous case. In the limit where the hopping term is neglected (which is also the mean-field ground state), the ground state is given by a perfect Mott insulator of the form $(g_A, g_B) = (g, 0)$

$$|MI\rangle = \prod_{i \in A} |g\rangle_i \prod_{j \in B} |0\rangle_j. \tag{C.1}$$

Let us start from the first-order term. The only non-vanishing terms are the ones for which a particle is removed from a site A and moved to one of the nearest-neighbor B sites. The energy difference is $\Delta = U(g-1) + \Delta\mu$ and the first-order correction has thus the form

$$-\frac{J}{\Delta} \sum_{\langle i,j \rangle} a_i^\dagger a_j |MI\rangle. \tag{C.2}$$

The quadratic correction is such that a particle is removed from an A site, moved to a nearest-neighbor B site and from there it is transferred again to an A site that is different from the original one. The final A site can be a nearest-neighbor A site or a next-nearest-neighbor one. The correction becomes

$$-\frac{2J^2}{U\Delta} \sum_{\langle i,j \rangle_A} a_i^\dagger a_j |MI\rangle - \frac{J^2}{U\Delta} \sum_{\langle\langle i,j \rangle\rangle_A} a_i^\dagger a_j |MI\rangle. \tag{C.3}$$

The ground state is therefore

$$|\psi_G\rangle = \left(1 - \frac{J^2}{2\Delta^2}\right) |MI\rangle - \frac{J}{\Delta} \sum_{\langle i,j \rangle} a_i^\dagger a_j |MI\rangle - \frac{2J^2}{U\Delta} \sum_{\langle i,j \rangle_A} a_i^\dagger a_j |MI\rangle$$

$$- \frac{J^2}{U\Delta} \sum_{\langle\langle i,j \rangle\rangle_A} a_i^\dagger a_j |MI\rangle, \tag{C.4}$$

where the first term is simply the unperturbed term with a wave function renormalization.

We can now calculate the momentum distribution

$$S(\mathbf{k}) = \frac{1}{N_s} \sum_{i,j} e^{i\mathbf{k}\cdot(\mathbf{r}_i - \mathbf{r}_j)} \langle a_i^\dagger a_j \rangle, \tag{C.5}$$

where N_s is the number of unit cells in the system. The visibility $\mathcal{V}$ is calculated at momenta $k_{\max} = (0,0)$ and $k_{\min} = (\sqrt{2}\pi, \sqrt{2}\pi)$. Therefore,

$$S_{\max} = \left(1 - \frac{J^2}{\Delta^2}\right)g - 8g(g+1)\frac{J}{\Delta}\left(\frac{3J}{U} + 1\right), \tag{C.6}$$

$$S_{\min} = \left(1 - \frac{J^2}{\Delta^2}\right)g - 4g(g+1)\left[\frac{J}{\Delta}(r_1 + 1) + \frac{2J^2}{U\Delta}(2r_1 + r_2)\right], \tag{C.7}$$

where $r_1 \equiv \cos(\sqrt{2}\pi) \approx -0.266$ and $r_2 \equiv \cos(\sqrt{8}\pi) \approx -0.858$, and we eventually find

$$\begin{aligned}
\mathcal{V} =& (S_{\max} - S_{\min})/(S_{\max} + S_{\min}) \\
=& -2(g+1)(1-r_1)\frac{J}{\Delta} + (g+1)(2r_1 + r_2 - 3)\frac{4J^2}{\Delta U} \\
& - 4(g+1)^2(r_1 + 3)(1 - r_1)\frac{J^2}{\Delta^2}.
\end{aligned} \tag{C.8}$$

SUMMARY

In extreme conditions, matter can behave in a very unexpected way compared to what we are used to experience on a daily basis. In this thesis, we discuss atomic gases at very low temperatures, just a few millionths of degrees above the absolute zero, much colder than the outer space temperature of 2.7K. When temperatures are lowered so much, the laws of Quantum Mechanics kick in and new remarkable phenomena manifest.

The focus of this work is on the study of quantum phase transitions. We are used to observe phase transitions in ordinary life. For instance, by increasing the temperature, metals or ice will melt. In this example, temperature drives a change in the symmetry of the material, from an ordered crystalline structure to a disordered system, namely a liquid. Quantum phase transitions manifest similarly as a change in the symmetry of the system, however thermal fluctuations are not responsible for this to happen, but quantum fluctuations. For instance, the increase of the strength of interactions in a bosonic gas can drive the system from a superfluid to an insulator. Throughout this thesis, we do not consider the effects of temperature and we assume that the gases are so cold that the effective temperature is exactly the absolute zero.

Atoms can be classified as bosons or fermions, depending whether their spin is integer or half-integer, respectively. The former are *social* atoms, meaning that they can occupy the same state: for instance, more than one identical atom can have the same velocity; the latter are atoms that prefer to *avoid* each other: using the same example as before, each identical fermion must have a different velocity. Fermions could move at the same velocity if they were not identical, for instance in a mixture of ^{40}K and ^{6}Li. The first part of this thesis deals with quantum phase transitions for fermionic atoms, while in the second part we discuss bosonic atoms.

Systems of cold atoms are a suitable tool to simulate models of interest because they can be tuned with a high control. They can therefore be used to observe or understand new physical phenomena. For instance, an important goal would be to unveil the mystery behind high-temperature superconductors, which are believed to be described by the Hubbard model. In this paradigm of quantum simulation, one wants to mimic what electrons (which are fermions) do in crystals. In a cold-atomic setup, the fermionic atoms move into a crystal of light realized by counter-propagating laser beams, the so-called optical lattice.

The high degree of control also allows one to play with the dimensionality of the system. One can therefore constrain the atoms to move on a plane or on a line by inhibiting the motion in the other directions via a strong confinement. In this way, very peculiar quantum phases can arise. For example,

when moving on a line, atoms cannot avoid each other and only a collective behavior is possible. Fermions typically are described by a new type of liquid, known as Luttinger liquid. Moreover, Mermin-Wagner theorem does not allow long-range order to appear in low-dimensional systems, and for this reason proper superfluidity or superconductivity cannot appear.

In the Introduction, we discuss the status of the field of cold atoms and its most recent developments. We focus on quantum simulation, time-dependent schemes used to engineer models of interest and the realization of exotic superfluids in higher energy states that break time-reversal symmetry.

In Chapter 2, we discuss how to realize a system of fermions on a lattice with additional interaction terms compared to the conventional Hubbard model. These new interactions affect the rate at which the atoms jump between neighboring sites and allow the model in one spatial dimension to have a ground state with unconventional superconductivity, known as η-superconductivity. This generalized Hubbard model is obtained by modulating the interactions with time.

In Chapter 3, we consider fermions loaded on a one-dimensional optical lattice with a unit cell containing two sites. The bipartite character of this lattice is described by hopping rates alternating in magnitude. With one particle per site, the system is a band insulator. By shaking the lattice one can dynamically obtain a quantum phase transition from the insulating phase to an unconventional metal with four Fermi-points.

In Chapter 4, we study a system of bosons in a two-dimensional square optical lattice. The unit cell contains two sites that differ by an energy offset. Since atoms prefer to stay in the deeper wells, the relative population of neighboring wells is affected. This system is realized in the experimental laboratory of Prof. Hemmerich in Hamburg and it is observed that superfluidity is lost when the detuning of the neighboring wells is sufficiently large. We model this system and describe it quantitatively concluding that the loss of superfluidity coincides with the regime in which the population in the higher wells disappears. The system becomes a Mott insulator with imbalanced density.

In Chapter 5, we study bosons in an unconvential geometry in two dimensions: the Lieb lattice. This is the lattice of the Cu-O plane in a class of high-temperature superconductors called cuprates. However, we focus on a system of bosons in an excited energy band and we analyze minimal models and the type of superfluid phases that can arise. Since in higher bands time-reversal symmetry can be broken, this system can realize the bosonic counterparts of the so-called Varma phases, which are proposed to explain the pseudo-gap phase of high-temperature superconductors. Among several possibilities, we find a bosonic Varma phase with topological excitations.

SAMENVATTING

Onder extreme omstandigheden kan materie zich anders gedragen dan dat we in het dagelijks leven gewend zijn. In dit proefschrift beschouwen we een voorbeeld van een dergelijk systeem, namelijk koude, atomaire gassen bij extreem lage temperaturen van ongeveer een miljoenste graad Kelvin boven het absolute nulpunt. Bij deze temperaturen die veel lager zijn dan de 2.7 Kelvin van de kosmische achtergrondstraling, gelden de wetten van de kwantummechanica en worden bijzondere fenomenen zichtbaar.

In dit proefschrift ligt de nadruk op kwantumfaseovergangen. Dagelijks hebben wij ook met faseovergangen te maken, denk aan het smelten van metalen of ijs door verhoging van de temperatuur. Een kenmerk van faseovergangen is dat de symmetrie van het systeem gedurende de transitie verandert. Bij de genoemde voorbeelden gaat het metaal of ijs van een geordend kristal naar een ongeordende vloeistof. Kwantumfaseovergangen worden ook gekarakteriseerd door het veranderen van de symmetrie van het systeem. Alleen wordt dat in dit geval niet veroorzaakt door fluctuaties in de temperatuur, maar door zogenaamde kwantumfluctuaties. Een voorbeeld van een systeem met een kwantumfaseovergang is een koud gas van bosonen. In dit systeem kan een toename van de interacties ervoor zorgen dat er een overgang plaatsvindt van een supervloeistof naar een isolator. In het vervolg van dit proefschrift verwaarlozen we de temperatuureffecten. We nemen dus aan dat de atomen dusdanig koud zijn dat ze zich hetzelfde gedragen als op het absolute nulpunt.

Het gedrag van een deeltje wordt mede bepaald door zijn spin. Deeltjes met heeltallige spin, de zogenaamde bosonen, zijn *sociale* deeltjes en kunnen dezelfde toestand bezetten. Een voorbeeld is een gas van identieke bosonen die allen dezelfde snelheid hebben. Daarentegen kunnen identieke deeltjes met halftallige spin, de zogenaamde fermionen, niet in dezelfde toestand zitten. Identieke fermionen kunnen dus niet dezelfde snelheid hebben. Dit principe is echter alleen van toepassing voor identieke fermionen en in een mengeling van ^{40}K en ^{6}Li kunnen fermionen wel bewegen met dezelfde snelheid. In het eerste gedeelte van dit proefschrift bekijken we kwantumfaseovergangen van fermionen en in het tweede gedeelte behandelen we bosonen.

Systemen die bestaan uit koude atomen zijn zeer geschikt om het gedrag van verschillende interessante modellen te bestuderen. Dit komt omdat de fysische eigenschappen met grote precisie kunnen worden ingesteld. Hierdoor kunnen in deze systemen nieuwe fenomenen voor het eerst worden geobserveerd. Koude atomen kunnen ook worden gebruikt om bepaalde fenomenen beter te begrijpen, zoals de fysica omtrent hoge-temperatuur supergeleiders. Met behulp van kwantumsimulaties kunnen we het gedrag van elek-

tronen in kristalstructuren nabootsen. Door gebruik te maken van lasers die in tegengestelde richting bewegen, kan deze kristalstructuur ook worden bewerkstelligd in systemen die uit koude atomen bestaan. Hierdoor ontstaat er een optisch rooster, waarbij de atomen in een kristalstructuur van licht bewegen.

Doordat het gedrag van atomen bij lage temperaturen relatief makkelijk kan worden gemanipuleerd, is het ook mogelijk om de dimensionaliteit van het systeem te veranderen. Door de bewegingsvrijheid van atomen in één of meerdere richtingen te beperken, kunnen de deeltjes zich alleen voortbewegen op een lijn of in een vlak. Met behulp van deze technieken kunnen systemen worden gemaakt die zeer speciale kwantumfaseovergangen bevatten. Als de atomen zich bijvoorbeeld alleen op een lijn kunnen verplaatsen, is het onmogelijk elkaar te ontwijken. Het gevolg is dat de atomen zich alleen als één collectief kunnen voortbewegen. In het geval van fermionen gedragen de deeltjes zich dan als een nieuw soort vloeistof, namelijk een Luttinger vloeistof. Verder volgt uit de stelling van Mermin-Wagner dat het onmogelijk is dat er een correlatie is tussen atomen, die zich op grote afstand van elkaar bevinden. Hierdoor is echte supergeleiding of superfluïditeit onmogelijk.

In de introductie van dit proefschrift geven we een overzicht van het onderzoek in het vakgebied van koude atomen en verder zullen ook recente ontwikkelingen aan bod komen. Hierna beschouwen we kwantumsimulaties en tijdafhankelijke schema's om bepaalde modellen te realiseren. Ook bekijken we exotische supervloeistoffen die zich in hoog energetische toestanden bevinden, waardoor invariantie onder tijdsomkering niet meer mogelijk is.

In Hoofdstuk 2 bespreken we verschillende manieren om een optisch rooster met fermionen te maken, waarbij in vergelijking met het normale Hubbard model meerdere interacties zijn toegevoegd. Dit beïnvloedt de frequentie waarmee atomen tussen aanliggende roosterpunten bewegen. In één dimensie kan dit ook leiden tot een grondtoestand met een bijzondere vorm van supergeleiding, namelijk η-supergeleiding. Dit gegeneraliseerde Hubbard model kan worden gemodelleerd door de interacties in tijd te variëren.

Vervolgens bekijken we in Hoofdstuk 3 fermionen in een ééndimensionaal rooster dat bestaat uit eenheidscellen met twee roosterpunten. Door de sterkte van de frequentie waarmee de atomen tussen de roosterpunten bewegen te laten alterneren, kunnen we dit systeem beschrijven. Als er zich precies één deeltje op een roosterpunt bevindt, is het systeem een bandisolator. Door het rooster te schudden, vindt er een dynamische kwantumfaseovergang plaats van een isolator naar een onconventioneel metaal met vier Fermipunten.

In Hoofdstuk 4 bestuderen we het gedrag van bosonen in een tweedimensionaal vierkant optisch rooster. Tussen de twee roosterpunten van een eenheidscel kan een energieverschil zitten. Dit kan gevolgen hebben voor de relatieve bezetting van atomen op aanliggende roosterpunten, omdat de atomen zich het liefst bevinden op plaatsen met de laagste energie. In een ex-

periment van prof. Hemmerich uit Hamburg is aangetoond dat in dit systeem de superfluïditeit verloren gaat als het energieverschil tussen aanliggende punten te groot wordt. We geven een kwalitatieve beschrijving van dit systeem en we vinden dat het verlies van superfluïditeit overeenkomt met het regime waar de roosterpunten met de grootste energie niet bezet zijn. In dit geval is het system een Mottisolator, waarbij de dichtheid in de verschillende roosterpunten ongelijk is.

Tot slot onderzoeken we in Hoofdstuk 5 bosonen in een meer onconventionele tweedimensionale geometrie, namelijk het Lieb rooster. Dit rooster van het Cu-O vlak is gerelateerd aan een bepaalde klasse van hoge-temperatuur supergeleiders, de zogenaamde cupraten. In het bijzonder bestuderen we de bosonen in een aangeslagen toestand en we analyseren de verschillende soorten superfluïde fases die kunnen ontstaan. Omdat in hogere banden invariantie onder tijdsomkering verloren gaat, kan in dit systeem een bosonische tegenhanger van de Varmafase gerealiseerd worden. Deze Varmafase kan een mogelijke verklaring geven voor het pseudogat dat we vinden in hoge-temperatuur supergeleiders. Van de vele mogelijke Varmafases vinden we een bosonische variant met topologische excitaties.

ACKNOWLEDGMENTS

I am grateful to my supervisor, Cristiane Morais Smith, for the opportunity to work with her and pursue original and fascinating research while living in such a stimulating and friendly environment. Optimism is a quality that I sometimes lack, but I have always known that I could find it in your office. Thank you once more for all the inspiring conversations, the enthusiastic attitude towards physics (but not only), the millions of good-hearted advices and all the help that I have received from you!

Special thanks go to my collaborators, whom I hope I can keep working together with. To Andreas Hemmerich, especially for the patience in explaining to us, poor theorists, how the real world works during the many enlightening discussions over the phone. To Gia Japaridze, with whom I have truly enjoyed learning and doing physics, in particular during my visit in Tbilisi. It has been a fascinating interaction and you have been a great host. To Charles Creffield, for being patient with me every time I was killing a running job on the computer and for the nice discussions over Floquet theory, and not only, during your stay in Utrecht. To Tommaso Comparin and Daniele Malpetti, who have been my first students and whom I enjoyed very much to supervise. You must know that I learned a lot from you too. To Matthias Ölschläger and Thorge Kock for producing the nice data that I was given the opportunity to analyze and to Netanel Lindner for the inspiring conversations that we have had across the world.

I want to thank also the scientists that I have met in my journeys around the globe and whom I enjoyed discussing and spending time with. An incomplete list includes: Alex Petrescu, André Eckardt, Arianna Montorsi, Brandon Anderson, Chiara Menotti, Dmitry Efimkin, Ewelina Hankiewicz, Fernanda Pinheiro, George Martins, Gilles Montambaux, Iacopo Carusotto, Ignacio Cirac, Jean-Noël Fuchs, Jonas Larson, Karyn Le Hur, Leonardo Fallani, Luis Santos, Marcello Dalmonte, Marco Roncaglia, Marco Polini, Mark Goerbig, Meera Parish, Nigel Cooper, Peter Barmettler, Philipp Hauke, Pietro Massignan, Sandro Stringari, Sebastian Greschner, Sebastian Huber, Thierry Giamarchi and many others.

I would like to thank the present and past members of Cristiane's group with whom I have shared nice moments in the institute or outside and happy Sinterklaas dinners (special thanks to Stefan for the lamb!!): Anton, Carmine, Dima, Emilio, Guido, Leandro, Lih-King, Natália, Ralph, Vladimir, Wouter.

I would like to thank my officemates, Arie-Willem and Benedetta. You have been really a nice company to share everyday's work with, to keep the atmosphere very friendly and fun, even when our life looked miserable because nothing was working, to discuss little Mathematica problems or big existen-

tial ones. In particular, I want to thank Arie-Willem for translating the Summary in Dutch.

I would also like to thank the present and past members of the Institute of Theoretical Physics for the enjoyable atmosphere. An incomplete list includes Alessandra, Alessandro, Andrew, Anja, Anne, Aron, Bram, Carolin, Chiara, Chris, Christoph, Clement, Dražen, Drian, Erik, Flavio, Giuseppe, Hai-Qing, Igor, Jan, Jasper, Javier, Jeffrey, Jiansen Zheng, Jildou, Joris, Jules, Kiril, Lei Liao, Leihua Liu, Liuba, Marcos, Martijn, Mathijs, Nava, Nick, Niklas, Olga, Olof, Panos, Phil, Philipp, Pietro, Piotr, Rick, Roberto, Sandeep, Sela, Simonas, Simone, Stefan, Stijn, Tara, Tatjana, Thomas, Tuna, Vivian, Watse, Wellington, Wilke and many others. I also want to thank the academic staff that I have met either as undergraduate student or during the years of my PhD: Bernard de Wit, Debabrata Panja, Dirk Schuricht, Enrico Pajer, Eric Laenen, Gerard Barkema, Gerard 't Hooft, Gleb Arutyunov, Renate Loll, Henk Stoof, Lars Fritz, Paul van der Schoot, Rembert Duine, René van Roij, Stefan Vandoren, Tomislav Prokopec, Umut Gürsoy. I would like to thank the supporting staff for the help provided over the years to solve minor and major problems: Els, Joost, Olga, Riny and Wanda.

Special thanks go to the friends that I have made in these years spent in Utrecht. To Anna, Riccardo and Shima with whom I have shared so many experiences, trips, fights, food (ricotta salata and caponata have to be mentioned here) and memorable episodes. I know I can always count on you, guys! I need to thank you in particular for not killing me all the times I was impossible to deal with (basically most of them), therefore allowing me to finish this PhD alive. To Jogundas for all the nice discussions, the crazy random comments and all the support I have received in these years. To Franz and Luìs whom I have shared some unforgettable experiences with in the first years of my PhD. To Carlo and Gosia, thanks for all the mocking and the fun that we have when we hang out, it will be dearly missed (sarcasm..). To Giuliana and Michele, I have enjoyed your company a lot in the few months that we have been knowing each other and I hope we can see each other soon again - in Sicily!-.

To the dear friends who have moved out of the Netherlands, in particular Magda and Michela. I have valued your friendship very much and you have been really missed in these last years.

To my favourite housemates Angie and I-Wen.

To many people who have crossed my path in the Netherlands: Andrea, Bruno, Chiara, Christina, Denia, Daniel, Dora, Federico, Gaetano, Gianrocco, Giuseppe, Irina, Jacopo, Joanna, Jorgos, Laura, Laurinha, Lisa, Marco, Matteo, Paolo, Pasquale, Sandro, Stefano, Yuki and many others..

I want to thank all the friends back in Italy or around the world that I rarely see but, when it happens, we know we can have a lot of fun together: Andrea, Angelo, Caterina, Cinzia, Daniela, Giada, Gigi, Gioele, Giuseppe, Mariella, Martina, Ornella, Paolo, Peppe G., Peppe S., Piero, Salvo, Salvuccio, Serafino,

Simona, Vincenzo and many others. In particular, I want to thank the ones who have come to my defence: Carla, Ciccio, Claudio, Emanuele, Gaspare, Gianni, Giovanna, Lorena, Mariaconcetta, Vito.

Finally, but most importantly, I want to thank my mother Paola and my father Biagio for all the support that I have received and all the pride that you have always shown over the years, despite the distance separating us or the technological limits of the communication media (worth mentioning the huge improvement provided by Whatsapp). Moreover, I want to thank all my relatives that always have good words to send me or share moments of joy in the few occasions that we have to see each other. In particular, I want to thank who made the big effort to take a plane and travel to this foreign and "dangerous" country to come for my defence: Ada, Ciccio, Emanuel, Marina.

CURRICULUM VITAE

I was born on April 11th, 1986 in Carini, a small town near Palermo in Sicily. I attended the Liceo Scientifico Santi Savarino in Partinico where I graduated in 2005.

In Fall 2005, I was admitted into the Scuola Superiore di Catania, a special structure for higher education of the University of Catania, after a selective admission test. At the same time, I enrolled in the Bachelor program in Physics at the University of Catania. As a student of the Scuola, I had to attend additional courses and to start early research activities. I worked in the Laboratory of Complex Systems with Prof. Latora during my second year. For my Bachelor thesis and the additional Diploma thesis of the Scuola (both awarded *cum laude*), I worked under the supervision of Prof. Branchina on the possibility to observe effects of the Cosmological constant in laboratory experiments with Josephson junctions.

In 2008, I enrolled in the Master program in Theoretical Physics. In 2010, I spent a semester in Utrecht as Erasmus exchange student. Later in the same year, I came back to Utrecht as a visiting student and I worked on my Master thesis under the supervision of Prof. Morais Smith, Dr. Tieleman and Prof. Branchina on Bose-Einstein condensates in optical lattices with finite momentum. After graduating *cum laude* from the University of Catania in March 2011, I started my PhD research in Utrecht in July 2011 under the supervision of Prof. Morais Smith. The results of this research are the main subjects of this thesis.

BIBLIOGRAPHY

[1] C. Pethick and H. Smith, *Bose-Einstein Condensation in Dilute Gases* (Cambridge University Press, 2002).

[2] M. H. Anderson, J. R. Ensher, M. R. Matthews, C. E. Wieman, and E. A. Cornell, Science **269**, 198 (1995).

[3] K. B. Davis, M. O. Mewes, M. R. Andrews, N. J. van Druten, D. S. Durfee, D. M. Kurn, and W. Ketterle, Phys. Rev. Lett. **75**, 3969 (1995).

[4] S. N. Bose, Zeitschrift fur Physik **26**, 178 (1924).

[5] A. Einstein, Sitzungsberichte der Preußischen Akademie der Wissenschaften **1**, 261 (1924).

[6] I. Bloch, J. Dalibard, and W. Zwerger, Rev. Mod. Phys. **80**, 885 (2008).

[7] J. Bardeen, L. N. Cooper, and J. R. Schrieffer, Phys. Rev. **108**, 1175 (1957).

[8] P. Nozières and S. Schmitt-Rink, Journal of Low Temperature Physics **59**, 195 (1985).

[9] E. Tiesinga, B. J. Verhaar, and H. T. C. Stoof, Phys. Rev. A **47**, 4114 (1993).

[10] C. Ching, R. Grimm, P. Julienne, and E. Tiesinga, Rev. Mod. Phys. **82**, 1225 (2010).

[11] M. Greiner, C. A. Regal, and D. S. Jin, Nature **426**, 537 (2003).

[12] M. Bartenstein, A. Altmeyer, S. Riedl, S. Jochim, C. Chin, J. H. Denschlag, and R. Grimm, Phys. Rev. Lett. **92**, 120401 (2004).

[13] T. Bourdel, L. Khaykovich, J. Cubizolles, J. Zhang, F. Chevy, M. Teichmann, L. Tarruell, S. J. J. M. F. Kokkelmans, and C. Salomon, Phys. Rev. Lett. **93**, 050401 (2004).

[14] M. Lewenstein, A. Sanpera, and V. Ahufinger, *Ultracold atomic gases in optical lattices: simulating quantum many-body systems* (Oxford University Press, 2012).

[15] M. Lewenstein, A. Sanpera, V. Ahufinger, B. Damski, A. Sen, and U. Sen, Advances in Physics **56**, 243 (2007).

[16] D. Jaksch, C. Bruder, J. I. Cirac, C. W. Gardiner, and P. Zoller, Phys. Rev. Lett. **81**, 3108 (1998).

[17] M. P. A. Fisher, P. B. Weichman, G. Grinstein, and D. S. Fisher, Phys. Rev. B **40**, 546 (1989).

[18] M. Greiner, O. Mandel, T. Esslinger, T. W. Hänsch, and I. Bloch, Nature **415**, 39 (2002).

[19] J. K. Freericks and H. Monien, Europhys. Lett. **26**, 545 (1994).

[20] D. van Oosten, P. van der Straten, and H. T. C. Stoof, Phys. Rev. A **63**, 053601 (2001).

[21] D. Jaksch and P. Zoller, Annals of Physics **315**, 52 (2005), special Issue.

[22] R. P. Feynman, International journal of theoretical physics **21**, 467 (1982).

[23] J. Hubbard, Proc. Roy. Soc. London A **276**, 238 (1963).

[24] W. Hofstetter, J. I. Cirac, P. Zoller, E. Demler, and M. D. Lukin, Phys. Rev. Lett. **89**, 220407 (2002).

[25] J. G. Bednorz and K. A. Müller, *Zeitschrift für Physik B Condensed Matter*, **64**, 189 (1986).

[26] P. A. Lee, N. Nagaosa, and X.-G. Wen, Rev. Mod. Phys. **78**, 17 (2006).

[27] S. Sachdev, *Quantum Phase Transitions* (Cambridge University Press, 2011).

[28] D. R. Hofstadter, Phys. Rev. B **14**, 2239 (1976).

[29] F. D. M. Haldane, Phys. Rev. Lett. **61**, 2015 (1988).

[30] A. Isacsson and S. M. Girvin, Phys. Rev. A **72**, 053604 (2005).

[31] W. V. Liu and C. Wu, Phys. Rev. A **74**, 013607 (2006).

[32] R. P. Feynman, *Statistical Mechanics: A Set of Lectures* (Addison Wesley, 1972).

[33] C. Wu, Mod. Phys. Lett. B **1**, 1 (2009).

[34] G. Wirth, M. Ölschläger, and A. Hemmerich, Nat. Phys. **7**, 147 (2011).

[35] M. Ölschläger, G. Wirth, and A. Hemmerich, Phys. Rev. Lett. **106**, 015302 (2011).

[36] M. Ölschläger, T. Kock, G. Wirth, A. Ewerbeck, C. Morais Smith, and A. Hemmerich, New J. Phys. **15**, 083041 (2013).

[37] K. Sun and E. Fradkin, Phys. Rev. B **78**, 245122 (2008).

[38] T. Stöferle, H. Moritz, C. Schori, M. Köhl, and T. Esslinger, Phys. Rev. Lett. **92**, 130403 (2004).

[39] I. B. Spielman, W. D. Phillips, and J. V. Porto, Phys. Rev. Lett. **98**, 080404 (2007).

[40] W. S. Bakr, J. I. Gillen, A. Peng, S. Folling, and M. Greiner, Nature **462**, 74 (2009).

[41] J. F. Sherson, C. Weitenberg, M. Endres, M. Cheneau, I. Bloch, and S. Kuhr, Nature **467**, 68 (2010).

[42] S. Trotzky, Y.-A. Chen, A. Flesch, I. P. McCulloch, U. Schollwock, J. Eisert, and I. Bloch, Nat Phys **8**, 325 (2012).

[43] F. H. L. Essler, H. Frahm, F. Göhmann, A. Klümper, and V. E. Korepin, *The One-Dimensional Hubbard Model* (Cambridge University Press, 2010).

[44] P. W. Anderson, *The Theory of Superconductivity in the High-Tc Cuprate Superconductors* (Princeton University Press, 1997).

[45] A. Paramekanti, M. Randeria, and N. Trivedi, Phys. Rev. Lett. **87**, 217002 (2001).

[46] M. Köhl, H. Moritz, T. Stöferle, K. Günter, and T. Esslinger, Phys. Rev. Lett. **94**, 080403 (2005).

[47] R. Jördens, N. Strohmaier, K. Günter, H. Moritz, and T. Esslinger, Nature **455**, 204 (2008).

[48] P. Fazekas, *Lecture Notes on Electron Correlation and Magnetism* (Wold Scientific, 1999).

[49] A. Auerbach, *Interacting Electrons and Quantum Magnetism* (Springer, 1998).

[50] R. A. Hart, P. M. Duarte, T.-L. Yang, X. Liu, T. Paiva, E. Khatami, R. T. Scaletter, N. Trivedi, D. A. Huse, and R. G. Hulet, Nature **519**, 211 (2015).

[51] D. Greif, T. Uehlinger, G. Jotzu, L. Tarruell, and T. Esslinger, Science **340**, 1307 (2013).

[52] M. Dolfi, A. Kantian, B. Bauer, and M. Troyer, Phys. Rev. A **91**, 033407 (2015).

[53] T. Esslinger, Annual Review of Condensed Matter Physics **1**, 129 (2010).

[54] A. Eckardt, C. Weiss, and M. Holthaus, Phys. Rev. Lett. **95**, 260404 (2005).

[55] C. E. Creffield and T. S. Monteiro, Phys. Rev. Lett. **96**, 210403 (2006).

[56] H. Lignier, C. Sias, D. Ciampini, Y. Singh, A. Zenesini, O. Morsch, and E. Arimondo, Phys. Rev. Lett. **99**, 220403 (2007).

[57] A. Zenesini, H. Lignier, D. Ciampini, O. Morsch, and E. Arimondo, Phys. Rev. Lett. **102**, 100403 (2009).

[58] C. E. Creffield, F. Sols, D. Ciampini, O. Morsch, and E. Arimondo, Phys. Rev. A **82**, 035601 (2010).

[59] C. V. Parker, L.-C. Ha, and C. Chin, Nat Phys **9**, 769 (2013).

[60] W. Zheng, B. Liu, J. Miao, C. Chin, and H. Zhai, Physical Review Letters **113**, 155303 (2014).

[61] L.-C. Ha, L. W. Clark, C. V. Parker, B. M. Anderson, and C. Chin, Physical Review Letters **114**, 055301 (2015).

[62] A. J. Leggett, *Quantum Liquids: Bose Condensation and Cooper Pairing in Condensed-Matter Systems* (Oxford University Press, 2006).

[63] A. Eckardt, P. Hauke, P. Soltan-Panahi, C. Becker, K. Sengstock, and M. Lewenstein, EPL (Europhysics Letters) **89**, 10010 (2010).

[64] J. Struck, C. Ölschläger, R. Le Targat, P. Soltan-Panahi, A. Eckardt, M. Lewenstein, P. Windpassinger, and K. Sengstock, Science **333**, 996 (2011).

[65] A. Altland and M. R. Zirnbauer, Phys. Rev. B **55**, 1142 (1997).

[66] S. Ryu, A. P. Schnyder, A. Furusaki, and A. W. W. Ludwig, New J. Phys. **12**, 065010 (2010).

[67] M. Z. Hasan and C. L. Kane, Rev. Mod. Phys. **82**, 3045 (2010).

[68] J. Struck, C. Ölschläger, M. Weinberg, P. Hauke, J. Simonet, A. Eckardt, M. Lewenstein, K. Sengstock, and P. Windpassinger, Phys. Rev. Lett. **108**, 225304 (2012).

[69] H. Miyake, G. A. Siviloglou, C. J. Kennedy, W. C. Burton, and W. Ketterle, Phys. Rev. Lett. **111**, 185302 (2013).

[70] M. Aidelsburger, M. Atala, M. Lohse, J. T. Barreiro, B. Paredes, and I. Bloch, Phys. Rev. Lett **111**, 185301 (2013).

[71] J. Dalibard, F. Gerbier, G. Juzeliunas, and P. Öhberg, Rev. Mod. Phys. **83**, 1523 (2011).

[72] J. Struck, M. Weinberg, C. Ölschläger, P. Windpassinger, J. Simonet, K. Sengstock, R. Hoppner, P. Hauke, A. Eckardt, M. Lewenstein, and L. Mathey, Nat. Phys. **9**, 738 (2013).

[73] P. Hauke, O. Tieleman, A. Celi, C. Ölschläger, J. Simonet, J. Struck, M. Weinberg, P. Windpassinger, K. Sengstock, M. Lewenstein, and A. Eckardt, Phys. Rev. Lett. **109**, 145301 (2012).

[74] G. Jotzu, M. Messer, R. Desbuquois, M. Lebrat, T. Uehlinger, D. Greif, and T. Esslinger, Nature **515**, 237 (2014).

[75] L. Tarruell, D. Greif, T. Uehlinger, G. Jotzu, and T. Esslinger, Nature **483**, 302 (2012).

[76] T. Uehlinger, G. Jotzu, M. Messer, D. Greif, W. Hofstetter, U. Bissbort, and T. Esslinger, Phys. Rev. Lett. **111**, 185307 (2013).

[77] C. L. Kane and E. J. Mele, Phys. Rev. Lett. **95**, 226801 (2005).

[78] C. L. Kane and E. J. Mele, Phys. Rev. Lett. **95**, 146802 (2005).

[79] M. König, S. Wiedmann, C. Brüne, A. Roth, H. Buhmann, L. W. Molenkamp, X.-L. Qi, and S.-C. Zhang, Science **318**, 766 (2007).

[80] N. Goldman, G. Juzeliūnas, P. Öhberg, and I. Spielman, Reports on progress in physics. Physical Society (Great Britain) **77**, 126401 (2014).

[81] O. Dutta, M. Gajda, P. Hauke, M. Lewenstein, D.-S. Lühman, B. A. Malomed, T. Sowinski, and J. Zakrzewski, "Non-standard hubbard models in optical lattices: a review," ArXiv:1406.0181.

[82] Á. Rapp, X. Deng, and L. Santos, Phys. Rev. Lett. **109**, 203005 (2012).

[83] C. N. Yang, Phys. Rev. Lett. **63**, 2144 (1989).

[84] R. Casalbuoni and G. Nardulli, Reviews of Modern Physics **76**, 263 (2004).

[85] M. M. Parish, F. M. Marchetti, A. Lamacraft, and B. D. Simons, Nat Phys **3**, 124 (2007).

[86] Y.-a. Liao, A. S. C. Rittner, T. Paprotta, W. Li, G. B. Partridge, R. G. Hulet, S. K. Baur, and E. J. Mueller, Nature **467**, 567 (2010).

[87] A. K. A. J. Daley, and P. Zoller, Phys. Rev. Lett. **104**, 240406 (2010).

[88] L. Arrachea and A. A. Aligia, Phys. Rev. Lett. **73**, 2240 (1994).

[89] S. Greschner, L. Santos, and S. Poletti, Phys. Rev. Lett. **113**, 183002 (2014).

[90] T. Giamarchi, *Quantum Physics in One Dimension* (Clarendon Press, 2003).

[91] R. Peierls, *Surprises in Theoretical Physics* (Princeton University Press, Princeton, 1979).

[92] W. P. Su, J. R. Schrieffer, and A. J. Heeger, Phys. Rev. B **22**, 2099 (1980).

[93] M. Ölschläger, G. Wirth, and A. Hemmerich, Phys. Rev. Lett. **106**, 015302 (2011).

[94] F. Gerbier, A. Widera, S. Fölling, O. Mandel, T. Gericke, and I. Bloch, Phys. Rev. Lett. **95**, 050404 (2005).

[95] C. M. Varma, Phys. Rev. B **73**, 155113 (2006).

[96] Y. He, J. Moore, and C. M. Varma, Phys. Rev. B **85**, 155106 (2012).

[97] I. Vasic, A. Petrescu, K. Le Hur, and W. Hofstetter, "Chiral bosonic phases on the haldane honeycomb lattice," (2014), arXiv:1408.1411.

[98] L.-K. Lim, C. Morais Smith, and A. Hemmerich, Phys. Rev. Lett. **100**, 130402 (2008).

[99] N. Goldman, W. Beugeling, and C. Morais Smith, Europhys. Lett. **97**, 23003 (2012).

[100] I. Bloch, J. Dalibard, and S. Nascimbène, Nature Physics **8**, 267 (2012).

[101] D. Greif, T. Uehlinger, G. Jotzu, L. Tarruell, and T. Esslinger, Science **340**, 1307 (2013).

[102] M. Foglio and L. Falicov, Phys. Rev. B **20**, 4554 (1979).

[103] M. Grifoni and P. Hänggi, Phys. Rep. **304**, 229 (1998).

[104] H. Sambe, Phys. Rev. A **7**, 2203 (1973).

[105] L. M. Duan, EPL (Europhysics Letters) **81**, 20001 (2008).

[106] J. P. Kestner, Phys. Rev. A **81**, 043618 (2010).

[107] C. N. Yang, Rev. Mod. Phys. **34**, 694 (1962).

[108] G. Sewell, J. Stat. Phys. **61**, 415 (1995).

[109] H. T. Nieh, G. Su, and B. H. Zhao, Phys. Rev. B **51**, 3760 (1995).

[110] R. R. P. Singh, and R. T. Scalettar, Phys. Rev. Lett. **66**, 3203 (1991).

[111] F. H. L. Essler, V. E. Korepin, and K. Schoutens, Phys. Rev. Lett. **68**, 2960 (1992).

[112] F. H. L. Essler, V. E. Korepin, and K. Schoutens, Phys. Rev. Lett. **70**, 73 (1993).

[113] J. de Boer, V. E. Korepin, and A. Schadschneider, Phys. Rev. Lett. **74**, 789 (1995).

[114] J. de Boer, and A. Schadschneider, Phys. Rev. Lett. **75**, 4298 (1995).

[115] A. Schadschneider, Phys. Rev. B **51**, 10386 (1995).

[116] L. Arrachea, A. A. Aligia, and E. Gagliano, Phys. Rev. Lett. **76**, 4396 (1996).

[117] G. I. Japaridze and A. P. Kampf, Phys. Rev. B **59**, 12822 (1999).

[118] A. A. Aligia and L. Arrachea, Phys. Rev. B **60**, 15332 (1999).

[119] H. Frahm and V. Korepin, Phys. Rev. B **42**, 10553 (1990).

[120] L. Arrachea, A. A. Aligia, E. Gagliano, K. Hallberg, and C. Balseiro, Phys. Rev. B **50**, 16044 (1994).

[121] M. Nakamura, Phys. Rev. B **61**, 16377 (2000).

[122] J. Hirsch, R. Sugar, D. Scalapino, and R. Blankenbecler, Phys. Rev. B **26**, 5033 (1982).

[123] R. T. Clay, A. W. Sandvik, and D. K. Campbell, Phys. Rev. B **59**, 4665 (1999).

[124] J. Zaanen and O. Gunnarsson, Phys. Rev. B **40**, 7391 (1989).

[125] A. Anfossi, C. Degli Esposti Boschi, A. Montorsi, and F. Ortolani, Phys. Rev. B **73**, 085113 (2006).

[126] A. A. Aligia, A. Anfossi, L. Arrachea, C. Degli Esposti Boschi, A. O. Dobry, C. Gazza, A. Montorsi, F. Ortolani, and M. E. Torio, Phys. Rev. Lett. **99**, 206401 (2007).

[127] J. E. Hirsch, and F. Marsiglio, Phys. Rev. B **39**, 11515 (1989).

[128] A. O. Dobry and A. A. Aligia, Nucl. Phys. B **843**, 767 (2011).

[129] L. Arrachea and A. A. Aligia, Phys. Rev. B **59**, 1333 (1999).

[130] N. Goldman and J. Dalibard, Phys. Rev. X **4**, 031027 (2014).

[131] C. V. Parker, L.-C. Ha, and C. Chin, Nat. Phys. **9**, 769 (2013).

[132] R. Ma, M. Eric Tai, P. Preiss, W. Bakr, J. Simon, and M. Greiner, Phys. Rev. Lett. **107**, 095301 (2011).

[133] N. Teichmann, M. Esmann, and C. Weiss, Phys. Rev. A **79**, 063620 (2009).

[134] Y.-A. Chen, S. Nascimbène, M. Aidelsburger, M. Atala, S. Trotzky, and I. Bloch, Phys. Rev. Lett. **107**, 210405 (2011).

[135] E. Haller, R. Hart, M. J. Mark, J. G. Danzl, L. Reichsöllner, and H.-C. Nägerl, Phys. Rev. Lett. **104**, 200403 (2010).

[136] S. Greschner, G. Sun, D. Poletti, and L. Santos, Phys. Rev. Lett. **113**, 215303 (2014).

[137] M. D. Liberto, C. E. Creffield, G. I. Japaridze, and C. M. Smith, Phys. Rev. A **89**, 013624 (2014).

[138] G. Wirth, M. Ölschläger, and A. Hemmerich, Nat. Phys. 7, 147 (2011).

[139] M. Di Liberto, T. Comparin, T. Kock, M. Ölschläger, A. Hemmerich, and C. Morais Smith, Nat. Comm. **5**, 5735 (2014).

[140] M. Atala, M. Aidelsburger, J. T. Barreiro, D. Abanin, T. Kitagawa, E. Demler, and I. Bloch, Nat. Phys. **9**, 795 (2013).

[141] N. Nagaosa and J. Takimoto, J. Phys. Soc. Jpn. **55**, 2735 (1986).

[142] T. Egami, S. Ishihara, and M.Tachiki, Science **261**, 1307 (1993).

[143] R. Resta and S. Sorella, Phys. Rev. Lett. **74**, 4738 (1995).

[144] M. Fabrizio, A. Gogolin, and A. Nersesyan, Phys. Rev. Lett. **83**, 2014 (1999).

[145] M. E. Torio, A. A. Aligia, and H. A. Ceccatto, Phys. Rev. B **64**, 121105(R) (2001).

[146] A. Kampf, G. I. M. Sekania, Japaridze, and P. Brune, J. Phys. C **15**, 5895 (2003).

[147] S. R. Manmana, V. Meden, R. M. Noack, and K. Schönhammer, Phys. Rev. B **70**, 155115 (2004).

[148] M. E. Torio, A. A. Aligia, G. I. Japaridze, and B. Normand, Phys. Rev. B **73**, 115109 (2006).

[149] G. Japaridze, R. Hayn, P. Lombardo, and E. Müller-Hartmann, Phys. Rev. B **75**, 245122 (2007).

[150] S. Kivelson, W.-P. Su, J. Schrieffer, and A. Heeger, Phys. Rev. Lett. **60**, 72 (1988).

[151] D. Baeriswyl, P. Horsch, and K. Maki, Phys. Rev. Lett. **60**, 70 (1988).

[152] J. Gammel and D. Campbell, Phys. Rev. Lett. **60**, 71 (1988).

[153] M. Modugno and G. Pettini, New J. Phys. **14**, 055004 (2012).

[154] K. Hai, Y. Luo, G. Lu, and W. Hai, Opt. Expr. **22**, 4277 (2014).

[155] N. W. Ashcroft and N. D. Mermin, *Solid State Physics* (Saunders College, Orlando, 1976).

[156] N. Marzari and D. Vanderbilt, Phys. Rev. B **56**, 12847 (1997).

[157] E. Arimondo, D. Ciampini, A. Eckardt, M. Holthaus, and O. Morsch, Adv. At. Mol. Opt. Phys. Advances In Atomic, Molecular, and Optical Physics, **61**, 515 (2012).

[158] A. Hemmerich, Phys. Rev. A **81**, 063626 (2010).

[159] A. B. Zamolodchikov, Int. J. Mod. Phys. A **10**, 1125 (1995).

[160] S. Lukyanov and A. Zamolodchikov, Nuc. Phys. B **493**, 571 (1997).

[161] M. Fabrizio, Phys. Rev. B **54**, 10054 (1996).

[162] K. Kuroki, R. Arita, and H. Aoki, J. Phys. Soc. Jpn. **66**, 3371 (1997).

[163] R. Arita, K. Kuroki, H. Aoki, and M. Fabrizio, Phys. Rev. B **57**, 10324 (1998).

[164] S. Daul and R. M. Noack, Phys. Rev. B **58**, 2635 (1998).

[165] S. Daul and R. M. Noack, Phys. Rev. B **61**, 1646 (2000).

[166] C. Aebischer, D. Baeriswyl, and R. M. Noack, Phys. Rev. Lett. **86**, 468 (2001).

[167] K. Louis, J. V. Alvarez, and C. Gros, Phys. Rev. B **64**, 113106 (2001).

[168] K. Hamacher, C. Gros, and W. Wenzel, Phys. Rev. Lett. **88**, 217203 (2002).

[169] M. E. Torio, A. A. Aligia, and H. A. Ceccatto, Phys. Rev. B **67**, 165102 (2003).

[170] C. Gros, K. Hamacher, and W. Wenzel, Europhys. Lett. **69**, 616 (2005).

[171] M. Capello, F. Becca, M. Fabrizio, S. Sorella, and E. Tosatti, Phys. Rev. Lett. **94**, 026406 (2005).

[172] J. Bardeen, Nobel Lectures, Physics 1942-1962 (1964).

[173] G. H. Jonker and J. H. van Santen, Physica **16**, 337 (1950).

[174] L. Sun, X.-J. Chen, J. Guo, P. Gao, Q.-Z. Huang, H. Wang, M. Fang, X. Chen, G. Chen, Q. Wu, C. Zhang, D. Gu, X. Dong, L. Wang, K. Yang, A. Li, X. Dai, H.-k. Mao, and Z. Zhao, Nature **483**, 67 (2012).

[175] D. Fausti, R. I. Tobey, N. Dean, S. Kaiser, A. Dienst, M. C. Hoffmann, S. Pyon, T. Takayama, H. Takagi, and A. Cavalleri, Science **331**, 189 (2011).

[176] J. M. Tranquada, AIP Conf. Proc. **1550**, 114 (2013).

[177] F. Gerbier, Phys. Rev. Lett. **101**, 155303 (2008).

[178] A. Hemmerich, D. Schropp, and T. W. Hänsch, Phys. Rev. A **44**, 1910 (1991).

[179] S. Paul and E. Tiesinga, Phys. Rev. A **88**, 033615 (2013).

[180] B. Chen, S. Kou, Y. Zhang, and S. Chen, Phys. Rev. A **81**, 053608 (2010).

[181] K. Sheshadri, R. Krishnamurthy, R. Pandit, and T. V. Ramakrishnan, Europhys. Lett. **22**, 257 (1993).

[182] C. Schroll, F. Marquardt, and C. Bruder, Phys. Rev. A **70**, 053609 (2004).

[183] J. Zakrzewski, Phys. Rev. A **71**, 043601 (2005).

[184] F. Gerbier, A. Widera, S. Fölling, O. Mandel, T. Gericke, and I. Bloch, Phys. Rev. A **72**, 053606 (2005).

[185] K. Jiménez-Garcia, R. L. Compton, Y.-J. Lin, W. D. Phillips, J. V. Porto, and I. B. Spielman, Phys. Rev. Lett. **105**, 110401 (2010).

[186] C. Becker, P. Soltan-Panahi, J. Kronjäger, S. Dörscher, K. Bongs, and K. Sengstock, New J. Phys. **12**, 065025 (2010).

[187] P. Sengupta, M. Rigol, G. G. Batrouni, P. J. H. Denteneer, and R. T. Scalettar, Phys. Rev. Lett. **95**, 220402 (2005).

[188] V. Kashurnikov, N. V. Prokof'ev, and B. V. Svistunov, Phys. Rev. A **66**, 031601 (2002).

[189] L. Pollet, C. Kollath, K. van Houcke, and M. Troyer, New J. Phys. **10**, 065001 (2008).

[190] B. Capogrosso-Sansone, S. G. Söyler, N. Prokof'ev, and B. Svistunov, Phys. Rev. A **77**, 015602 (2008).

[191] A. F. Albuquerque, J. Magn. Magn. Mater. **310**, 1187 (2007).

[192] B. Bauer, J. Stat. Mech. , P05001 (2011).

[193] J. D. Axe, A. H. Moudden, D. Hohlwein, D. E. Cox, K. M. Mohanty, A. R. Moodenbaugh, and X. Youwen, Phys. Rev. Lett. **62**, 2751 (1989).

[194] B. Büchner, M. Breuer, A. Freimuth, and A. P. Kampf, Phys. Rev. Lett. **73**, 1841 (1994).

[195] I. Affleck and J. B. Marston, Phys. Rev. B **37**, 3774 (1988).

[196] A. Hemmerich, "Private communication," .

[197] S. D. Huber and E. Altman, Phys. Rev. B **82**, 184502 (2010).

[198] G. Engelhardt and T. Brandes, ArXiv:1503.02503.

[199] T. Fukui, Y. Hatsugai, and H. Suzuki, Journal of the Physical Society of Japan **74**, 1674 (2005).

[200] H. M. Price and N. R. Cooper, Phys. Rev. A **85**, 033620 (2012).

[201] H. M. Price and N. R. Cooper, Phys. Rev. Lett. **111**, 220407 (2013).

[202] A. Collin, J. Larson, and J. P. Martikainen, Phys. Rev. A **81**, 023605 (2010).

[203] J. J. Sakurai, *Modern Quantum Mechanics* (Addison Wesley, 2009).